JOURNAL OF ENGINEERING, EMERGING TECHNOLOGIES AND APPLIED SCIENCES (JEETAS)

A PUBLICATION OF THE FACULTY OF ENGINEERING, NIGER DELTA UNIVERSITY

APRIL 2023 VOLUME 01 ISSUE 01

ARTICLES

NIGER DELTA UNIVERSITY

Journal of Engineering, Emerging Technologies and Applied Sciences (JEETAS)

ABOUT US

The Journal of Engineering, Emerging Technologies and Applied Sciences (JEETAS) is a peer reviewed, international and biannual publication of the Faculty of Engineering, Niger Delta University, Nigeria. The journal aims to facilitate scholarly work on recent theoretical and practical aspects of engineering research and related multidisciplinary fields.

SCOPE

The journal covers scholarly articles in all the fields of Engineering, Technology and Applied Sciences, including but not limited to:
Agricultural / Environmental Engineering, Biomedical Engineering, Biochemical / Chemical Engineering, Civil / Structural Engineering, Electrical and Electronics Engineering, Engineering Management, Marine Engineering, Mechanical / Mechatronics Engineering, Oil and Gas Engineering, Petroleum Engineering, Informatics Engineering, Industrial Engineering, Artificial Intelligence and Machine Learning Applications etc.

EDITORIAL BOARD

EDITORIAL ADVISORY BOARD

S/N	Name	Affiliation
1	Emeritus Prof Joseph C. Igbeka	University of Ibadan
2	Emeritus Prof Sulaiman Adeniyi Adekola	Federal University Otuoke
3	Prof Daukiye Samuel Zibokere	Federal University Otuoke
4	Prof Christopher Ahiakwo	Rivers State University
5	Prof Samuel Enahoro Agarry	Ladoke Akintola University of Technology
6	Prof Inengite Azibaola Kesiye	Niger Delta University
7	Prof Kenneth S. Okiongbo	Niger Delta University
8	Prof Kenneth Dagde	Rivers State University
9	Prof Jackson G. Akpa	Rivers State University
10	Prof Sunday Ikiensikimama	University of Port Harcourt
11	Prof Abdulkarim Nasir	Federal University of Technology Minna
12	Prof Baba Shehu Waziri	University of Maiduguri
13	Prof Mike Oyekonwu	University of Port Harcourt

EDITORIAL OPEN ACCESS

A Message From the Editor-in-Chief

I am delighted to celebrate the launch of the *Journal of Engineering, Emerging Technologies and Applied Sciences* (JEETAS), a new peer-reviewed, biannual, open-access journal that publishes original scholarly work on recent theoretical and practical aspects of engineering research and related multidisciplinary fields. JEETAS is a publication of the Faculty of Engineering, Niger Delta University, Nigeria.

The opportunity to serve as the first Editor-in-Chief is a huge privilege but also a significant responsibility to shape the future of engineering education in this part of the world. JEETAS aims to provide a platform for researchers, practitioners, and industry experts to share their latest discoveries and insights in the field.

As the editor-in-chief of this journal, I am committed to upholding the highest standards of scientific integrity, transparency, and rigor in the peer-review process. Our editorial team comprises of experienced professionals with a passion for engineering, who will work tirelessly to ensure that every paper published in our journal meets the highest quality standards.

We welcome submissions from all branches of engineering, including but not limited to electrical, mechanical, civil, chemical, biomedical, and environmental engineering. We are particularly interested in papers that focuses on interdisciplinary collaborations and promote the development of new technologies and solutions to real-world problems.

All the articles presented in this maiden issue of the Journal were subjected to Turnitin plagiarism check and a rigorous blind peer-review process. We operate a zero tolerance policy on plagiarism and some manuscripts that did not meet the plagiarism threshold policy of the Journal were rejected. Manuscripts that passed the plagiarism check were sent to three expert reviewers in the subject areas.

We also recognize the importance of open access to scientific knowledge, and our journal will be fully open access, meaning that all articles will be freely available to readers worldwide. We believe that this will not only increase the visibility and impact of our authors' research but also promote collaboration and innovation in the engineering community.

The success of any journal is built on the support of the contributors, the reviewers, associate editors and the publication staffs. I would like to thank you all for your tremendous contributions and I look forward to receiving your suggestions and ideas to make JEETAS more valuable for the research community.

We invite you to submit your best work to our new journal and become part of a vibrant community of engineers dedicated to advancing the field. Thank you for your support, and we look forward to receiving your submissions in the next issue of the Journal.

ZEKIENI R. YELEBE, *Editor-in-Chief*
Journal of Engineering, Emerging Technologies
and Applied Sciences (JEETAS)
e-mail: robert.yelebe@ndu.edu.ng

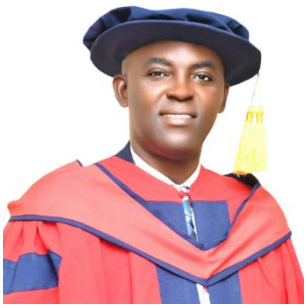

Zekieni R. Yelebe is a distinguished professor of Chemical Engineering and Dean of the Faculty of Engineering at the Niger Delta University, Bayelsa State, Nigeria. He received the Ph.D. degree in Chemical Engineering from the Rivers State University of Science and Technology (now Rivers State University) in 2010 and became a Full Professor of Chemical Engineering at the Niger Delta University in 2019. Prof. Yelebe is a member of the governing board of the Council for the Regulation of Engineering in Nigeria (COREN).

Journal of Engineering, Emerging Technologies and Applied Sciences -– Volume 1 Issue 1, April 2023

Available at ***www.ndu.edu.ng/ journalofengineering***

RESEARCH ARTICLE OPEN ACCESS

Evaluation of an Alternative Source of Power for Ship Operations in Ports

G. O. Nwaorgu[1] and E. A. Ogbonnaya[2]

[1]*Department of Marine Engineering, Nigerian Maritime University, Okerenkoko, Delta State, Nigeria*

[2]*Department of Marine Engineering, Niger Delta University, Amassoma, Bayelsa State, Nigeria*

Corresponding Author: gpdwise@gmail.com

----------**********----------

Abstract:

This research undertakes the provision of an alternate source of power of vessel that berths in Nigeria ports. Renewable energy such as solar power will be used to power these vessels. Port Harcourt port was used as a case study for this research. A total of 2.5mW was observed as the constant power needed to power vessels that berth in Port Harcourt port. A total of 10800 panels is connected in 1080 parallel and 10 series while 6578 Batteries are connected in 274 parallel and 24 series will be used to generate 2.5mW needed to power vessels that berth in Port Harcourt port. The cost of running this solar generator for 25 years which is estimated as the life span of the solar panel is shown in this research. The Solar batteries is replaced after 10 years as the assumption of the solar power plant (SPP) maintenance cost. This research will help reduce pollution and generate an alternative revenue source for Nigeria Port Authority. ETAP and MATLAB software will be used to carryout necessary analysis in this research.

Keywords: Renewable Energy, Nigeria Port Authority, Revenue Generation, Pollution, Solar Power Plant

----------**********----------

I. INTRODUCTION

The exhaust gas emission from vessels can be pollution emission (Achilleas et al, 2021). The emission of these gases is on the increase due to heavy demand of moving cargo from one point to another. The activities from marine operations in port such as loading and discharging of cargo is a major contribution to climate change due to this (Corbett, et al, 2007). The Nigeria Port Authority (NPA) operates and governs activities of ports in Nigeria. Calabar Port, Warri Port, Apapa port Complex and Tin Can Island Port in Lagos, Onne port and Port Harcourt port are major ports controlled by the NPA. In 2005 the federal government implemented its concessioning programme with an aim of promoting efficiency through public and private partnership.

Cold ironing, a process that enables ships to receive electrical power from the shore side while at berth, has been implemented in several ports worldwide as a means of reducing ship emissions and noise. This technology, also known as shore supply of power, has been successfully introduced in ports such as Los Angeles, Antwerp, Genoa, Gothenburg, and Oslo (Parth et al, 2016). By

providing ships with an alternative power source during their stay at the port, cold ironing allows them to turn off their auxiliary engines, leading to a significant reduction in their environmental impact (Zis et al, 2014).

Many developing countries, including Nigeria, have not yet adopted shore power as a means of providing electricity to their ports. As a result, the emissions generated by port operations are causing health issues for nearby communities. Due to the epileptic power supply in Nigeria an alternative and reliable means of renewable energy such as solar generator will be used. To provide an effective shore supply of power, cost analysis of the solar/diesel generator will be compared as used in ports by ships that come to call.

II. LITERATURE REVIEW

Emodi and Yusuf (2015) identified various constraints on power access in Nigeria, including low competency and implementation, security of fuel source, administrative impediments, inattentive institutional organization, information inefficiency, ramshackle transmission and distribution, meager grid structure, and lack of approach and venture advancement. Solar power systems can offer solutions to these problems, such as no fuel cost for power generation, reduced running costs, and a more robust transmission grid structure (Dumkhana and Idoniboyeobu,

To determine the hourly yield force of photovoltaic (PV) and wind blend system, the hourly load variety of the examined region is drawn and the loss of load probability (LOLP) is assessed through Monte Carlo simulation. The battery storage system is then integrated into the system, and the LOLP unswerving quality list at several battery measures, PV, and wind blend are determined. Stiel and Skyllas (2012) have used Vanadium Redox Battery as an integrated technology model in extensive large-scale remote wind/diesel control systems using Hybrid Optimization of Multiple Energy Resources (HOMER) Micro-Power Optimization Model computer program built by the US National Renewable Energy Laboratory.

The results from this study show significant financial and ecological benefits to be achieved in mounting energy storage. A metering system will be installed in this research to charge batteries during low radiation of sunlight to reduce LOLP that may arise as a result of insufficient storage of power on the battery, and Surrette/Roll is used, having a rated capacity of 4560AH.

Girma (2013) recommended the most reasonable design of a solar PV system with a diesel generator as support for suggested rural school electrification. The technical and economic evaluation of the ideal system was prepared, contrasting the economic energy of a sunlight-based PV/generator/battery mixture control system with that of a separate diesel generator system, using HOMER simulation software for the analysis. In this research, Matrix laboratory (Matlab) and Electrical Power System Analysis (ETAP) software are used to analyze a solar power plant (SPP) in electrifying NPA, and it gave a reasonable result compared to the diesel generator currently in use.

Zaheeruddin et al. (2015) examined a blend of one or more renewable sources like PV and wind, either in separate or grid-connected mode with energy storage capacity-based energy systems. The hybrid system was modeled, optimized, and analyzed using HOMER software built by the National Renewable Energy Laboratory, Colorado USA. The hybrid systems were evaluated based on Net Present Cost, Cost of Energy, Initial Cost, Operation Cost, and Renewable Fraction attained on the basis of analyzed outcomes.

To assess the technical state and economic potentials of new energy systems or sources that appear to match economic development, engineers, technologists, and students concerned with renewable energy systems must undertake modern-related software and hardware tutoring to aid them in carrying out both technical and economic analysis on other energy systems. This research aims to analyze real-time life cost analysis and the rate of pollution that auxiliary generation vessels produce using a diesel generator and compare its operating cost to a solar generator. It will also enable NPA to generate funds through cold ironing processes and reduce pollution present in Nigerian ports.

III. MATERIALS AND METHODS

A power audit is shown in Tables 1 to 3 on the auxiliary engines and the various metric tonnes (MT) of fuels on Ships that berth in Port and Terminal Operator Nigeria Limited (PTOL). This data was obtained by me from 4th of January 2018 to 31st of May 2023. A 2.5mW solar generator power as observed from the table will be capable of powering all vessel that loads and unload cargo at this berth. An analysis of using SPP will be carried out during this research with the aim of reducing operational cost, pollution and generating revenue for NPA.

TABLE 1:

The power and running cost of a vessel in PTOL terminal in January 2018

Days in a week	Name of vessel	Number of days in a port	Gross Registered Tonnage	Cargo carried	Generator power used in port (KW)	Fuel consumption MT/Day	Total power used in 24hrs	Total fuel used in a week	Total cost of running vessel in port (N)
1st week of January	MV. Leonarisso	4	27989	Wheat	1210	5.0	5.0*4+ 4.3*2+ 4.16*4	45.24* 206,280=	9332107.20
	MSC.Maria	2		Container	900	4.3			
	MV. Bold Voyager	4	25905	Salt	880	4.16			
2nd week of January	MV. Frio Shinano	4		Fish	1100	4.7	4.7*4+4.3*1	23.1*206,280=	4765068.00
	MSC. Maria	1		Container	900	4.3			
4th week of January	MV. Secombus	4		Fish	900	4.42	4.42*4 + 4.74*4+4.35*1	40.99*206280	8455417.20
	MV. Angara	4		Fish	1200	4.74			
	MV. Andermatt	1		Salt	910	4.35			

TABLE 2:

The power and running cost of a vessel in PTOL terminal in February 2018

Days in a week	**Name of vessel**	**Number of days in a port**	**Gross Registered Tonnage**	**Cargo carried**	**Generator power used in port (KW)**	**Fuel consumption MT/Day**	**Total power used in 24hrs**	**Total fuel used in a week**	**Total cost of running vessel in port (N)**
1st week of February	MT. Biskra	2	8744	Bitumen	660	3.92	3.92*2+4.35*5 +4.16*7 +4.75*4+4.3*2	86.31*206280	17804026.80
	MV. Andermatt	5	12578	Salt	910	4.35			
	MV. Paraskevi	7	26330	Wheat	850	4.16			
	MV. MercsKelani	4		Bulk malt	1100	4.75			
	MV. MSC Maria	2		Container	900	4.3			
2nd week of February	MV. Bold Voyager	4		Salt	880	4.16	4.16*4+2.75*7 +4.32*7	66.13*206280	13641296.40
	MV. Hibisus	7		Bulk wheat	400	2.75			
	MV. Pamyatillic he	7		Fish	960	4.32			
3rd week of February	MV. PamyatIllic he	1		Fish	960	4.32	4.35*1+2.75*6 +4.3*4+2.62*4	48.53*206280	10010768.40
	MV.Hibisus	6		Bulk malt	400	2.75			
	MV. Maria	4		Container	900	4.3			
	MV. Interlink Levity	4		Wheat	350	2.62			
4th week of February	MV. Sierra Leyra	4		Fish	820	4.21	4.21*4 + 4.02*4 + 4.3*2	41.52*206280	8564745.60
	MV. China Frost	4		Fish	740	4.02			
	MV. MSC Maria	2		Container	900KW	4.3			

TABLE 3:

The power and running cost of a vessel in PTOL terminal in March 2018

Days in a week	**Name of vessel**	**Number of days in a port**	**Gross Registered Tonnage**	**Cargo carried**	**Generator power used in port**	**Fuel consumption MT/Day**	**Total power used in 24hrs**	**Total fuel used in a week**	**Total cost of running vessel in port (N)**
1st week of March	MT. Biskra	1	8744	Bitumen	660	3.92	3.92*1 + 4.21*4 + 3.86*7	47.78*206280	9856058.40
	MV. Da Qing	4	12578	Cargo	870	4.21			
	MV. Discover	7	26330	Wheat	550	3.86			
2nd week of March	MV. MSC Maria	2		Container	900	4.3	4.3*2 + 4.15*1 + 4.29*7 + 4.16*1	46.94*206280	9682783.20
	MV. Numalik	1		Cargo	740	4.15			
	MV. Sweet Lady	7		Bulk salt	810	4.29			
	MV. Bold Voyager	1		Salt	880	4.16			
3rd week of March	MV. Sweet Lady	1		Bulk salt	810	4.29	4.29*1 +4.16*3 + 4.42*4	34.45*206280	7106346.00
	MV. Bold Voyager	3		Salt	880	4.16			
	MV. PamyatKirova	4		Cargo	930	4.42			
4th week of March	MV MSC Maria	4		Container	900	4.3	4.3*4+ 3.92*1	21.12*206280	4356633.60
	MV Briska	1		Bitumen	660	3.92			

After closely observing the power used in ports by vessels when they berth as shown in the Tables 1 to 3 in which both power requirement and fuel consumption for each vessel was tabulated. A 2.5mW power generator set is selected to be used initially for port operation and during the course of this research, a comparative analysis is carried out between a solar and diesel generator.

A. *Data Collection on Power Consumption of Ship Operations in Port*

Various vessel such as dry, liquid and bulk carriers predominantly occupy this berth. The current available power requirement for this research work was carried out from 4th of January to April 31st 2018. The full power requirement carried out in this research work entails that the power during working hours of the vessel and crew comfort was placed into consideration.

Tables 1 to 3 shows the expected power requirement of vessels when in port and terminal operations limited (PTOL) berth with respect to the generators used and the running cost due to Intermediate fuel oil (IFO) needed to run the vessel. The price of IFO 180 sales for $573 (N206,280.00) for one Metric Ton (MT).

B. *Solar Panel Sizing for 2.5MW*

The size of a PV array depends on both technical and economic factors related to the PV panel. It is generally assumed that the output of a PV panel is directly proportional to the amount of incident radiation it receives (Podder et al, 2015). In order to determine the appropriate size for a PV panel, several key parameters must be taken into consideration, including the total daily energy (E) in watt hours, the average number of sun hours per day (T_{min}), and the Direct Current (DC) voltage of the system. Once these parameters have been determined, the sizing process can begin.

For this particular project, the Solar Panel Model 270W Polycrystalline Solar Panel is to be used. This panel boasts a cell efficiency of around 30% and utilizes advanced low sunlight technology, which ensures high performance even in low light conditions. Additionally, it comes with a 25-year warranty and can handle high charging currents. The unit cost for this panel is N 55,000.

C. *Peak Power*

Equation 1 allows us to calculate the total number of PV panels required based on the required power (P) and the average sun hours per day (T_{min}).

$$E_{rough} = P * T_{min} \quad (1)$$

To ensure that the system is not undersized, we first divide the total daily energy demand (E) by the efficiency (η) of the system components. This gives us the daily energy requirement from the solar array, which can be obtained using equation 2.

$$\frac{E}{\eta} = E_r \quad (2)$$

Where E_r is the dialy energy requirement, E is the dialy average energy consumption; and η_{overal} is the product of component efficiencies as shown in equation 3.

$$E_r = \frac{E}{\eta_{overall}} \quad (3)$$

To achieve the Peak power (P_p), the result of equation 3 is divided by the average sun hour per day T_{min} for the geographical location as shown in equation 4.

$$P_{peak} = \frac{\text{dialy energy requirement}}{\text{average sun hours per day}}$$

$$P_{peak} = \frac{E_r}{T_{min}} \; Kwp \quad (4)$$

To obtain the total current required in DC, Equation 5 indicates that the peak power must be divided by the DC voltage of the system (Dumkhana and Idoniboyeobu, 2018).

$$I_{DC} = \frac{Peak\ Power}{System\ DC\ Voltage}$$

$$I_{DC} = \frac{Peak\ Power}{System\ DC\ Voltage}$$

$$I_{DC} = \frac{P_{peak}}{V_{DC}} \quad \text{Amps} \qquad (5)$$

D. *Number of Series (N_s) and Parallel (N_P) Modules*

To meet the desired voltage and current requirements, the module needs to be connected in both series and parallel. To calculate the number of modules connected in series *(Ns)*, the DC voltage of the system (V_{DC}) needs to be divided by the rated voltage of each module (V_M), assuming V_M =34.5 as shown in Equation 6. This will determine the string length of the module. As a result, TN_S represents the number of modules in series.

$$\text{TNs} = \frac{\text{V}_{\text{DC}}}{\text{V}_{\text{M}}} \qquad (6)$$

To determine the number of parallel modules (TN_P), we divide the total peak power of all modules (P_P) by the peak power capacity of one module (P_M), and then multiply the result by the number of series modules (*Ns*), as shown in Equation 7.

$$TN_p = \frac{P_P}{P_M * TN_S} \qquad (7)$$

To calculate the total number of modules (TN_M), we multiply the number of series modules (TN_S) by the number of parallel modules (TN_P), as shown in Equation 8. These calculations are based on a 2500kW load and a PV lifespan of 25 years, according to Franklin (2017).

$$TN_m = \text{TN}_\text{p} * \text{TN}_\text{S} \qquad (8)$$

E. *Total cost of PV Panel for a 2500KW System*

The total cost of the solar panel is calculated by multiplying the total number of PV modules (TN_m) and the unit cost of PV panel (U_{ppv}) in which a unit price of PV panel in Nigeria is ₦55,000.00. Total Module Area occupied is calculating by multiplying the total number of PV module (TN_m) and the dimension of solar panel as shown equation 9 and 10.

$$\boldsymbol{TC_{PV}} = TN_M * U_{PPV} \qquad (9)$$

$$\text{A} = \text{TN}_\text{m} * \text{Dimension of SP } mm^2 \qquad (10)$$

F. *Battery Sizing and Cost*

The choices of the batteries are taking into consideration the capacity, the load time and depth of discharge. They are designed to be recharged hundreds or thousands of times. The batteries are rated in amp hours (AH) and its properties are shown in table 4. Like solar panels, batteries are wired in series or parallel to increase voltage to the desired level and increase amp hours.

TABLE 4:
The Specification/Details of the Batteries (Dumkhana and Idoniboyeobu, 2018)

Model	2YS-62P
Series	5000
Manufacturer	Surrette/Rolls
Type	Flooded- Dual Wall
Dimension	27.38”*9”*31.63”
Weight	570lb
Nominal Voltage	2V
Rated Capacity (24 hours)	4560AH

G. *Calculating for twenty-four (24) hour a day autonomy using solar Battery*

In view of the full load calculated from the power review of the building, the energy required is 2500kW. Presently computing for twenty four hours a day independence by using Battery. The safe energy storage $E_{safe}$is equal to the E_{rough} divided by

the maximum allowable level of discharge (MDOD) as shown in equation 11.

$$E_{safe} = \frac{E_{rough}}{MDOD} \qquad (11)$$

The capacity of the battery bank as shown in equation 12 is in ampere hour is equal to the E_{safe} divided by the rated voltage for each battery V_h to be used in the battery bank.

$$c = \frac{E_{safe}}{V_b} \quad \text{Ah} \qquad (12)$$

Where C is the capacity of the battery bank and V_b is the battery bank voltage. The total number of batteries ($TN_{batteries}$) used are obtained by dividing the capacity of the battery bank needed (C) in ampere hours by the capacity of one of the battery C_b selected in ampere hours as shown in equation 12, since the battery bank is composed of batteries we have

$$\text{TN}_{\text{batterie}} = \frac{C}{C_b} \qquad (13)$$

The number of series connection (TN_s) equals to the DC voltage of the system divided by the voltage rating of one of the batteries selected is presented in equation 14. The number of parallel paths (TN_p) is obtained by dividing the total number of batteries by TNs as shown in equation 13

$$TN_s = \frac{V_{dc}}{V_b}$$
$$TN_p = \frac{TN_{batteries}}{TN_S} \qquad (14)$$

Therefore the total cost of battery (TC_b) is the product of the number of battery to the unit price of one battery (U_{pb}) as represented in equation 14 (Ishaq et al, 2013).

$$TC_b = TN_b * U_{pb} \qquad (15)$$

H. ***Inflation and Replacement Cost of batteries:***

The National Bureau of Statistics disclosed that the consumer price index has dropped from 11.37% to 11.3% as price rose at a slower rate for all categories. Inflation rate in Nigeria average 12.46% from 1996 to 2019 (World Bank, 2019). A rate of 11.37% inflation will be used as commodity inflation rate of batteries, maintenance cost of diesel engine and replacement cost of diesel engine.

$$TC_b = TC_b * (1 + \text{r})^{ni} \qquad (16)$$

Grid power supply or generator can also be used to power the vessels in Port during nighttime. It requires a battery to store the DC generated from the solar cell DC to power all lighting appliances, motors and so on and are designed to use AC power while most solar power systems generate DC current which is transmitted to the inverter (Jayakumar, 2009).

A 4680AH battery system will deliver power using a power for one day autonomy. In view of the fact that we are neither designing nor constructing the battery for this research work a 2YS-62P Surrette/ Rolls battery is used with a replacement cost (TC_b) of 10 years with a unit cost of ₦500,000.

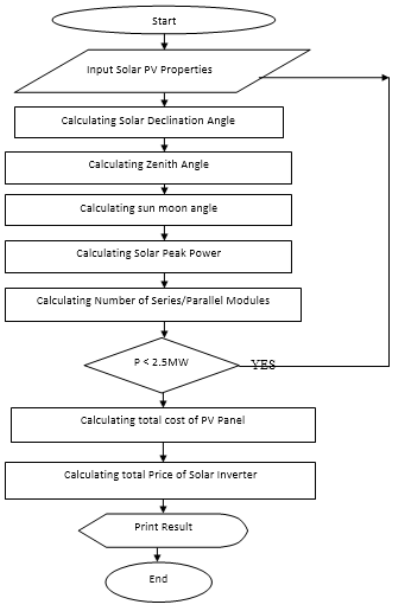

Fig 1 Flow Chart of 2.5mW Solar Generator for Powering Vessels in Port Harcourt Port

3.9 Inverter Cost

The total load calculated is 2500KW and a 500kVA inverter is suitable. In view of the fact that we are neither designing nor constructing the inverters for this research work, we will recommend: A 500kVA, 3-Phase Solar UK Xantra with Product Code: FR-UK33500; Weight: 3,300.00kg; Dimensions: 1000mm *42000mm * 2000mm is recommended with a cost price of₦ 52,000,000.

APP B shows the individual property of the selected inverter. A total of six (6) pieces of this inverter will be needed for this design. A flow chart showing the implementation of the above steps to obtain the total costing of this 2.5mW solar generator plant is shown in Fig 1.

IV. RESULTS AND DISCUSSION

1. PV Arrangement

Matlab and ETAP simulation are used to verify the arrangement of PV panels, which are suitable for analyzing the Solar Generator behavior of a PV module. The proposed PV model is validated by the results shown in figure 2a and figure 2b ETAP simulation. The specification of the user defined PV module and batteries which demonstrates the series and parallel parameters PV module operating under standard test conditions.

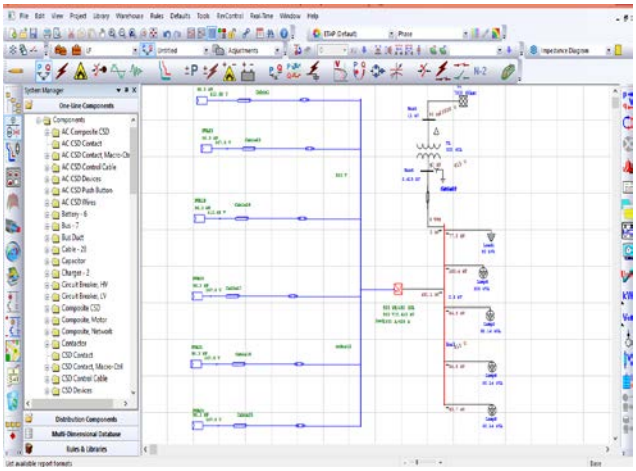

Fig 2: The ETAP Simulation of the Alternating Current (AC) 500KVA Solar Generator

Figs 2 and 3 shows the ETAP simulation of 500KW solar Generator set in which the PV module is arranged in 10 series and 180 parallel and a total of 1800 panel was used.

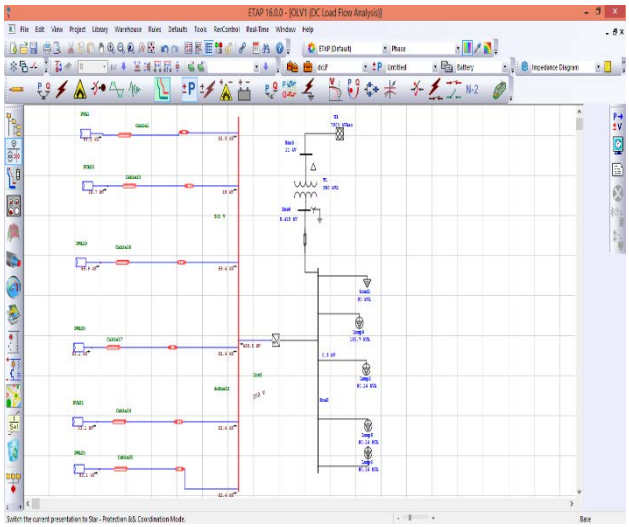

Fig 3: The ETAP DC Simulation of 500kva Solar Generator

Fuses and line wire cost was considered negligible. Loads shown in Figs. 2 and 3 represent watercraft load as shown in table 1 to 3. The inverter connects converts the DC to AC current. Figure 3 shows the ETAP simulation for a 2.5MW Solar Generator system that runs for 24 hours. A total of 10800 Panels was used to generate 2.5MW Power in which 1080 panels was connected in series and 10 parallel and 6578 batteries was used and connected in 24 parallel and 274 series.

2. Cost of Running Solar Generator

The total cost of running solar generator for 25 years was calculated to be ₦ 8,867,000,000 for the initial cost and ₦ 22,889,000,000 as the final cost after 25 years with battery replacement as the only maintenance cost of running the solar generator since inverters and solar panel are said to have 25 years warrantee. The battery replacement cost for 10 and 20 years caused a spike in the cost of the solar generator as shown in figure 4. The main costing of the solar generator was obtained from the number and unit cost of PV panel, batteries and inverter used

while cable, fuse and metering cost were considered negligible.

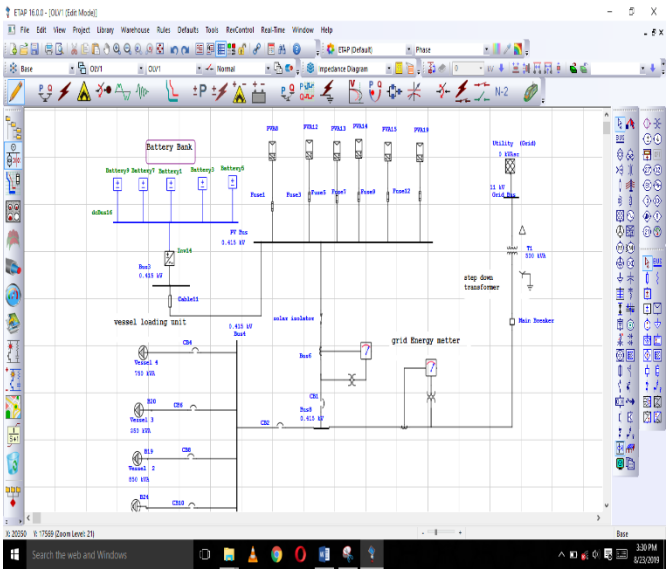

Fig 4: The ETAP Simulation of 2.5mW Solar Generator Power System

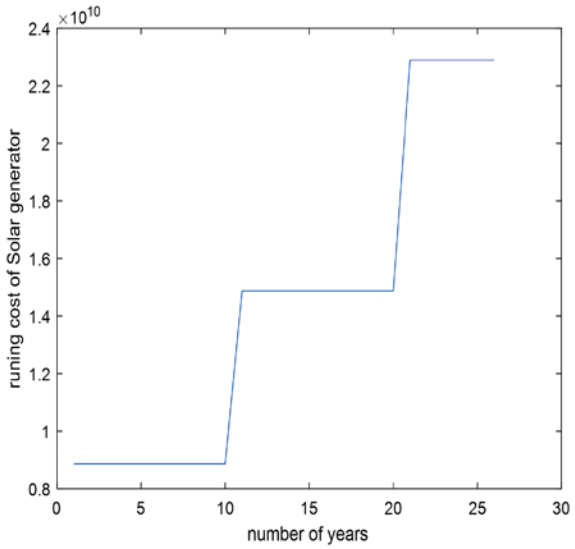

Fig 5: Cost of Running Solar Generator for 25 years

V. CONCLUSION AND RECOMMENDATIONS

The mainstay of NPA is to provide a good working environment for its staff, generate revenue for federal government and have a low operational cost for ship owners. It is therefore needed to implement an alternative source of power for vessels when they berth in Ports to facilitate speedy port operation and reduce auxiliary engine downtime that may occur as a result of engine failure due to over usage.

A life cycle cost analysis of a solar generator set in which initial cost, maintenance and replacement cost of the generator component was considered. The maintenance cost of solar generator is comparatively low as to when compared with its initial cost, and hence considered as the best choice for comparison.

The result of using this choice of generation as to the traditional diesel engine used in our ports today will reduce the rate of pollution produced. The diesel engine due to its fuel consumption will cause greenhouse gas effect and make the ports a potential health hazard to NPA staff. A step-by-step analysis of the SPP parameters obtained was used to write a program to determine the cost analysis of the generator thereby holistically monitoring this generator for 25 years. This program could be extended to other power plant such as gas and wind turbine plants.

Based on the results obtained in the course of this work, the following recommendations are hereby made:

a) A solar generator should be aimed at during implementation of shore supply of electricity in Port Harcourt port.

b) There should be an increase in research in shore supply of electricity on old vessels.

c) More stringent laws should be enacted and enforced to reduce the rate of pollution that occurs due to fuel consumption of diesel engines

REFERENCES

Achilleas G., Sokratis M, Ioannis I, Elisa M, Jukka-Pekka J, Leonidas N, Development of exhaust emission factors for vessels: A review and meta-analysis of available data, Atmospheric Environment: X, Volume 12, 2021, 100142, ISSN 2590-1621

Corbett, J., Winebrake, 1., Green, E. H., Kasibhatla, P., Eyring, V & Lauer, M. (2007). Mortality from Ship Emissions:A Global Assessment. *Environmental Science Technology*, 41 (24), pp 8512-8518

Dumkhana, L & Idoniboyeobu, D.C. (2018). Solar PV/Battery System Analysis for Faculty of Engineering Building, Rivers State University, Port Harcourt, Nigeria. *IOSR Journal of Electrical and Electronics Engineering (IOSR-JEEE)*, 45-51.

Emodi, N.V & Yusuf, S.D. (2015). Improving Electricity Access in Nigeria: Obstacles and the Way Forward. *International Journal of Energy Economics and Policy*, vol5(1), Pp 335-351.

Franklin, E. (2017, August). Solar Photovoltaic (PV) Site Assessment. Retrieved from Cooperative extention: https://extension.arizona. edu/sites/extension.Arizona.edu/ files /pubs /az1697-2017.pdf

Girma, Z. (2013). Technical & Economic Assessment of Solar PV/diesel Hybrid Power System for Rural School Electrification in Ethiopia. *International Journal of Renewable Energy Research*, 3(3), 736-744. Retrieved on 2 February, 2016 fromhttp://www.pscsolaruk.com/ solar-panels?product_id=202

Ishaq M., Ibrahim U. H & Abubakar, H (2013) "Design of an off grid photovoltaic system: a case study of government technical college, Wudil, Kano State," *International Journal of Scientific and Technology Research* Vol 2, Issue 12, 2013.Published

Jayakumar.K., N.Srihash & Rambabu, Ch. (2009) Voltage Unbalance Correction in a Grid Using Inverter *International Journal of Computational Engineering Research* (ijceronline.com) Vol 2 Issue. 8

Parth V, Paul S, Fischbeck, M, Granger M, and James J.C. Shore Power for Vessels Calling at United State Port: Benefits and Costs. *Environmental Science & Technology* **2016** *50* (3), 1102-1110 DOI: 10.1021/acs.est.5b0 4860

Podder, S., Khan, R.S. & Mohon, S.Md A.A. (2015). The Technical and Economic Study of Solar-Wind Hybrid Energy System in Coastal Area of Chittagong, Bangladesh. *Journal of Renewable Energy*. 1-10. Retrieved on 22 April 2016 from http://dx.doi.org/10.115 5/2015 /482543

Stiel, A. & Skyllas, K.M. (2012). Feasibility Study of Energy Storage Systems in Wind/Diesel Applications Using the HOMER Model. Article in *Applied Sciences*, (2), 726-737. Retrieved on 09 January, 2016 from https://www.mdpi.com/journal/applsci

Zaheeruddin, M.M., Saharia, B.J & Ganguly, A. (2015). Optimal Sizing and Cost Assessment of Hybrid Renewable Energy System for Assam Engineering College. *Research Gate*, 1-7.

World Bank, 2019, "Inflation in Emerging and Developing Economies, edited by Ha J., Kose, M.A., and Ohnsorge F. (https://www.worldbank.org/en/research/publication/inflation-in-emerging-and-developing-economies

Zis, T., North, R. J., Angeloudis, P., Ochieng, W. Y., & Bell, M. G. H. (2014). Evaluation of cold ironing and speed reduction policies to reduce ship emissions near and at ports. *Maritime Economics & Logistics*, 16(4), 371-398.

Journal of Engineering, Emerging Technologies and Applied Sciences -– Volume 1 Issue 1, April 2023

Available at ***www.ndu.edu.ng/ journalofengineering***

RESEARCH ARTICLE OPEN ACCESS

Design and Implementation of an Online Coronavirus Testing Software

SHOEWU Oluwagbemiga Omotayo*, AKINYEMI Lateef Adesola*, MUMUNI Quadri Ademola*, AJASA Abiodun Afis*, FOLORUNSO Comfort Oluwaseyi**, and RAFIU Moshood Olakunle*

*Department of Electronic and Computer Engineering, Lagos State University, Nigeria

Email: Oluwagbemiga.shoewu@lasu.edu.ng

**Department of Systems Engineering, Faculty of Engineering, University of Lagos, Nigeria

----------**********----------

Abstract:

The coronavirus disease (COVID-19) has spread across the world and has been classified as a pandemic and a public health emergency of global importance. Researchers have claimed that one of the reasons the coronavirus is deadly is because it attacks the respiratory system, which is like severe acute respiratory syndrome (SARS). The coronavirus causes shortness of breath and reduces the oxygen level in the blood. The coronavirus can also cause fever, taste and smell loss, and other symptoms. Early detection of infected persons and thorough contact tracing helps in reducing and mitigating the transmission of this virus. However, in rural communities where resources for testing are little or are not even available, this aim becomes unachievable. This system focuses on designing and implementing a coronavirus testing software that utilizes a deep neural model to detect the probability of COVID-19 based on user input data. After a one-time registration, users answer a few questions about how they feel, and the input data is then fed into the DNN model. The model is designed to detect if the individual is a suspect of COVID-19, providing a list of COVID-19 test laboratories based on their current location. With early detection of infected individuals and thorough contact tracing, this system aims to reduce and mitigate the transmission of COVID-19, especially in rural communities with limited resources for testing.

***Keywords* —** COVID-19; Web application; Deep learning**;** Coronavirus

----------**********----------

I. INTRODUCTION

SARS-COV-2, a critical respiratory disease, was first identified as a pulmonary incident of uncertain cause in China's Wuhan province in December 2019 (Ceci et. al, 2021), which subsequently led to the coronavirus disease epidemic (National Center for Biotechnology Information, 2021). Since the first public case, the rest of the world has faced numerous health challenges, including uneven public health policy implementation, a lack of widely available testing, and confusion over reliable diagnostics (Sofra, 2021). The World Health Organization declared COVID-19 a global infectious disease on March 11, 2020, as it had already infected around 100,000 people in roughly 100 states (Beta South-Ayrshire, 2021). The symptoms of COVID-19 begin with shortness of breath and evolve into a fever, cough, respiratory symptoms, and difficulty breathing. The disease is fatal and can cause bronchitis, pneumonia, acute respiratory suffering, and severe breathing conditions like SARS. The elderly, infants, those with cardiac illnesses, and immune-conceded persons are at higher risk of complications due to their weak immune systems. The global expiry proportion of the disease is estimated to be around 3.41 per cent (Coronavirus CDC, 2019). Experts have warned of the risks of the

virus's spread in Africa due to the region's delicate medical facilities and adjacent marketable relations with Beijing. Although coronavirus germs are expected to have minor existence proportions in hot Africa (SOAS University London, 2020), the continent has still been significantly affected. Nigeria has recorded 323 COVID-19 cases and ten deaths as of April 13, 2022. It is essential to acknowledge that Nigeria, being the most populated country in the region, has a significant role to play in controlling and managing the spread of COVID-19. Research has indicated that early detection and diagnosis of the virus can significantly increase the chances of recovery, particularly if there are no delays between assessment and analysis. A well-improved investigation scheme would encourage more individuals to get tested, leading to a better understanding of the extent of the disease. Viral infections have been a significant concern in human health, and COVID-19 has affected 221 countries and territories with over 230 million confirmed cases and 4.7 million deaths. In Nigeria, there have been over 203,000 confirmed cases and 2,644 deaths, indicating the need for better control measures. Effective contact tracing and timely diagnosis of infected patients is critical for healthcare organizations to manage and alleviate the COVID-19 illness. However, in remote areas where testing facilities are limited, controlling the spread of the virus becomes more challenging. To address this issue, self-testing can help people identify the symptoms before seeking medical attention, preventing false alarms, and wasting time. Therefore, improving the investigation scheme in Nigeria is crucial for controlling and containing the COVID-19 pandemic.

II. LITERATURE REVIEW AND THEORETICAL ANALYSIS

A. Literature Review

The National Institutes of Health conducted a study on the applicability of smartphone apps in conjunction with the QuidelQuickVue At-Home COVID-19 Test. This was supported by NIH through the RADx initiative. Over 200 participants enrolled on this study, and it involved a two-week testing period. Then a software called Mydatahelps was developed by CareEvolution LLC, which provided step-by-step instructions for taking the test, but unhappily it was only beneficial to America only. Using the terms "Coronavirus," "respirational condition coronavirus 2," and COVID-19, a previous study that was focused on the analytical and serological analyses for SARS-Cov-2 was disregarded. From their launch to 16 April 2020, the PubMed, Google Scholar, and EMBASE databases were searchable in any language. They were then updated on 15 May 2020. The preprint attendees for both fitness disciplines and genetic records were analyzed for the quickly emerging arena and fast dissemination of systematic responses concerning COVID-19 (Li M, 2020). Using machine learning techniques, some authors created a prediction model to tackle COVID-19 in China and other impacted places worldwide (Li M, 2020). To calculate the number of illnesses and catastrophes that have been reported around the universe, particularly in China, the authors employed a methodology. Between January 20 and March 1, 2020, data that served as the basis for the models were collected. According to their calculations, on the 22nd of February, and 10th of April 2020, in mainland China and globally respectively, the COVID-19 epidemic reached its climax. Additionally, the scientists estimated that global eradication of COVID-19 would be around mid-June 2020 and in China, at the start of April 2020. They estimated that there would be approximately 89,000 COVID-19 patients in 2010. Using the ARIMA model, which is an auto-regressive integrated moving average, some authors forecast that COVID-19 would greatly spread in the globe’s 15 most contaminated nations. They forecast that conditions will deteriorate in both Europe and Iran. Additionally, they anticipated that South Korea's and China's mainland's severity of illness will stabilize. Additionally, the study predicted that COVID-19 would spread swiftly in the US and that swift, rigorous government intervention would be needed to halt the disease's growth. However, there were expected to be one million COVID-19 cases in

the US between April 8 and April 30, 2020, there were only 677,570 instances on April 17, 2020. Additionally, despite an anticipated 300,000 cases, Italy only reported 168,941 cases. 100 different chest X-ray images, fifty per cent (50%) of Coronavirus victims and fifty per cent (50%) who were not infected were used by some authors to develop a CNN-based framework that could be used to detect COVID-19 sufferers. ResNet-50 demonstrated the greatest detection performance when three (3) CNN versions—Inception-ResNet-v2, Inception-v3, and Inception-v3—were tested utilizing five-fold inter (98 per cent). Also, some authors classified chest X-ray images as healthy or sick using a support vector machine after extracting attributes from the images using a deep-learning method (SVM) (Narin et al, 2021). The authors used AlexNet, Inception-ResNet-v2, ResNet-18, DenseNet-20, Inception-v3, XceptionNet, GoogLeNet, ResNet-50, VGG16, VGG19, and ResNet-101 (Chen et al, 2020), (Sharma et al, 2021). They collected two datasets: one had 133 infected patients (including those with MERS, SARS, and ARDS) and 133 uninfected clients, whereas the other had 25 infected people and 25 uninfected sick people. With ResNet-50 and SVM, they were able to extract independent features from each dataset with 95.38 per cent accuracy (Sethy and Behera, 2020). Additionally, some authors unveiled COVIDX-Net, a method that could aid radiologists in using X-rays to diagnose COVID-19 patients (Hemdan et al, 2020). 50 distinct X-ray images, divided into 25 COVID-19-negative images and 25 COVID-19-positive images, were employed to validate their framework of theirs. The employed photos were reduced to pixels 224224. The ResNet-v2, Xception, MobileNet, and Inception-v3 deep learning models are employed by the COVIDX-Net framework., modified VGG19, and Inception-ResNet-v2. The VGG19 and DeneNet models fared well, based on their analysis results and equally, having a COVID-19 F-score rate of 91% (Redie et al, 2022). More also, work on tuberculosis regarding patients in rural areas using the E-health solution scheme was carried out by (Shoewu, O.O. et.al, 2019). Additionally, Other machine learning, game theory, and metaheuristic algorithms, including genetic algorithm (GA), particle swarm optimisation (PSO), and others such as game theory, will be used to expand and validate this study in the future (Ekwe,S.O., 2020, Ekwe,S.O., 2021). Numerous engineering issues, including those involving wireless networks, automation, and process control, to name a few, have been successfully solved using these techniques (Oladejo. S.O., et al, 2021) and (Oladejo. S.O., et al, 2021). Also, a deep learning approach has been employed in autonomous robotic car (Shoewu, O.O. et al, 2021) and (Shoewu, O.O. et al., 2023). This scheme can equally be employed in health-related case. There is a wide variety of commercial software on the market that may be evaluated online for the COVID-19 virus. The contribution of this study lies in the strength to predict any pandemic before it occurs to avoid such deadly disease that ravaged the world in 2019. The following is a list of such global COVID software-based tests:

B. Theoretical Analysis

1. Viral Testing Tool: The Coronavirus Infectious Toolkit is a collaborating online software aimed to assist both fitness care suppliers and people comprehend COVID-19 testing choices. This software delivers pertinent, actionable data for persons to make knowledgeable conclusions regarding which test they might require. Once you have the assessment outcome, the software would take you to CDC references for that trial outcome. This virtual, mobile-friendly software inquires a sequence of queries and delivers suggested schedules and means based on the consumer's answers (Coronavirus CDC, 2019).

2. Detection Management Software for Coronavirus: Due to physical Coronavirus Test supervision methods, clinics, analytical workrooms, portable testing sites, hospitals, and fitness care providers all over the biosphere waste hours of productivity that could be spent on patient care. Xybion provides COVAPP which is a thorough

point-to-point Coronavirus Check Supervision app, in rebuttal to the Coronavirus pandemic and the requirement to quickly educate infected persons of the outcomes of their testing. COVAPP eradicates physiological processes with full regulatory requirements and fully automated test result notices.

3. Cloud COVID-19 LIMS: To evaluate, identify, and enhance coronavirus disease vaccines, medical testing and investigation workshops around the world are working nonstop. By using FDA permission and well-organized work streams, CloudLIMS has already helped several workshops get up and running in a week. The following are some of the common situations that COVID-19 testing labs deal with:

- Fast confirmation of FDA-permitted COVID-19 test work movements.
- Growth, regulation, and authentication of innovative approaches for detecting Coronavirus.
- Recording detection consequences according to CDC and FDA strategies.
- Ensuring global supervisory rules, like ISO 15189:2012, HIPAA, and CLIA.

Perfectly timed analysis of Coronavirus presumed cases plays a key role in effective isolation and medication handling. To combat the SARS-CoV-2 epidemic, for automatic COVID-19 identification on chest CT, a deep learning-focused prototype is being created. A poorly managed deep learning-built system was designed to comprehend COVID-19 utilizing 3D CT dimensions. The chest region of each victim was divided using an effective UNet, and a 3D deep neural network was then given the segmented 3D chest region to forecast the likelihood of Coronavirus infection. 499 CT dimensions were collected between 13 December 2019 and 23 January 2020 for teaching, whereas 131 CT sections were obtained between 24 January and 6 February 2020 for learning (Zheng et al, 2020). The deep learning system achieved a 0.976 PR AUC and a 0.959 ROC AUC. In the ROC curvature, there was an effective terminal with a sensitivity of 0.907 and 0.911. By classifying COVID-negative and COVID-positive utilizing a probability margin of 0.5, the method was able to attain an efficiency of (90.1%), a positive prefiguring rate of (84.0%), with a large negative prefiguring rate of (98.2%) (Zheng et al, 2020). Running a single client's CT data through a special GPU only took 1.93 seconds. Without the need to interpret the cuts for learning, the shakily implemented deep learning prototype could accurately anticipate the likelihood of COVID-19 infection in chest CT collections. A casual method of classifying COVID-19 sufferers is made possible by the simple-to-use yet very successful deep learning approach, which is useful for preventing the spread of SARS-CoV-2 (Zheng et al, 2020).

III. METHODOLOGY

This section discusses the methodology employed in this study. The Figure 1 depicts the block diagram used for this study using the deep neural network model for the COVID case.

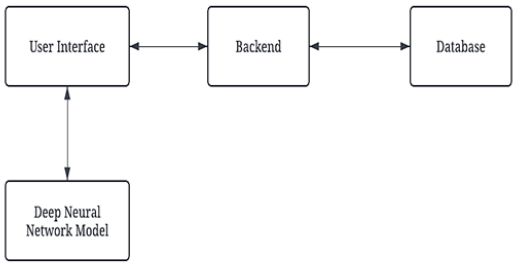

Fig 1: Block diagram of the system

A. Literature Review

1. ***User Interface:*** This is the graphical user interface of the application that allows communication between the system and the user. This component is a web application to be used on a web browser and it was built with modern web technologies such as HTML, CSS, and VueJS (JavaScript). This system's user interface was created as a Single Page Application (SPA), which implies that data is passed from one page to the next without the need to download new HTML content from the server.

2. ***Backend:*** The backend was built using Laravel, a PHP framework that enables developers to create

server-side applications and web services. Employing the REST Application Programming Interface, the backend delivered endpoints to enable the communication between the interface and the database. It serves as an intermediary between the user interface and the database.

3. Deep neural network model: The proposed system incorporates a deep neural network (DNN) model as the backbone of the COVID-19 testing software. The DNN model serves as the decision-making component, where it receives an input tensor from the user interface and returns a probability that the user has COVID-19 based on the provided input. The model was designed and trained in a Colab notebook using the Python programming language and several libraries such as Pandas, Numpy, PyTorch, and sklearn. These libraries enabled the creation of a high-performing and efficient model that accurately classifies the user's input as positive or negative for COVID-19. The DNN model's ability to learn and generalize from large datasets makes it an ideal choice for COVID-19 diagnosis, allowing for efficient and reliable testing even in areas with limited resources. Overall, the deep neural network model represents a critical component of the COVID-19 testing software, providing accurate and reliable predictions to aid in the fight against this global pandemic.

4. Database: The database stores the data sent from the Frontend through the Backend service. It is the source of data for the whole system. The database technology that was used in this system is MySQL.

B. System Design

In the deep neural network model, the classification was handled by a feed-forward neural network that used deep learning. Multi-layer perceptron (or MLPs) is another name for feedforward topologies. The outputs from units in each layer are transmitted to units in the next higher layer, with no outputs being passed back to lower levels in a feedforward arrangement. An artificial neural network (ANN) having multiple levels between both the layer of input and output is known as a deep neural network (DNN). Both neural networks employ the same modules: neurons, weights, biases, and functions. The neural network algorithm resembles how the human brain works. Any neural network needs input and output layers. The objective parameter is present in the layer of the output, whereas the layer of the input includes system parameters. An input layer, hidden layers nodes, and an output layer make up the model (Tawadrou and Katsabani, 2005). The layer of the input of the model has 18 nodes, the initial unknown level of the process has 11 nodes, the second hidden layer of the model has 3 nodes, and the output layer has just a single node (Geoffrey, 2002).

In this study, Figures 2 and 3 depict the flowchart of the deep neural network model and architectural structure of the deep neural network, respectively. The flowchart indicates every step taken from the feeding the input data to output using the dataset to train the developed model.

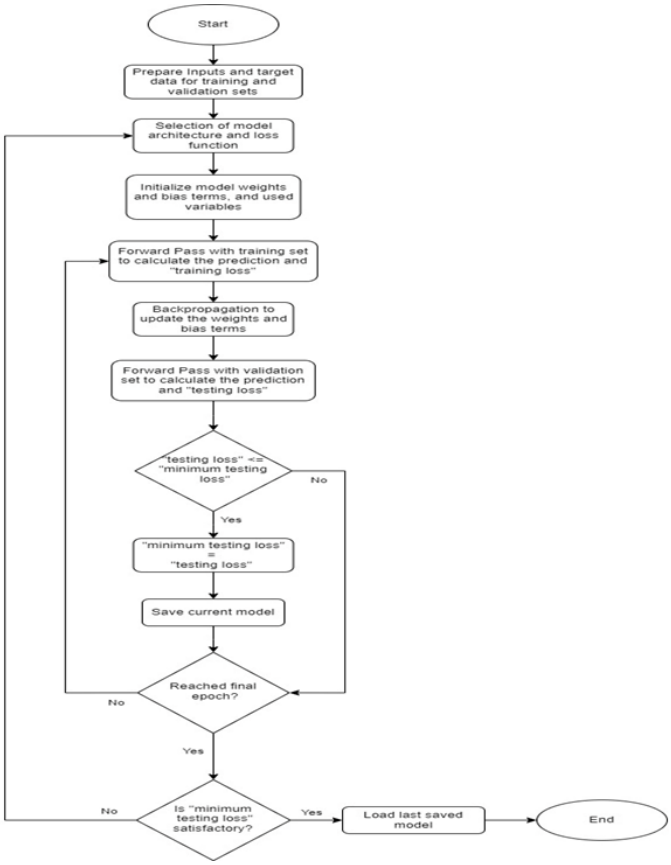

Fig 2: Flowchart of the deep neural network model.

IV. RESULTS AND DISCUSSIONS

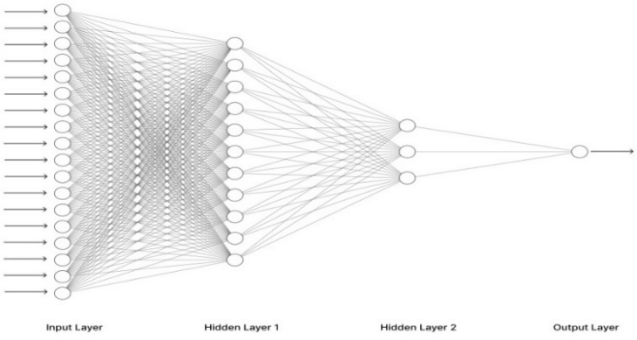

Fig 3: Architectural structure of the deep neural network**.**

The dataset is prepared by converting all the parameters from "Yes" and "No" to 1s and 0s (1 representing "Yes" and 0 representing "No") and then dividing the data into training and testing data. The deep neural network architecture of linear layers and a binary cross-loss function is chosen. The model weights and bias terms, epoch, minimum testing loss, and all other required variables are initialized.

To derive the prediction and training loss, forward propagation is used with the training data from the input layer to the output layer. After the training loss has been obtained, a backward propagation is then carried out to update the weight and bias terms and then increase the accuracy (en.wikipedia.org, 2020).

The forward pass is now repeated with the validation sets in other to obtain the testing loss (Kumar, 2020). If the testing loss is less than or equal to the minimum testing loss, the minimum testing loss is updated with the value of the current testing loss and the model's current state is saved. The process is repeated for the selected number of iterations. If the minimum testing loss is not satisfactory, the architecture is changed a little and the process repeats. After the iteration has been completed, and the minimum testing loss satisfied, the last saved state of the model is loaded. The activation function of the last layer is a sigmoid function which converts the single node output into probability.

A. Results

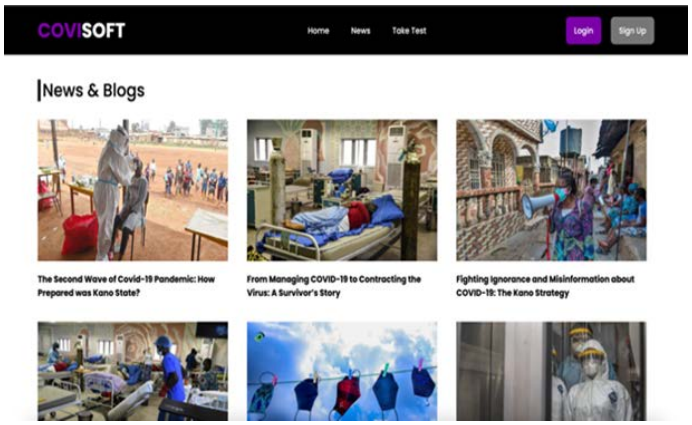

Fig 5: COVID-19 news page.

Figure 4 is a snapshot of the Covisoft news page which is the online page for publishing the latest news on the damages caused by the pandemic. In Figure 5, a patient is captured trying to do covid self-assessment after login into his dashboard on the Covisoft app by answering some questions which are automatically used in determining the status of the patient. A total of about 13 different questions are programmed on the app.

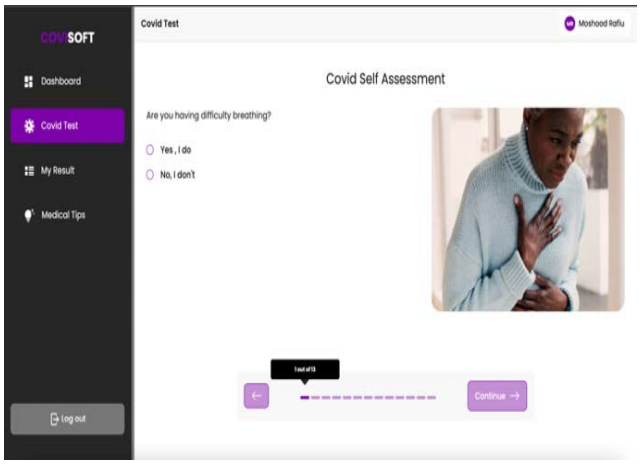

Fig 4: COVID-19 assessment start page.

Figure 6 captures the last stage of the self-assessment page which queries the suspected patient

if they contacted anyone who has directly or indirectly contacted a covid patient or medical personnel.

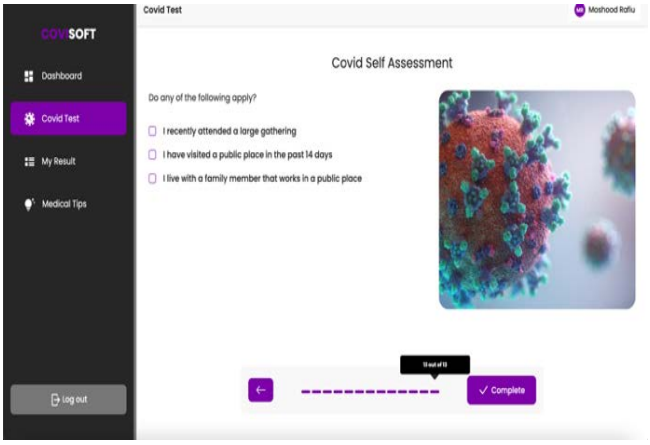

Fig 6: COVID-19 assessment complete page.

The result of the self-assessment session is displayed in Figure 7 based on the analysis of the answers provided and a recommendation is made available for the patient. In addition, it suggests a possible and close-by hospital for easy access to treatment.

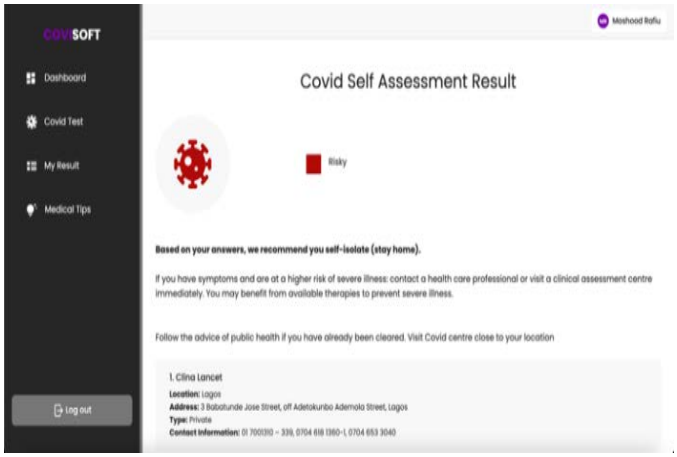

Fig 7: COVID-19 assessment result page.

Figure 8 shows the summary list of previous results generated on the online testing software. The results table shows four distinct parameters which are result ID, risk level, date of the test, and the review button. The risk levels are in 3 categories namely: pass, risky, and warning.

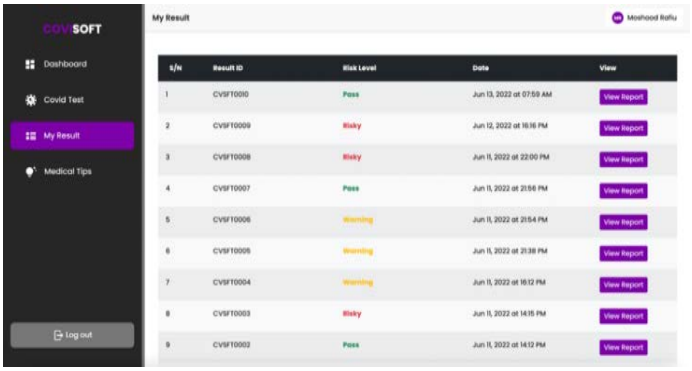

Fig 8: List of assessment results on the page.

In Figure 9, medical tips on curbing the spread of covid are itemized, which is the last icon on the dashboard.

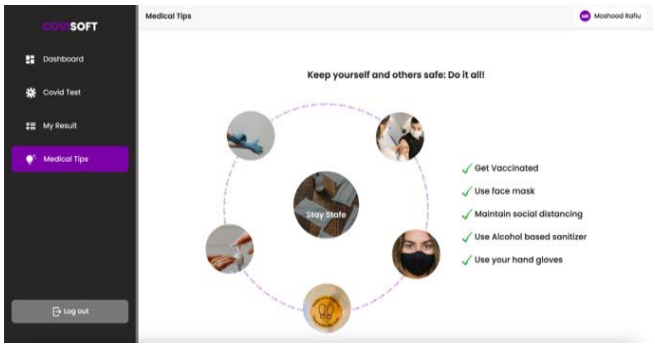

Fig 9: Medical tips page.

Figure 10 shows the graph of binary cross-entropy against the epochs or iterations to reveal the neural network training convergence from a global dataset. A steady state was achieved from about 20000 iterations against about 1.5 binary.

In Figure 11, the rise was constant up until the 20000 epoch and remained steady until it ultimately converged at around 0.94. After the 150000 epochs, a final accuracy of roughly 94% was attained (iterations). After 20000 epochs (iterations), the model converged, yielding an average training rate of 95%.

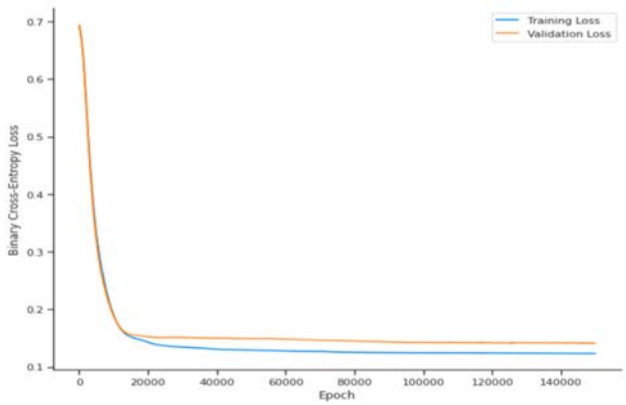

Fig 11: Neural network training convergence from a global dataset.

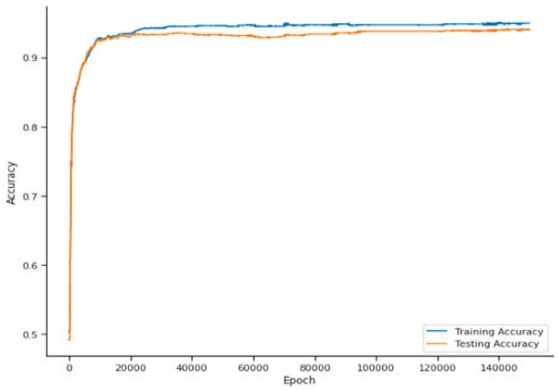

Fig 12: Accuracy neural network model from a global dataset.

Figure 12 is the confusion matrix for testing the global dataset and matrices [2, 2] show the highest prediction of 1057. Meanwhile,

Figure 13 is the neural network training convergence from the synthetic local dataset. The convergence diminished from about 20000 epochs. However, the convergence rate between the training and the testing dataset increases as compared to that of the global dataset.

Also, Figure 14 shows a steady rise up to the 17000th epoch before remaining steadily rising until it ultimately converged at around 0.86. After 150000 epochs, a final accuracy of roughly 86% was attained (iterations). After roughly 100000 epochs (iterations), the model converged, with an average training rate of 86%.

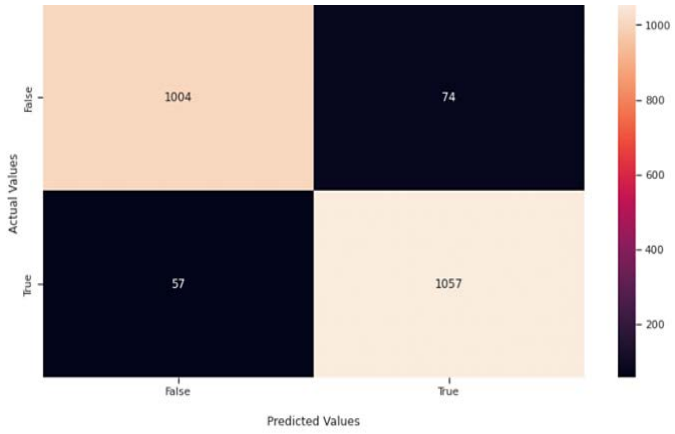

Fig 13: Confusion matrix for testing the global data model.

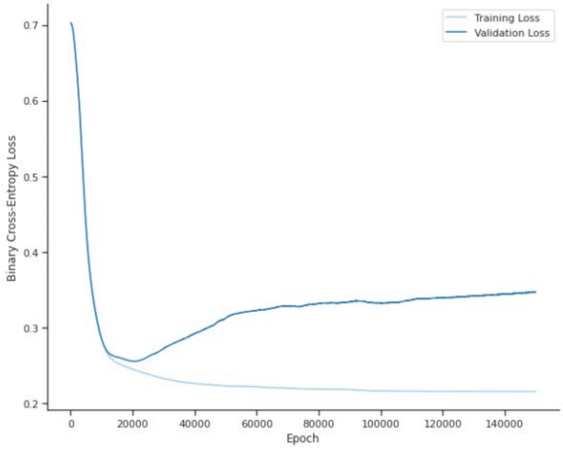

Fig 10: Neural network training convergence from the synthetic local dataset.

The confusion matrix of Figure 15 shows that matrices [1, 1] have the highest prediction of 449 which is lower than that of the global dataset.

Figure 16 are depicting the histograms to represent the effect of each symptom on the patient's result, while Figure 17 are the histograms to represent the effect of each symptom on the patient's result.

Figure 18 are the doughnut charts representing the COVID and non-COVID patients based on symptoms for local data while Figure 19 are the doughnut charts representing the COVID and non-COVID patients based on symptoms for global data.

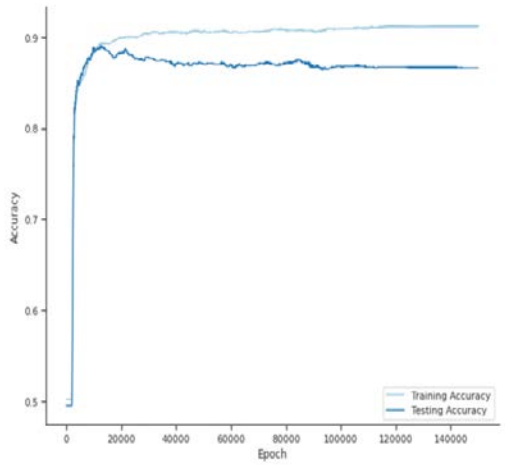

Fig 14: Accuracy neural network model from the local dataset.

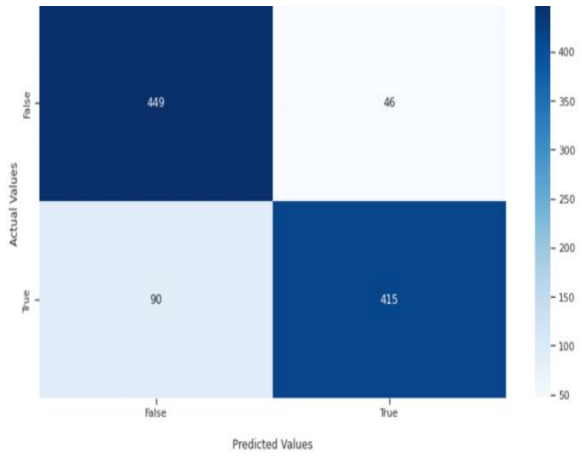

Fig 15: Confusion matrix for testing the local data model.

B. Discussions

1. *Statistical Analysis from Dataset*

The feature parameters from the global and local datasets were visualized using histograms and doughnut charts and pie charts to show how each feature parameter contributes to the goal parameter. It should be noted that the obtained numerical results could not be compared with other machine learning algorithms or metaheuristic algorithms because of the lack of dataset locally or globally and more importantly paucity of time. To extend this study in the future, other machine learning algorithms and metaheuristic algorithms such as genetic algorithm (GA), particle swarm optimization (PSO) and so on will be employed to validate this study. These schemes have been extensively employed to solve engineering problems such as wireless networks, automation and process control to mention a few

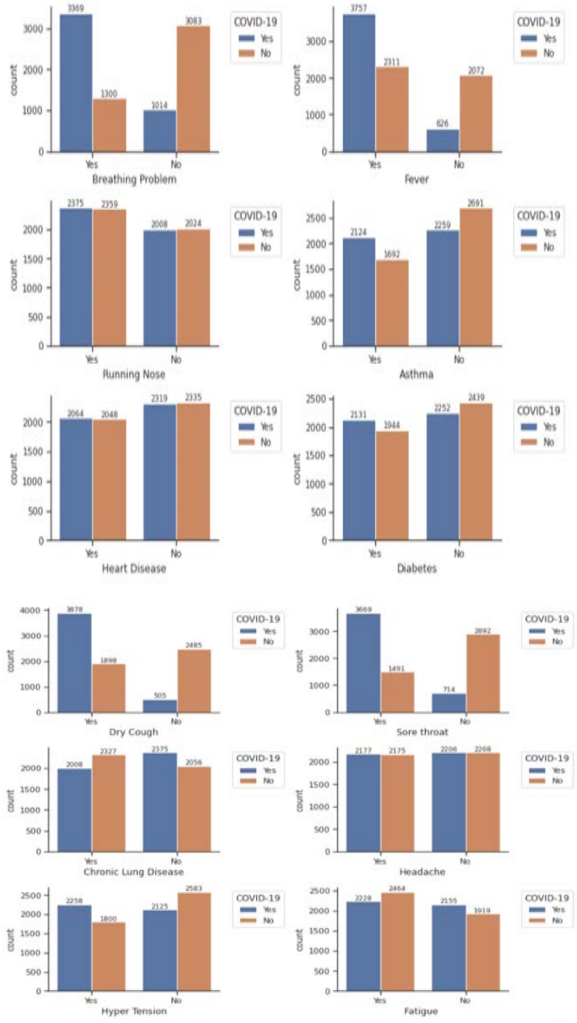

Fig 16: Histograms for global data

V. CONCLUSION

In conclusion, the proposed system of designing and implementing a coronavirus testing software that utilizes a deep neural model to detect the probability

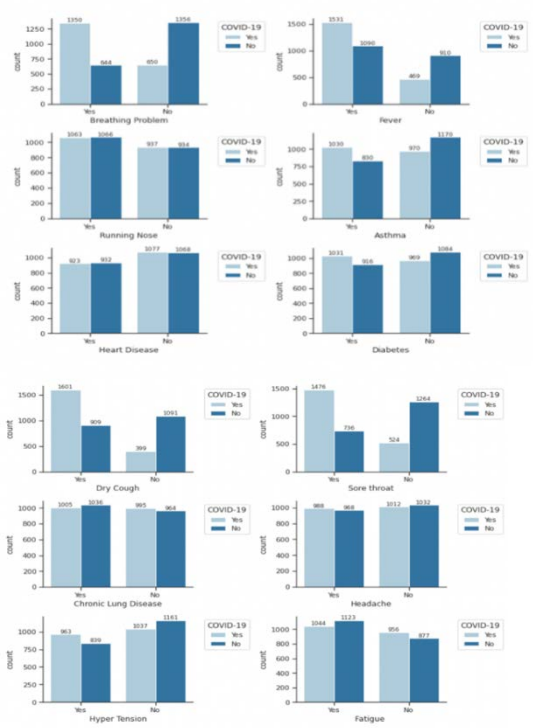

Fig 18: Histograms for local data

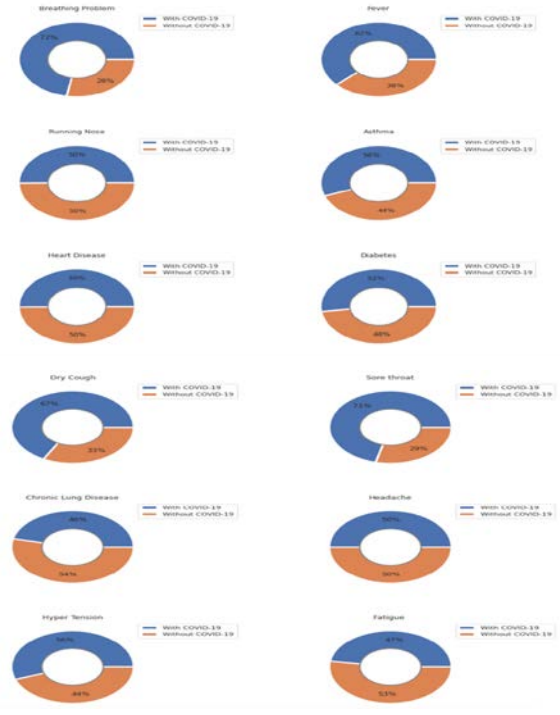

Fig 18: Doughnut charts for local data.

Fig 17: Doughnut charts for global data.

of COVID-19 based on user input data offers a solution to this challenge. After a one-time registration, users answer a few questions about how they feel, and the input data is then fed into the DNN model, which provides a list of COVID-19 test laboratories based on their current location. With early detection of infected individuals and thorough contact

tracing, this system aims to reduce and mitigate the transmission of COVID-19, especially in rural communities with limited resources for testing. The system offers a practical solution to enhance the fight against the spread of COVID-19, particularly in resource-limited settings, and it highlights the critical role of technology in global public health

emergencies. After accurate examination and analysis of the software created it could be resolved that the software is an effective, practical, and consistent online COVID-19 testing software system. It is functioning appropriately and sufficiently fulfils the least prospects from the task. The innovative software is anticipated to assist the user concerning efficacy in the practice of the COVID-19 testing system. Therefore, this study has demonstrated that DNN is a perfect candidate to predict and classify any form of the pandemic in the near future.

RECOMMENDATION

To get the maximum benefits, the web-based COVID-19 testing software should be able to have the following features as well.

- If someone is found to be at a high risk of contracting COVID-19 infection, the web-based COVID-19 testing software should schedule them for physical tests.
- The web-based COVID-19 testing software should be able to book appointments and contact doctors directly or other paramedical staff.

REFERENCES

Absar N, Mamur B, Mahmud A, Talha B.E et al. (2022). Development of a computer-aided tool for detection of COVID-19 pneumonia from CXR images using machine learning algorithm, Journal of Radiation Research and Applied Sciences.

Ceci A, Muñoz-B.C, Tegge A, Brown K. et al. (2021). Development and implementation of a scalable and versatile test for COVID-19 diagnostics in rural communities, Cold Spring Harbor Laboratory.

Chen Y, Jiang G, Li Y, Tang Y, Xu Y, Ding S, Xin Y, Lu Y. (2020). A Survey on Artificial Intelligence in Chest Imaging of COVID-19, BIO Integration.en.wikipedia.org

Ekwe, S.O, Akinyemi, L.A, Oladejo, S.O, and Neco Ventura (2021) "Social-Aware Joint Uplink and Downlink Resource Allocation Scheme Using Genetic Algorithm" IEEE AFRICON

Ekwe, S.O, Oladejo, S.O, Akinyemi, L.A, and Neco Ventura (2020). A Socially-Inspired Efficient Resource Allocation for Future Wireless Network" IEEE 16th International Computer Engineering Conference (ICENCO)

Hassan H, Ren Z, Zhao H, Huang S, Li D, Xiang S, Kang Y, Chen S, Huang B. (2022). Review and classification of AI-enabled COVID-19 CT imaging models based on computer vision tasks', Computers in Biology and Medicine.

Hemdan E.E., Shouman M., and Karar M. (2020). COVIDX-Net: A Framework of Deep Learning Classifiers to Diagnose COVID-19 in X-Ray Images, *ArXiv*.

Kumar P. (2020). Forecasting the dynamics of the COVID-19 Pandemic in Top 15 Countries', ARIMA Model with Machine Learning Approach. medRxiv, p. 2020.03.30.20046227, Apr. 05,

Li M. (2020). Predicting the epidemic trend of COVID-19 in China and across the world using the machine learning approach, medRxiv; 03 (18) 2003-8117

Narin A, Kaya C, and Pamuk Z. (2021). Automatic detection of coronavirus disease (COVID-19) using X-ray images and deep convolutional neural networks, *Pattern Anal Applic*, Aug.; 24 (3) 1207–1220

Okigbo P.O. (2021). Nigeria must not forget its poor in the Covid-19 world, ORF. https://www.orfonline.org/expert-speak/nigeria-must-not-forget-its-poor-in-the-covid-19-world-64389/

Oladejo, S.O, Ekwe, S.O, and Akinyemi, L.A (2021). Multi-tier multi-tenant network slicing: A multi-domain games approach ITU Journal on Future and Evolving Technologies, Wireless Communication systems in beyond 5G era, pp. 57-82, vol. 2, Issue 6**,**

Oladejo, S.O, Ekwe, S.O, and Akinyemi, L.A (2021). Multi-Tier Multi-Domain Network Slicing: A Resource Allocation Perspective" IEEE AFRICON.

Peters D.J. (2020). Community Susceptibility and Resiliency to COVID-19 across the Rural-Urban Continuum in the United States, J Rural Health, Jun.; 36 (3) 446–456

Redie D.K, Sirko A.H.E, Demissie TM, Teferi SS et al. (2022). Diagnosis of COVID-19 using chest X-ray images based on modified DarkCovidNet model, Evolutionary Intelligence,

Sethy PK. and Behera S.K. (2020). Detection of Coronavirus Disease (COVID-19) Based on Deep Features, Mar.

Sharma N, Sharma R, Jindal N. (2021). Machine Learning and Deep Learning Applications-A Vision, Global Transitions Proceedings.

Shoewu, O.O., Akinyemi, L.A., Folorunso, C.O. (2019). An E-Health Solution Provider for Tuberculosis Patient in Rural Areas, The Fourteenth

(14th) Annual ***Research Conference*** and ***Fair*** of the University at the Jelili Adebisi Omotola Halls, ***UNILAG***, Akoka, on August 21 – 23.

Shoewu, O.O., Adebayo, S.O, Ayangbekun, J.O, Akinyemi, L.A (2021) Application of Deep Learning to Autonomous Robotic Car" International Journal of Computer Applications

Shoewu, O.O., Akinyemi, L.A., and Edozie, R. (2023) UAV Cellular Communication in 5G New Radio Wireless Standards" Under Processing for Publication by Springer

Sofra X. (2021). Vaccines' Safety and Effectiveness amid Covid-19 Mutations, *Health;* 13(03):283–298

Tawadrou A.S, Katsabani P.D. (2002). Prediction of surface blast patterns in limestone quarries using artificial neural networks, Fragblast, 2005Geoffrey EH. Training Products of Experts by Minimizing Contrastive Divergence, Neural Computation,

Yvonne M and Yap B. (2020). Coronavirus: Amid the global pandemic, lessons for Africa, *Brookings*, https://www.brookings.edu/blog/africa-in-focus/2020/03/20/coronavirus-amid-the-global-pandemic-lessons-for-africa/

Zheng C, Deng X, Fu Q, Zhou Q, Feng J, Ma H, Liu W, Wang X. (2020). Deep Learning-based Detection for COVID-19 from Chest CT using Weak Label, Cold Spring Harbor Laboratory.

Journal of Engineering, Emerging Technologies and Applied Sciences -– Volume 1 Issue 1, April 2023

Available at ***www.ndu.edu.ng/ journalofengineering***

RESEARCH ARTICLE OPEN ACCESS

Reinforcement of Cast Iron with the Ashes of Animal Bone for the Production of Engineering Components

Ajoko Tolumoye John*, Amula Emomotimi*

**Department of Mechanical Engineering, Faculty of Engineering,*
Niger Delta University, Wilberforce Island, Bayelsa State.
Email: tjajoko@ndu.edu.ng, amula.emmomotimi@ndu.edu.ng

----------**********----------

Abstract:

The durability of engineering components is the main focus and concern of a maintenance engineer. Therefore, the study of reinforcing cast iron (CI) with the ashes of animal bones to enhance the production of engineering components is innovative in the engineering industry. Thus, investigating the potentials of cow bone ash used as composite materials to improve the mechanical properties of CI in engine components construction is a lead way to techno-industrialization. Several methods such as heat treatment analysis of samples, corrosion test, investigation of material hardness, tensile stress, strain and the determination of modulus of elasticity of the sampled materials were carried out in this research. Established results obtained from practical examination showed appreciable improvement for material hardness and tensile stress. As percentage composition of CI to cow bone ash increases. However, the sampled specimens were found more corroded in sea water medium than the fresh water. The corresponding weight loss result of the specimens is from 33.77% – 5.44% for sea water and 7.28% – 3.62% for fresh water respectively over the test duration for the hybrid CI with cow bone ash. Other results are the rate of corrosion of the CI and cow bone hybrids where the sampled specimens in the sea water corrode faster than the fresh water. Conclusively, the carried out research is found to be feasible and it is recommended that the hybrid CI with cow bone ash be used for engine components construction to avoid unforeseen damages from engine block explosions, corrosion emission, etc.

Keywords — Bone ash, Cast iron, Corrosion, hardness test, heat treatment.

----------**********----------

I. INTRODUCTION

The use of CI for structural purposes, constructions and other vital engineering and technical applications cannot be over emphasized (Pankaj, 2017; Satnam, et al., 2019). The structure of CI is a composition of different metallic materials put together by the process of liquefaction. The end product from this process is the formation of CI. CI serves in different capacity in manufacturing and production industries. It is most often the raw material to the construction of engine components, such as cylinder heads, engine blocks, piston rings, flywheels, machine beds, brake drums, etc, (Attila et al., 2004; Salihu and Sulieman, 2018). Thus, the vital features of a CI in its numerous applications is subject to its good thermal conductivity, vibration damping ability and good machinability (Attila et al., 2004; Salihu and Sulieman, 2018; Mousa and Daniel, 2014). Cast irons are of various types but the most commonly used in engineering is the grey CI. Hence, the

selection criteria of a CI for engineering applications are based on good resistance, weight consideration, low cost, compressive strength, exhibition of fairly high temperature, high fluidity for easy shaping to complex form, etc (Salihu and Sulieman, 2018).

Inspite of these numerous advantageous factors surrounding CI, the said engineering material is seriously liable to corrosion in its application in sea-water and other medium (Ojo and Abimbola, 2019; Ojo et al., 2020). A scholarly report affirms that the cast iron mostly made of grey deforms and fracture, thus; corrodes and wear-off due to its weak nature in its molecular composition (Pankaj, 2017). Corrosion is a limiting factor militating high rate of organizational spending. It is the destructive degradation of CI and other engineering materials like metals and alloys. It can cause unplanned shutdown and jeopardize the technological progress of engineering equipment (Ojo and Abimbola, 2019). A reviewed study attest to this fact and confirmed the cost implication of engineering materials corrosion in the US as high as $300 billion per year. This could be reduced by the application of innovative technology from material scientists (Ojo and Abimbola, 2019).

Conversely, improving CI material optimization for the design production of engine components is the heart beat of this research paper. This needful act will tend to reduce unplanned downtime and maintainability but rather increase durability and availability of an engineering equipment. Hence, the experimentation of hybridizing CI with animal ashes will reinforce CI against corrosion and other similar deteriorative elements. This is the pivotal aim of this paper. Thus, the hybridization of animal ashes with engineering materials is a new innovative technology in the engineering industry. Studies revealed that ashes of animal bones such as cow from abattoir wastes are used as alternative and replacement of lime and limestone dust to improve the engineering properties of asphaltic concrete mixtures in construction of flexible pavement roads (Modupe et al., 2019). Similarly, a revealed investigation attests that the ashes from cow bone have been proven as reinforcement agents in polyester for the development of polymer based composites for structural application (Temitope and Isiaka, 2015). No doubt, the trend of research is towards the production of automotive engine blocks with network polymers which comprises of vital mechanical properties with graphite fiber reinforcement (Namata, 2015).

Consequently, a deep research into studying CI hybrids and relative organic wastes such as the ashes of animal bones are imperative features for the development and improvement of corrosion resistance engine components. Therefore, the study is to bridge the gap of improving the tensile properties of the hybrid CI. This will allow it to operate at higher pressures, effective improvement in the combustion process to reduce the emission of pollutants.

II. EXPERIMENTATION

In order to achieve the goals of this research paper, a practical evaluation of CI and selected animal bone ashes were put together for experimentation as shown Figs 1 – 3.

Fig 1: Sample of Cast Iron

Fig 2: Ashes of cow bone

Fig 3: Ashes of goat bone

These selected specimens of animal bones were sourced from the Edepie cow slaughter in Yenagoa metropolis, Bayelsa State. The reason for the selection of the two bones is to make a close comparative analysis in terms of their chemical composition so as to choose the sample with richer chemical properties. Meanwhile, the animal bones were dry-oven and grinded in the Niger Delta University chemical engineering laboratory equipment as shown in Fig 4.

Fig 4: Boekel Chemical Dryer and Oven

Consequently, a tabular information in table 1 describes the bone chemistry of the selected animal bones and the cow bone is obviously selected due to its reported chemical composition.

Table 1: Chemical Composition Report of Animal Bone

Chemical Compound	Cow	Goat Bone
Calcium Oxide (%)	37	28.11
Phosphorus	18.03	16.71
Water Content (%)	1.71	1.79
Melting Point Temperature (^{0}C)	350	330
Density (g/cm^3)	2.16	2.23
Sodium (%)	3.5	-
Sulphur (%)	1.78	-
Potassium (%)	3.29	0.44
Magnesium (%)	-	0.58

III. HEAT TREATMENT

The selected specimens were subjected to heat treatment process to test for the corresponding thermal characteristics to ascertain its acceptability. They were introduced to the furnace to determine the material melting temperatures; meanwhile, their weights were measured before and after the experiment. This is carried out with the samples placed in a 33.56g crucible plate inserted into the furnace as shown in Fig 5. The crucible plate allows the specimens to liquefy inside it at their respective melting temperatures. After liquefaction, the materials in the crucible plate are brought out for measurement to determine their weight differences with an electronic compact scale shown in Fig 6.

Fig 5: Specimens inside Heat Treatment Furnace

Fig 6: Electronic Compact Scale

The process continued with the combination of CI and the ashes of cow bone by percentage ratio as shown in table 2.

Table 2: Order of CI /Ashes of Cow Bone Experiment

Materials	Percentage Composition (%)	
	CI	Bone Ash
CI /Bone Ash	99	1
CI /Bone Ash	98	2
CI /Bone Ash	97	3
CI /Bone Ash	96	4
CI /Bone Ash	95	5
CI /Bone Ash	90	10
CI /Bone Ash	85	15
CI /Bone Ash	80	20
CI /Bone Ash	75	25
CI /Bone Ash	70	30

IV. DETERMINATION OF CORROSION RATE

The test specimens in this research work was subjected to corrosion examination where materials are meant to undergo a total immersion test analysis. This test is carried out due to its effectiveness in evaluating metals corrosion. Conversely, a MH – Series Pocket Scale equipment shown in Fig 7 was used for specimens measurement before and after immersion test analysis in sea and fresh water medium respectively.

Fig 7: MH – Series Pocket Scale

Thus, the measurement of the specimens was all based on weight loss, density, area and the exposure time of the corresponding corrosion rate which is calculated using the governing equations in equations 1 and 2. Meanwhile, the corrosion test bed for the experimentation is shown in Fig 8.

$$R_{corr.} = 87.6 \times 10^4 \left[\frac{W}{DAT}\right] \quad 1$$

$$\%\, weight\ loss = \frac{W_o - W_f}{W_o} \times 100\% \quad 2$$

Where,

R_{corr} = Corrosion rate
D = Density
A = Cross Sectional Area
T = Exposure Time
W_o = Original weight of specimens before corrosion test
W_f = Final weight of specimens after corrosion test

Fig 8: Corrosion Test Bed

V. HARDNESS TEST

The hardness of a material is the resistance to penetrate through an object. This property of a material is to resist indentation and wear. Thus, the objective of this test is to identify the level of resistance of the test samples used in the experimental process. Therefore, in order to achieve this purpose, Universal Testing Machine as shown in Fig 9 is used in carrying out the prescribed experiment with the aid of Vernier calliper in Fig 10 for smaller measurement of distance. The practical procedure carried out according to the Brinell hardness test process. In this test method, a

ball made of hardness steel is used as test body. The ball is pressed onto the sample with a defined test force which depends on the diameter of the ball and test material, where measurement of the impression of the ball is taken. The hardness of the material according to Brinell is calculated from the test force, F and the surface diameter, D of the ball with the impression diameter, d caused by the impression of the ball on the material as shown in the hardness governing expression in equation 3.

Fig 9: Universal Testing Machine

Fig 10: Vernier Calliper

$$Material\ Hardness = \frac{0.102F}{0.5\pi D\ (D-\sqrt{D^2-d^2})} \quad 3$$

VI. RESULTS PRESENTATION AND DISCUSSION

Presented in table 3 is heat treatment result for the CI and the ashes of the cow bone with corresponding melting temperatures of 1204℃ and 350℃ respectively. Thus, this result enables the evaluation of the percentage composition ratio of the specimens at the appropriate temperatures for complete liquefaction of samples.

Table 3: Heat Treatment Results

Materials	Melting Point Temperature (^{0}C)	Mass of Specimens (g)		Weight Difference (g)
		Weight before Heating	Weight after Heating	
Cast Iron	1204	47.71	31.24	16.47
Ashes of Cow Bone	350	25	13.42	11.58

Subsequently, table 4 presents heat analysis results of CI in combination with the cow bone ash in varying percentage ratios.

The weight percentage composition results in terms of ratio of CI to the bone ash before and after the heat treatment is shown in Figs 11. The two curve plots demonstrate linearity as the ratio progresses. The result interprets the acceptability of bone ash as reinforcement to CI which will eventually enhance the production of engine component.

Table 4: Percentage Composition of CI /Cow Bone Ash at Melting Temperature of 1204^{0}C

Percentage Composition (w%)		Mass of Specimens (g)		Weight Difference (g)
CI	Cow Bone Ash	Weight before Heating	Weight after Heating	
99	1	10	9.89	0.11
98	2	9.1	8.49	0.61
97	3	9.2	9.33	-0.13
96	4	12.64	12.96	-0.32
95	5	13.39	13.58	-0.19
90	10	16.64	16.65	-0.01
85	15	19.41	19.45	-0.04
80	20	20.87	21.43	-0.56
75	25	21.5	22	-0.5
70	30	10.28	10.48	-1.2

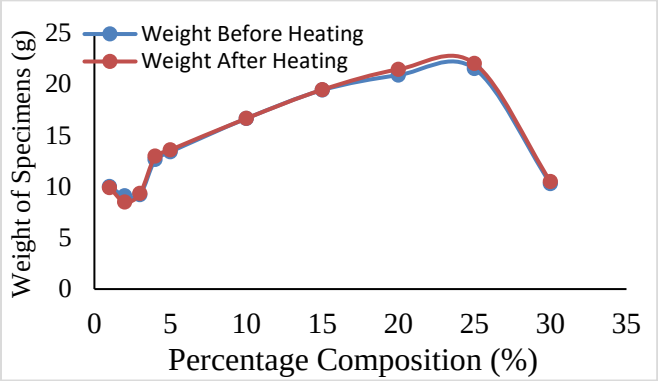

Fig 11: Graph Plot of Percentage Composition

Similarly, graphical plots of corrosion rate analysis of the specimens in the fresh and sea water testing medium are presented in Figs 12 – 15.

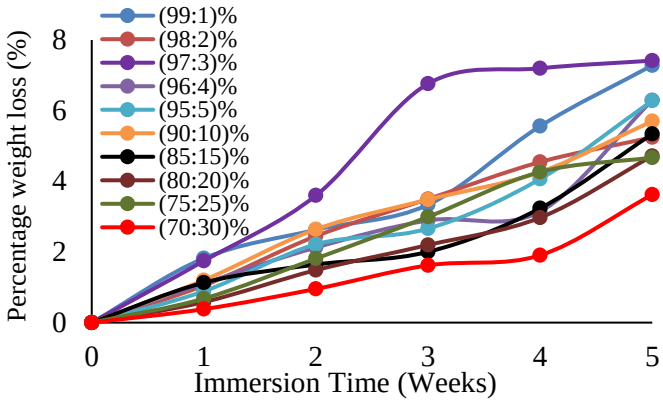

Fig 12: Weight Percentage of CI /Bone Ash in Fresh Water

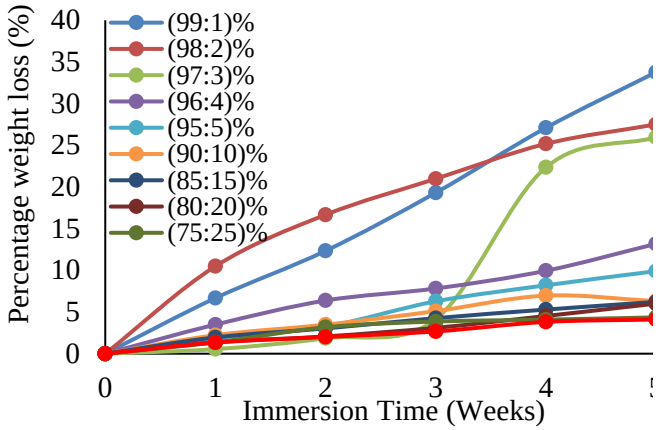

Fig 13: Weight Percentage of CI /Bone Ash in sea Water

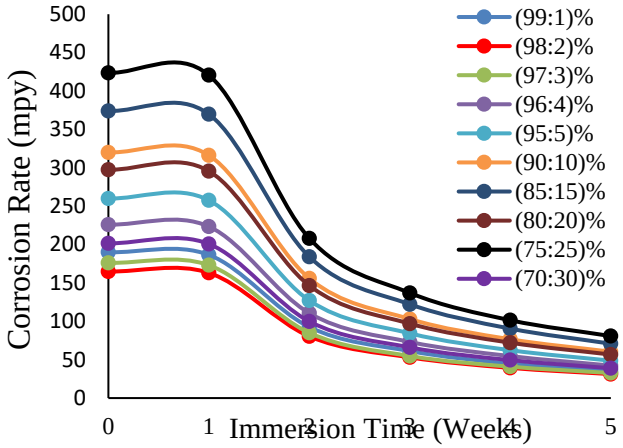

Fig 14: Corrosion Rate Analysis of CI /Bone Ash in Fresh Water

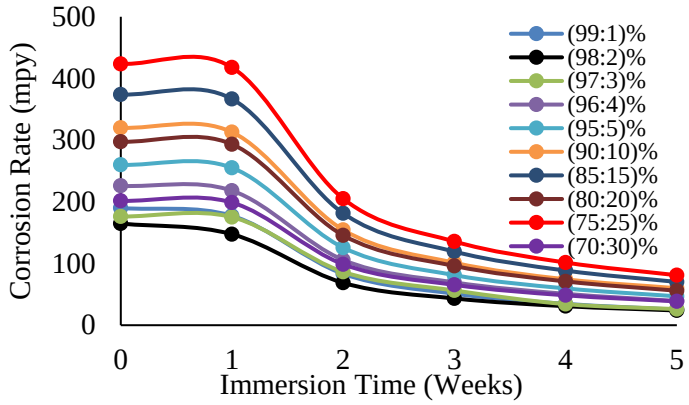

Fig 15: Corrosion Rate Analysis of CI /Bone Ash in Sea Water

The graphical results of corrosion rate analysis and percentage weight loss against time of immersion of the sample in the testing medium describes the thermodynamic capacity of specimens in engineering applications. It is observed that the weight loss in percentage in seawater for the specimens is higher than the fresh water medium under the same ratio consideration of the cast iron to bone ash combination. Results show specimens weight loss of 33.77%, 27.51%, 25.95%, 13.18%, 9.90%, 6.30%, 6.21%, 6.01%, 5.44% and 6.29% at sea water and a corresponding trend for fresh water as 7.28%, 5.24%, 7.42%, 6.29%, 6.28%, 5.7%, 5.34%, 4.72%, 4.67% and 3.62% as presented in Fig 12 and 13 respectively.

Similarly, results attest that sampled specimens corrodes more in sea water than fresh water. Thus,

in a summarised result for corrosion rate for sea and fresh water is 25.16mpy against 35.23mpy at a ratio of 99% of CI to 1% of bone ash composition. Conversely, in a progressive ratios of (98:2)%, (97:3)%, (94:6)%, (95:5)%, (90:10)%, (85:15)%, (80:20)%, (75:25)% and (70:30)% of CI to bone ash composition; corresponding results for sea water are 23.90mpy, 26.09mpy, 39.23mpy, 46.83mpy, 59.97mpy, 70.15mpy, 55.90mpy, 80.10mpy and 37.77mpy. Similarly, for fresh water the corrosion rate obtained are 31.24mpy, 32.62mpy, 42.34mpy, 48.72mpy, 60.36mpy, 70.81mpy, 56.67mpy, 80.76mpy and 38.84mpy respectively. However, the increase in percentage composition of the bone ash on the CI reduces the corrosion rate.

The hardness and tensile test results of the materials under study are presented in table 5 with the aid of the governing equation as shown in equation 3. The presented test results for the material hardness and tensile test analysis affirms to the review literature. Consequently, percentage composition of the cow bone ash to the CI test analysis reveals that the bone ash is identified as a reinforcement agent and it is capable of improving the mechanical properties of the ordinary CI in terms of its stress – strain characteristics.

Table 5: Universal Tensile Test Results

Cast Iron/ Bone Ash Composition	Applied Force (N)	Material Stress Analysis			
		Tensile Stress (σ) MPa	Strain (ε) δl/L	Ductility (%)	Modulus of Elasticity (*E*) Mpa
99:1%	9550	143.603	0.978	2.222	146.794
98:2%	9710	146.966	0.96	4.205	153.145
97:3%	9965	151.485	0.902	10.909	168.011
96:4%	10280	156.959	0.893	12.025	175.833
95:5%	10310	158.109	0.889	12.469	177.824
90:10%	10550	162.503	0.886	12.919	183.497
85:15%	10750	167.05	0.885	12.984	188.739
80:20%	10890	170.353	0.87	14.904	195.743
75:25%	11150	175.196	0.861	16.129	203.454
70:30%	11325	177.946	0.856	16.883	207.989

It is affirmed from the tabular results as shown that as the applied force increases down the percentage composition ratio of the CI /bone ash, the tensile stress, strain and the modulus of elasticity both increases with a rise in percentage ductility. The ductile characteristic feature confirms that the added load up to 11.325KN to the testing specimens will not fracture the material even as high as 16.883% which is a corresponding percentage composition of (70:30)% of CI to bone ash. Another affirmed factor is the young modulus of elasticity which is a numerical value of tensile stress that is applied to a metallic material that will increase its length as the material remains perfectly elastic throughout such an excessive strain. Thus, the young modulus of elasticity is defined within a range of values for CI as (100 – 160)MPa (Khurmi, 2004). However, the test result for the CI /bone ash confirms this value for the modulus of elasticity to be (146.794 – 207.989)MPa within the defined percentage composition. Perhaps, these set of results seems to improve due to the reinforce CI with the bone ash. Similarly, it is observed that the fracture diameter gradually reduce as the percentage composition increase to (70:30)% of CI to bone ash.

Finally, the obtained results from the practical section confirms some level of improvement of the CI as cow bone ash is combined with it to serve as reinforcement substance. It confirms some level of enhancement in terms of hardness, corrosion resistance, improved modulus of elasticity, tensile stress, ductility, etc. Therefore, the reinforced CI with good percentage of animal bone ash will stand the test of time to be used for the design and construction of engine components in the engineering industry.

VII. VALIDATION OF RESULTS

The research work carried out could be validated using Ojo et al (2020) to improve the structural properties of CI in order withstand engineering material stresses. Also to enhance the production of engineering components and ensuring their durability.

VIII. CONCLUSION

The study of reinforcing CI with ashes of animal bone for effective production of engineering materials will resist some amount of regular engine components degradations. Therefore, it is evidently obvious to conclude that:

- The combination of CI with ashes of animal bone is a good hybrid for the production of machine parts and components.
- The hybrid is also confirmed as a good corrosion resistance mostly in salty medium like the sea water.
- Study also affirms the use of animal waste such as animal bone as substitute to improve the desired properties of metallic materials for engine components construction.
- This also creates waste conversion, thus promoting synergy in an abattoir wastes not only as a replacement to lime and limestone to improve the engineering properties of asphaltic concrete mixtures in road construction industries as stated in the literature (Modupe et al., 2019); but also as means to improve metallic properties.

IX. RECOMMENDATIONS

The result findings from this research will proffer solution to future failure and deterioration of CI used for the production of engine parts.

REFERENCES

Attila, D.; Vasilios, F. and Ingvar, L.S. (2004). Microstructure and Tensile Properties of Grey Cast Iron, Research Report: School of Engineering, Jonkoping University, Sweden. ISSN:1404 – 0018.

Khurmi, R. S. (2004). Strength of Materials (Machanics of Solids). S. Chand and Company LTD, Ram-Nagar, New Delhi, India.

Ojo, S. I. F. and Abimbola, P. I. P. (2019). Corrosion propagation challenges of mild steel in industrial operations and response to problem definition. *International Conference on Engineering for Sustainable World - Journal of Physics*, 1378(2019). https://doi.org/10.1088/1742-6596/1378/2/022006.

Ojo, S. I. F., Adedamola, S., Itopa, G. A., Abimbola, P. I. P. and Oluranti, A. (2020). Improving the structural properties and corrosion behaviour of electroless deposited Ni–P–Zn coatings on mild steel for advanced processes. *AIMS Materials Science*, 7(4), 441–452. https://doi.org/10.3934/matersci.2020.4.441.

Modupe, A.E.; Olayanju, T.M.A.; Atoyebi, O.D.; Aladegboye, S.J.; Awolusi, T.F.; Busari, A.A.; Aderemi, P.O. Modupe, O.C. (2019). Performance evaluation of hot mix asphaltic concrete incorporating cow bone ash (CBA) as partial replacement for filler, *IOP Conf. Ser.: Mater. Sci. Eng.* 640, 012082. https://doi.org/10.1088/1757-899X/640/1/012082.

Mousa, J. and Daniel, L. (2014). Application of cast Al–Si alloys in internal combustion engine components, *International Materials Reviews*, 59(3),132-158. https://doi.org/10.1179/1743280413Y.0000000027

Pankaj, A. (2017). Engineering Materials and Additive Processes Used in Automotive Engine Blocks. *International Journal of Advances in Scientific Research and Engineering (IJASRE)*, 3(4), 151-161.

Salihu, S. A. and Sulieman, Y. I. (2018). Effects of Mould Additives on Hardness Property of Grey Cast Iron, *International Journal of Scientific Research in Mechanical and Materials Engineering*, 2(5), 72-78.

Satnam, S., Praveen, S., Dheeraj, G., Vivek, J., Rohit, K. and Sarbjeet, K. (2019). Development and characterization of microwave processed cast iron joint. *Engineering Science and Technology, an International Journal*, 22, 569–577. https://doi.org/10.1016/j.jestch.2018.10.012.

Temitope, A. and Isiaka, O. (2015). Effect of Cow Bone Ash Particle Size Distribution on the Mechanical Properties of Cow Bone Ash-Reinforced Polyester Composites, *Chemistry and Materials Research*, 7(3), 40-46.

Namata, S. (2015). Using Polymers as the Main Material in Engine Blocks and Components. *Journal of Applied Mechanical Engineering* , 4(5), 1-4. https://doi.org/10.4172/2168-9873.1000182.

Journal of Engineering, Emerging Technologies and Applied Sciences -– Volume 1 Issue 1, April 2023

Available at ***www.ndu.edu.ng/ journalofengineering***

RESEARCH ARTICLE OPEN ACCESS

Synthesis and characterization of Zinc oxide nanoparticles-polyvinyl alcohol-polyethylene glycol nanofluids (ZNO-Nps-PVA-PEG-NF)

Orlando Ketebu
Department of Chemical Engineering, Niger Delta University, Wilberforce Island, Bayelsa State
Email: ketebu.orlando@ndu.edu.ng

----------**********----------

Abstract

Water and oil are known conventional fluids used in heat transfer processes due to their availability at low cost. The limited heat transfer potentialities of these conventional fluids in the industries for heat and mass transfer equipment such as heat exchangers, air coolers and chemical unit processes, has been a major challenge over the years. This is due to the poor thermal conductivity of these conventional fluids. Nanofluid offers a promising future for such industries because they give better performance than conventional fluids due to the presence of suspended nanoparticle which has high thermal conductivity. Nanofluid is a fluid containing particles in nanometer range called nanoparticles. This research work looks at the synthesis and characterization of Zinc oxide nanoparticles polyvinyl alcohol/polyethylene glycol nanofluids (ZnO-Nps-PVA-PEG-NF). The results from the experiment showed that ZnO Nps with hexagonal wurtzite structure and average size 15 nm was formed using X-ray Diffraction (XRD) analysis to determine the sample crystalline structure and sizes. Scanning electron microscopy (SEM) image used to determine the morphology of the prepared ZnO Nps-PVA-PEG NF showed a well dispersed ZnO Nps in PVA-PEG base fluid. The ZnO Nps-PVA-PEG NF also showed stability for up to two weeks before aggregation and the PVA-PEG composite base fluid also acted as a stabilizing agent for the ZnO Nps in ZnO Nps-PVA-PEG NF. These findings make ZnO Nps-PVA-PEG NF a possible replacement for conventional fluids with its unique properties.

Keywords — Zinc oxide nanopaticles, Polyvinyl alcohol, Polyethylene glycol, Nanofluid, X-ray diffraction, Scanning electron microscopy

----------**********----------

I. INTRODUCTION

Fluids for heat and mass transfer equipment such as heat exchanger, air coolers, towers and chemical unit processes has been a major challenge over the years. Conventional fluid such as water, oils and ethylene glycol are often used as heat transfer fluids due to their availability at low cost. But these fluids are known to have poor thermal conductivity which limits their heat transfer potentials, and this drawback impedes their effectiveness in heat exchangers and other heat and mass transfer equipment (Czaplicka, et al., 2021, Okonkwo, et al., 2021). This has made researchers to look for alternative fluids to these conventional fluids that are effective, cheap with good thermal conductivities. One of such fluids is nanofluids. Nanofluid offers a promising future for industries making use of heat and mass transfer equipment, because they give better performance than

conventional fluid due to the presence of suspended nanoparticle which has high thermal conductivity.

Nanofluids are colloidal suspension of nanometer-sized particles also known as nanoparticles in a base fluid (Samir and Mandal, 2015). Nanoparticles such as metal nanoparticles, carbon base nanoparticles, metal oxide nanoparticles are used in the formation of nanofluid. These nanoparticles have their individual unique properties that contribute effectively to the thermal conductivities of heat and mass transfer operation, fuel cell design, microelectronics and pharmaceutical processes etc. (Das et al., 2007). Nanofluids are known to have enhanced thermal conductivity with effective heat transfer coefficient (convective heat transfer) when compared to their base fluid (Kakac et al., 2009, John et al, 2022). Nanofluids can be a single phase or two phase fluid depending on the components involved in the synthesis. It is a single phase fluid when the physical properties of the nanofluid is due to its constituents and concentrations, or a two phase fluids when two component are involve in its synthesis (Lu et al., 2013). Nanofluids can be synthesized through a one-step method or two step method. The one step method concurrently disperses the nanoparticles in the base fluid and is often used in synthesizing of metal nanoparticles nanofluids. The two step method involves agitating the nanoparticles in the base fluid with an agitator to homogenize the nanoparticles in the base fluid forming nanofluid and is suitable for large scale nanofluid production.

There are different techniques for synthesizing nanofluids such chemical precipitation, direct evaporation, chemical vapour condensation, gas condensation /dispersion, and bio-base methods. This work focuses on the synthesis and characterization of nanofluids using polyvinyl alcohol (PVA), polyethylene glycol (PEG) mixture as base fluid and zinc oxide nanoparticles (ZnO Nps) as nanoparticles source.

PVA is non-hazardous water soluble synthetic polymer made up of vinyl alcohol unit connected together in a repeating pattern (Rigved and Jatin, 2019). PVA can be fully or partially hydrolyzed depending on the amount of vinyl acetate replaced by hydroxyl group in the ester group. PVA is used in the manufacture of adhesives, medical and biomedical applications, food processing, coating industries, films and elastomers, biopolymer etc.

PEG is also a synthetic water soluble polymer synthesized when ethylene oxide interacts with water. PEG has a wide range of applications such as in medical and biomedical processes, industrial and chemical processes and for commercial activities (Hoang Thi et al., 2020).

Zinc Oxide nanoparticle is a metal oxide nanoparticles with unique properties such as its semiconducting and piezo-electric properties, antifungal and antibacterial properties, photochemical and ultraviolet filtering properties (Sirelkhatim, et al., 2015). ZnO Nps can be synthesized using micro-emulsion, sol-gel, thermal evaporation, laser ablation and chemical vapour deposition techniques and these techniques also affects the nanoparticles sizes.

Researchers have synthesized ZnO Nps with polymers such as PEG, PEG-PVA nanocomposites (Irina et al, 2021, Nibiyouni et al., 2011, Liufu et al., 2004, Minea et al., 2022) but were interested in the synthesis route, for drug storage, monitoring the adsorption of PVA/PEG nanocomposites and heat transfer analysis of PEG 400 on ZnO Nps. Non looked at combining PVA-PEG with ZnO Nps to synthesize nanofluid that might be a good alternative for conventional fluids.

II. MATERIALS AND METHOD

The following chemicals and equipment were used to carry out the experiment.

The chemicals are; hydrolyzed PVA (98%), PEG-4000, Zinc acetate dehydrate, distilled water, Methanol, Potassium hydroxide, and the equipment are; Magnetic stirrer, Hot plate, Centrifuge, 100 milliliter Beakers, 100 milliliter volumetric flasks, Ultrasonicator, syringe, weighing balance, X-ray diffractommetry (XRD), and Scanning electron microscopy (SEM).

A. Synthesis of ZnO Nps

ZnO Nps were prepared following similar method adopted by Singh and co researchers (Singh et al, 2012). The procedure involves dissolving 294.1 mg of zinc acetate dihydrate in methanol (100 ml) to form 13.4 millimole of zinc acetate dihydrate mixture followed by drop wise addition of potassium hydroxide solution at 52^{o}C with constant agitation for two hours. The two hours is the time range for precipitation to occur and 52^{o}C is the temperature required for the solvothermal process. Potassium hydroxide solution was prepared by dissolving 162.5 mg of potassium hydroxide in 100 ml methanol to form 28.96 millimole of potassium hydroxide solution (100 ml). Precipitates of ZnO Nps were formed as the agitation continues at 52^{o}C when the solution turns turbid. The heating and agitation process was stopped and the precipitate allowed to cool at room temperature for two hours. The excess liquid was decanted and the precipitated ZnO Nps was washed with 50 milliliters of methanol twice and centrifuged to collect the nanoparticles. The ZnO Nps were dried at room and placed in an airtight container.

B. Synthesis of Polyvinyl alcohol-Polyethylene glycol- base fluid (PVA-PEG)

Three weight percent of PVA-PEG base fluid were synthesized by dissolving 2.55 grams of PEG and PVA in distilled water (80 milliliters) at 60^{o}C. The mixture were stirred continuously for complete dissolution and formation of homogeneous mixture. After complete dissolution, the mixture were left at room temperature to cool.

C. Formation of Polyvinyl alcohol-Polyethylene glycol-Zinc oxide Nanoparticles nanofluid (ZnO Nps PEG-PVA-NF)

Grounded powder of ZnO Nps (5 weight percent) were obtained by crushing the dried ZnO Nps. The ZnO Nps powder were then dispersed in 3 weight percent of PVA-PEG base fluid through ultrasonication. The dispersed solution were allowed to stand for 2 weeks to monitor its stability and aggregation. This in turn affects the size and shape of the nanoparticles as evaporation of the base fluid occurs.

D. Characterization of ZnO Nps -PVA- PEG-NF

The synthesized ZnO Nps PEG-PVA-NF were characterized with SEM to determine the nanoparticles and base fluid surface morphologies and XRD to determine the crystalline nature of ZnO Nps formed and the presence of PEG, PVA and ZnO Nps peaks at desired Bragg's angles.

III. RESULT AND DISCUSSION

Fig. 1a shows the synthesized ZnO Nps which is the whitish particles on the plate. Fig. 1b shows the prepared PVA-PEG base fluid. In Fig. 1b the base fluid is a transparent homogeneous mixture resulting from the combination of water soluble PVA and PEG.

Fig. 1 (a) shows the synthesized ZnO Nps (b) synthesized PVA-PEG base fluid

Fig. 2 Synthesized ZnO Nps-PVA-PEG nanofluid

Fig. 2 shows the synthesized ZnO Nps-PVA-PEG nanofluid. The ZnO Nps are homogenized in the base fluid through ultrasonication process. The ZnO Nps-PVA-PEG nanofluid remained stable for two week without aggregation of the ZnO Nps. This shows that the combination of PVA and PEG to form base fluid also acted as a stabilizing agent for the ZnO Nps preventing the nanoparticles from aggregating.

Fig. 3 shows the XRD image of the synthesized ZnO Nps-PVA-PEG nanofluid. The diffraction peaks (100), (002), (101), (102), (110), (103), and (201) located at 31.84◦, 34.52◦, 36.33◦, 47.63◦, 56.71◦, 62.96◦ and 69.18◦ respectively indicate that the ZnO Nps formed had hexagonal wurtzite phase of Zinc oxide based on JPCDS card number: 36-1451. The average nanoparticles size diameter (D) was approximately 15 nm applying Debye-Scherrer formula in equation 1.

$$D = \frac{0.89\lambda}{\beta \cos \theta} \qquad (1)$$

Where λ is X-ray wavelength, β is the full width at half-maximum (FWHM), 0.89 is Scherrer's constant, and θ is the Bragg diffraction angle.

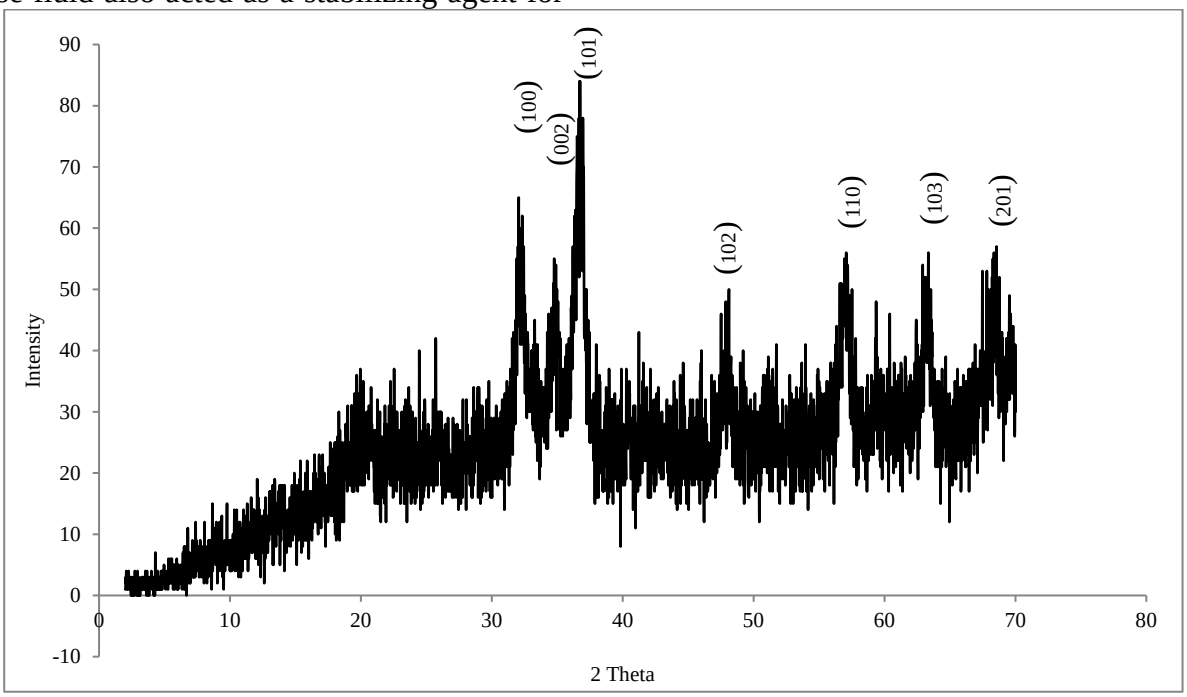

Fig. 3 XRD analysis of ZnO Nps-PVA-PEG-NF

Fig. 4 showed the XRD pattern for the synthesized ZnO Nps powder. The diffraction peaks 002, 102 and 110 indicate ZnO Nps was formed. The presence of diffraction peaks denoted as X, might be due to impurities during synthesis.

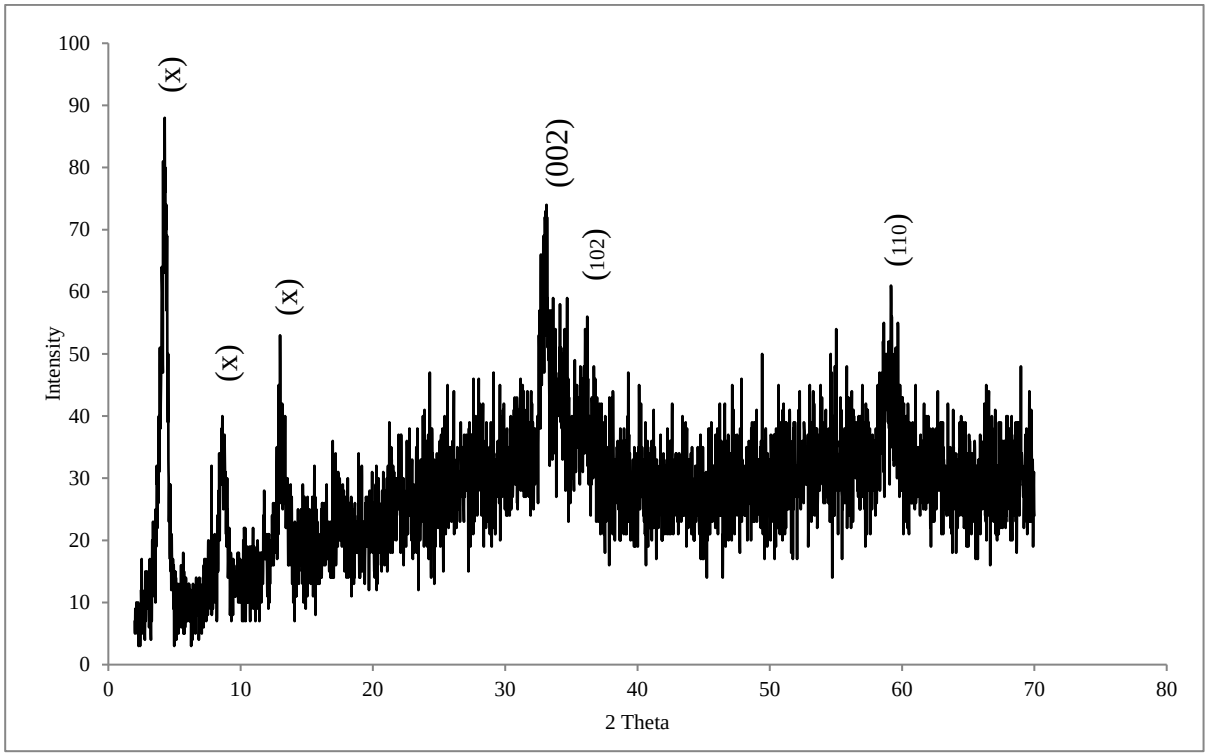

Fig. 4 XRD plot for ZnO Nps

Fig. 5 shows the SEM image of ZnO Nps-PVA-PEG nanocomposite nanofluid synthesized. The figure showed a well dispersed ZnO Nps in the PVA-PEG base fluid forming ZnO Nps-PVA-PEG nanocomposite nanofluid. This also indicates that the PVA-PEG composite base fluid also acts as a stabilizing agent for dispersing the ZnO Nps thus preventing aggregation of the particles.

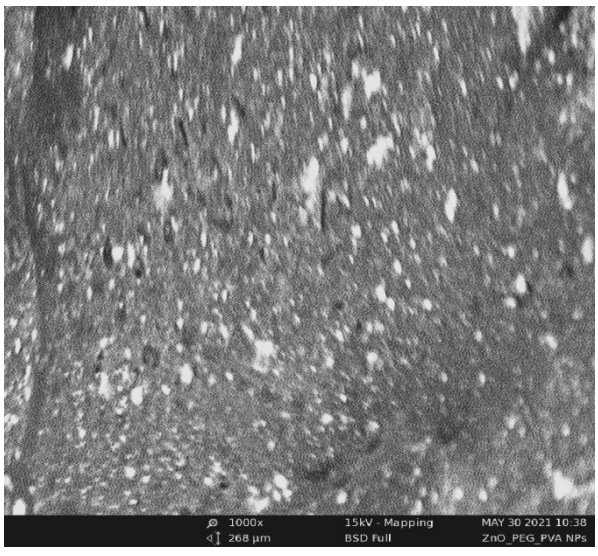

Fig. 5 SEM image of ZnO Nps-PVA-PEG-NF synthesized

Fig. 6 is the SEM image of the synthesized ZnO Nps. The figure shows aggregated ZnO Nps which is normal with nanoparticles as they aggregate over time. But the addition of PVA-PEG composite stabilized the ZnO Nps as shown in Fig. 5.

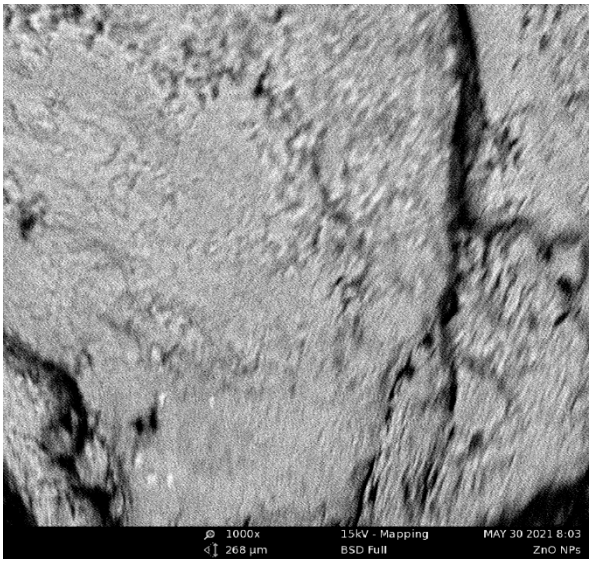

Fig. 6 SEM image of aggregated ZnO Nps without PVA-PEG composite

IV. CONCLUSION

In conclusion the results showed that Zinc oxide nanoparticles were successfully synthesized and ZnO Nps-PVA-PEG nanocomposite nanofluid were prepared with the Zinc oxide nanoparticles. The nanofluid showed stability for up to two weeks before aggregation and the PVA-PEG composite base fluid also acted as stabilizing agent for the ZnO Nps in ZnO Nps-PVA-PEG nanocomposite nanofluid. The average nanoparticles size of the ZnO Nps in ZnO Nps-PVA-PEG nanocomposite nanofluid was calculated to be 15nm using diffraction peaks 002, 100 and 102. The XRD analysis of the diffraction peaks showed that the synthesized ZnO Nps had hexagonal wurtzite phase of ZnO. The hexagonal wurtzite phase of ZnO is known for its unique properties including its thermal conductivity. The SEM image of ZnO Nps-PVA-PEG-NF showed well dispersed ZnO Nps in PVA-PEG base fluid. This also indicates that the unique properties of ZnO Nps including its thermal potentials are well distributed in the base fluid.

REFERENCES

Czaplicka , N., Grzegórska, A., Wajs, J., Sobczak, J., Rogala, A. (2021). Promising Nanoparticle-Based Heat Transfer Fluids-Environmental and Techno-Economic Analysis Compared to Conventional Fluids. *International Journal of Molecular Science,. 22*, (17), 9201.

Okonkwo, E.C., Wole-Osho, I., Almanassra, I.W. *et al.* (2021). An updated review of nanofluids in various heat transfer devices. *Journa of Thermal Analysis and Calorim*etry, *145*, 2817–2872

Samir, K. N., Rajib, K. M. (2015). MHD Stagnation-Point Flow and Heat Transfer of Nanofluid over a Shrinking Surface. *Journal of Nanoscience and Nanoengineering*, *1* (4), 183-192

Das, S.K., Choi, S.U.S., Yu, W., Pradeep, T. (2007). Nanofluids: science and technology. *Wiley-Interscience*, 397.

Kakac, S., Cao, L. (2009). Analysis of convective two-phase flow instabilities in vertical and horizontal in-tube boiling systems. *International Journal of Heat and Mass Transfer*, *52*, 3984–3993

Joshua, B., Michael, P., Kallie ,I., Jake, W., Marcus, C., Ryan, F., Branden ,S., Saeid, V. (2022). Heat Transfer Enhancement in the Microscale: Optimization of Fluid Flow. *nanomaterials,12*, 3628

Lu, G.; Hu, H.; Duan, Y.; Sun, Y. (2013). Wetting kinetic of water nano-droplet containing non-surfactant nanoparticles: A molecular dynamic study. *Applied Phyics Lett*er, *103* (25): 253104

Rigved, N., Jatin, Patel. (2019). Polyvinyl Alcohol: A Comprehensive Study. *Acta Scientific Pharmaceutical Sciences*, *3*, (4), 34 - 44

Hoang Thi, T.T., Pilkington, E.H., Nguyen, D.H., Lee, J.S., Park, K.D., Truong, N.P. (2020). The Importance of Poly(ethylene glycol) Alternatives for Overcoming PEG Immunogenicity in Drug Delivery and Bioconjugation. *Polymers (Basel).* *12*, (2), 298. doi: 10.3390/polym12020298. PMID: 32024289; PMCID: PMC7077443.

Sirelkhatim, A., Mahmud, S., Seeni, A., Kaus, N.H.M., Ann, L.C., Bakhori, S.K.M., Hasan, H., Mohamad,

D. (2015). Review on Zinc Oxide Nanoparticles: Antibacterial Activity and Toxicity Mechanism. *Nano-micro Letters. 7*, (3), 219-242.

Irina ,M.F., Júlia, M. A., Paulo, H. C., Derval S. R., Bruna A. L., Marcelo B., Emerson, R. D., Juliana, S. S. (2021). ZnO Nanoparticle/Poly(vinyl alcohol) Nanocomposites via Microwave-Assisted Sol–Gel Synthesis for Structural Materials, UV Shielding, and Antimicrobial Activity *ACS Applied Nano Materials* **,** *4* (7), 7371-7383

Nabiyouni, G., Barati, A., Saadat, M. (2011). Surface Adsorption of Polyethylene Glycol and Polyvinyl Alcohol with Variable Molecular Weights on Zinc Oxide Nanoparticles. *Iranian Journal of Chemical Engineering. 8*.

Shengcong, L., Hanning, X.., Yuping, L. (2004). Investigation of PEG adsorption on the surface of zinc oxide nanoparticles, *Powder Technology*, *145*, (1), 20-24

Minea, A.A.; El-Maghlany, W.M.; Massoud, E.Z. (2022) Heat Transfer Analysis of Nanocolloids Based on Zinc Oxide Nanoparticles Dispersed in PEG 400. *Nanomaterials*, *12*, 2344

Singh, D.K., Pandey, D.K., Yadav, R.R. (2012). A study of nanosized zinc oxide and its nanofluid. *Pramana Journal of Physics*, *78*, 759–766, https://doi.org/10.1007/s12043-012-0275-8

Journal of Engineering, Emerging Technologies and Applied Sciences -– Volume 1 Issue 1, April 2023

Available at ***www.ndu.edu.ng/ journalofengineering***

RESEARCH ARTICLE OPEN ACCESS

Production of Perfume and Determination of the Physiochemical Features from Locally Available Lemongrass Leaves Extract

Sakwe Adianimovie and Uku Eruni Philip

Department of Chemical Engineering, Federal University Otuoke, Bayelsa State, Nigeria

Corresponding Author: sakwea@fuotuoke.edu.ng

----------**********----------

Abstract

The main purpose of this work is to extract essential oil from locally and readily available Lemongrass as natural plants for the formulation of perfume as opposed to synthetic chemicals, with the end goal of eliminating the negative consequences that are associated with the usage of synthetic chemicals. Plants with no established edible use are considered waste in most parts of Nigeria, especially those considered as wild. However lemongrass (Cymbopogon citratus) leaves containing essential oils, can be used for the production of perfumes that can mask body odours and living homes. Lemongrass essential oil obtained through Soxhlet Extraction was used to formulate perfume using n-Hexane as Solvent media. At 65°C and 150 minutes, the oil yields obtained during extractions were 1.55%, 1.67%, 1.710%, %, 1.73% and 1.80%, respectively. The physicochemical properties of the formulations revealed that the essential oil has a saponification value of 21.04mgKOH/g. And at the same temperature, the density of the lemongrass oil was 0.8865gcm3 at a boiling point of 224℃. The essential oil was used successfully for the formulation and production of perfume resulted at 15% to 20% strength with Sandalwood as the top note, Lemongrass as the middle note and Lavender as the base note.

Keywords: Essential oil, Solvent Extraction, Perfume, Fragrance, Physiochemical Parameters, Lemongrass, Formulation, Solvents, Techniques, Yield, Notes, Perfume Concentration

----------**********----------

I. INTRODUCTION

In recent years, there has been a rise in researches being conducted on a diverse assortment of plants all over the world for the use in the production of food, pharmaceuticals cosmetics, and others. Often, the production of synthetic chemicals is one example of an industrial activity that contributes to pollution and other environmental problems due to its direct negative impacts on the natural world; therefore, there is a global move towards the use of raw material sources that are less harmful to the environment in a variety of manufacturing processes.

In an effort to reduce reliance on essence derived from synthetic sources and to save money that would otherwise be spent on the purchase of essential oils for the production of high-end perfumes, a novel search has been initiated for underutilized plants that can serve as sources of essential oils. The use of locally available lemongrass (Cymbopogon citratus) for the production of essential oil and perfume formulation is of very essence, as people have utilized a variety of methods, including the application of perfumes and other aromatic materials for the benefits of scent (www.worldhistory.org 2021), in order to mask or accentuate the fragrance of their bodies Oloyede (2009). Perfume refreshes the air and its fragrance like flowers around living environment is made up of three different notes, which are the base note, middle note and the top note, which these distinctive components blend to form an

harmonious scent that complements one another (Newton, 2020; Aftel, 2001; Groom, 2012). The essential oil from lemongrass leaves is also widely used in perfumes, cosmetics, medicines, germicides and insecticides (Agbafor and Akubugwo, 2007; Kotzekidou et al., 2008, Mahanta, et al., 2007), which therefore serve as a consumable plant by the general population Ekpenyong (2017).

In Nigeria, there exists a wide array of plants ranging from the largely known and highly utilized to the underutilized plants for which in-depth studies have not being done on their potential uses (Ugbogu et al., 2014). Locally, the lemongrass (Cymbopogon citratus) plant is known as "Eti" by the Edo's, "Ikon eti" by the Efik's, "Tsauri" by the Hausa's, "Myoyaka makara" by the Ibibio's, "Achara ehi" by the Igbo's, and "Kooko oba" by the Yoruba's and Ikpoo Okom by the Epie-Atissa's (Ijaw). Essential oils are made from various parts of plants, such as stems, leaves, roots, flowers (Hesham, Rassem et al., 2016), and at such lemongrass which is locally and readily available is harvested four times per annum and have a lifespan of four to eight years (www.nhb.gov.in, 2014).

There are numerous techniques such as solvent extraction, hydro-distillation, enfleurage, microwave aided hydro-distillation, superficial Carbon dioxide extraction, cold pressing, and soxhlet extraction that can be utilized in the distillation of essential oils and the formulation of perfumes. However, the three most popular techniques are solvent extraction (Suryawanshi et al., 2016), hydro-distillation Hydro-distillation (Jigisha K. Parish et al., 2011), effleurage extraction (Hunter, M. (2010); Manniche, L. (1999). But, solvent extraction is one extraction technique used to obtain the extract which increases oil output and regulate the oil's composition. It could also be applied to fragile plants in order to achieve a better yield of essential oil with a smaller amount of harvesting (Chrissie et al., 1996), and at a low temperature it could achieve a higher yield of extract while suffering a lower loss of heat-sensitive bioactive components (Suryawanshi et al., 2016). This is a preferred method that exceeds the optimal temperature and will trigger the enzymatic and chemical breakdown of the polyphenolic components (Akowuah and Zhari, 2010). This proves that extract of essential oil from locally and available Lemon grass as natural plants for the formulation of perfume as opposed to synthetic chemicals is achievable, which also determine the extent of oil yield as well as the physiochemical parameters of the extracted oil from dried lemongrass.

Furthermore, numerous in-depth analyses have been carried out in order to evaluate the quality of lemongrass powder that was made using a variety of drying techniques, including drying in the sun, drying in the shade, drying in the oven, drying in the microwave, and drying in the freezer (Hanaa et al., 2012). The extraction procedures and the type of solvent used have a large influence on the quality and quantity of essential oil produced. The results obtained in the extraction of oil using n-Hexane as solvent are stated in table 4.3a and 4.2b. After extraction was completed, a simple distillation was set-up and used to separate the solvent from the oil at 60^{o}C until complete separation was achieved. The solvent reduces over time, leaving the essential oil. The resulting oil was pale yellow-green in color, with an aromatic odour. Because of its high volatility, it has a cooling taste. It was kept in an airtight container and kept out of direct sunlight. The essential oil was water-insoluble but soluble in alcohol and oil, in which case the locally and readily available Lemongrass for the production of essential oil and perfume formulation as a natural plant sources as opposed to synthetic chemicals was achievable, both in terms of oil yield as well as the physiochemical parameters. And the end goal of eliminating the negative consequences that are associated with the usage of synthetic chemicals was also tenable.

II. MATERIALS AND METHODS

A. *Experimental Materials*

Detailed descriptions of the materials used in this work are given in this section.

1. **Lemongrass (Cymbopogon citratus):** The fresh leaves of Lemongrass (Cymbopogon

citratus) leaves were collected from a local garden, sorted to remove unwanted plants, washed and dried in a shaded moisture free environment.

2. **Chemicals:** All chemicals used in this study are analytical grades and they include: n-Hexane, diethyl-ether and ethanol, potassium hydroxide (KOH), ethanoic potassium hydroxide, phenolphthalein, HCl and benzyl salicylate.
3. **Glassware:** Various sizes of Duran beakers, conical flasks, round-bottom flasks and decanters was used. Glassware utilized is the separation funnel, condenser, thermometer, pipette and burette.

B. ***Equipment***

The detailed descriptions of the equipment used in this work in this section.

1. **Digital Weighing Balance:** The weighing balance of Model No.FA2104 was used to determine the absolute weight of chemicals, oils and other substances used throughout this work.
2. **Heating Mantle:** Heating mantle was used for heating to temperature up to 100℃ and used to evaporate the excess n-Hexane left after the oil has being extracted.
3. **Viscometer:** A viscometer of Model NDJ-55 was used to determine the viscosity of the oil.
4. **Sieve Shaker:** A sieve shaker was used for the particle analysis of the dried and powdered lemongrass sample.
5. **Other materials required**: Other materials utilized are rubber stopper, ice cubes maker, knives, olive oil, aluminum foils, and Crusher (Mortar and Pestle).

.

III. DETERMINATION OF OIL YIELD

The yields of the oil was determined by taking the ratio of the weight of the extracted oil to the weight of the sample with respect to varying temperature and time.

$$\%\ oil\ yield\ (w/w) = \frac{Weight\ in\ gram\ of\ extracted\ oil}{Weight\ in\ gram\ of\ sample} \quad (1)$$

The yield obtained with varying temperature and time is shown in Table 1 and 2 respectively.

Table 1: Solvent extraction at varying temperature.

Weight of dried sample (g)	Temp (℃)	Weight of extracted oil (g)	Yield (%)
130	45	2.09	1.58
127.91	50	2.17	1.69
125.74	55	2.24	1.78
123.50	60	2.29	1.85
121.21	65	2.34	1.93

Table 2: Solvent Extraction at Varying Time.

Weight of dried sample (g)	Time (minutes)	Weight of extracted oil (g)	Yield (%)
130	30	2.11	1.62
127.89	60	2.18	1.68
125.74	90	2.26	1.73
123.45	120	2.29	1.76
121.16	150	2.36	1.82

IV. RESULTS AND DISCUSSIONS

The experiment was carried out to extract essential oil from lemongrass, which has high essential oil content and was used in the formulation of perfume. The lemongrass essential oil was successfully extracted from dry lemongrass leaves using solvent extraction (soxhlet extraction method). The essential oil was used successfully in perfume formulation by using fixatives and different solvents (alcohols) as ingredient as the type of solvent, quality of sample and type of equipment used are the factors that affected the yield in this research experiment. Changes in the quantity of solvent used also affected the yield hugely. Proper particle analysis of the dried

lemongrass sample ensured that the particles of the sample used in this experiment were of uniform sizes to prevent discrepancies in the results and reduce the time spent on the experiments. Fig. 1 shows the effect of varying temperature on the yield and it indicates that the yield increases with temperature, but never exceed 65^{o}C, with regards to related literature beyond destroying the extract. While the effect of varying time on the yield is shown in Fig. 2.

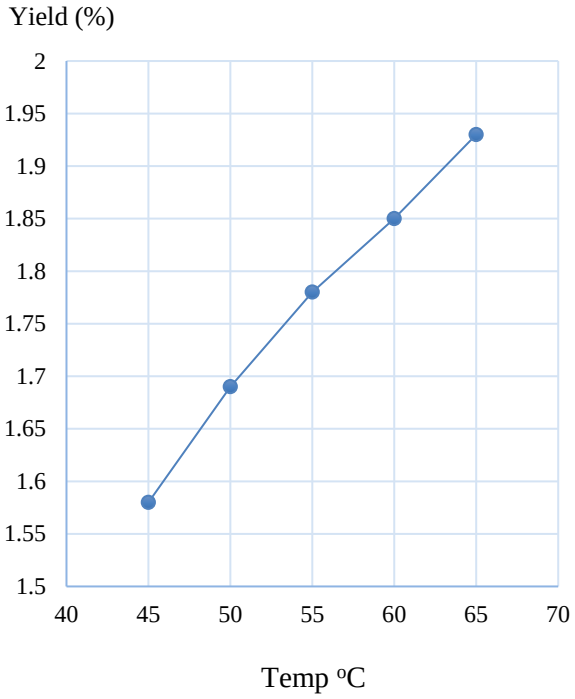

Fig. 1: Graph of yield against temperature

With respect to the Physiochemical analysis of the extracted lemongrass oil, Table 3 shows the evaluation of the physicochemical properties of the extract from the lemongrass such as moisture content, relative density, acid value, viscosity, saponification value and pH in accordance with the Association of Official Analytical Chemists (AOAC), specific gravity value by methods of Pearson (1976) and American Petroleum Institute (API) value (Haldar *et al*, 2009). It further shows that the liquid had a

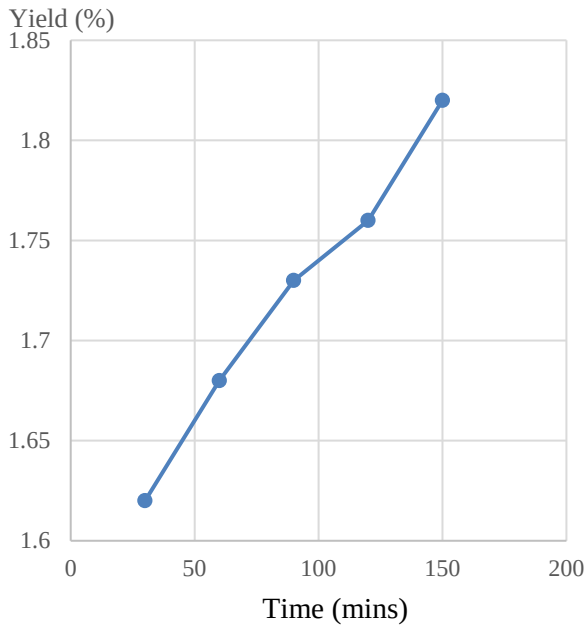

Fig. 2: Graph of yield against Time

density of less than one (ρ = 0.8865) at room temperature, indicating that the essential oil was lighter than water. Comparatively with Table 3, some physicochemical properties from lemongrass extract as determined by Atitegeb Abera 2020 gives the following result such as moisture content, percentage yield, pH, boiling temperature, acid value and saponification values are 20.7%, 6.27%, 5.6, 212^{o}C, 2.805 mg KOH/g, 140.25mg KOH/g respectively. Precisely, both results shows that the higher the acid value of oil, the lower storage quality and vice versa, though with varying saponification value, but was exactly 21.04 mg KOH/g as reported by Alhazan *et al*, 2018, which all values indicates that saponification value also has the potential to be an input for soap production The boiling temperatures was similar to the former at 212^{o}C, though higher than the later at 85^{o}C, though with varying yields percentage to both at 3.8% as shown Table 1.

In the same vain, on the particle analysis of the dried powdered lemongrass**,** Table 4 shows the sieving analysis performances carried out at the Chemical Engineering Department of the Federal University Otuoke (FOU).

Table 3: Physicochemical Properties of Lemongrass Oil

Physio-chemical properties	**Lemongrass oil (C. citratus essential oil)**
Acid Value	2.948 mg KOH/g
Saponification Value	21.04mgKOH/g
Specific Gravity	0.890 @ 20°C
Viscosity	0.887 kg/L
API	27.488
Colour	Yellow-Green
Odour	Specific
Density	0.8865
Ester Index	6.402
Boiling Point	224°C

Table 4: Results for Particle Analysis for the Powdered Lemongrass Sample

Sieve Number	**Pore Diameter (mm)**	**Initial Weight of Dry Sample (g)**	**Final Weight of Dry Sample (g)**
8	2.36	1200	28.0
10	2.00	1172	51.2
12	1.70	1120	74.4
20	0.85	1046.4	260.4
30	0.60	786	278.8
40	0.425	507.2	279.8
60	0.25	227.4	97.2
Pan		130.20	0.4

The process was by stacking and vibrating the sieve on a sieve shaker for 20 minutes with a test sieve (size 250 m) at amplitude of 60. The samples were then sieved and the final weight was recorded. The particle analysis of the powdered lemongrass sample was placed on a stack of seven sieves with sieve numbering 8, 10, 12, 20, 30, 40, 50 and 60 respectively. The total weight of 1200g dried powdered lemongrass sampled was weighed and poured to the topmost sieve on the stack which is sieve number 8, then the timer and the electronic sieve shaker was turned on at the same time. After 20 minutes the shaker was turned off and each sieve was separated and the sample on each sieve was weighed and recorded. A small brush was used to clean each sieve properly before the sample on each sieve was weighed to prevent losses. From the results on table 4, the sieve with the sieve number 30 and opening size of 0.6 had the highest amount of sample at 278.8g while the sieve with sieve number 8 with an opening size of 2.36 had the least amount of sample at 28.0g.

Similarly, on the formulation of perfume, 15ml carrier oil (Olive oil) was placed in a beaker containing 25ml of 42%vol vodka. 15 drops of lavender were added as the base note, 25 drops of lemongrass oil as the middle note and 10 drops of sandalwood as top note. To improve the longevity of the perfume, 5ml of benzyl salicylate which is a fixative was added to the solution. The beaker containing the solution was covered and placed in a cool dark place to allow the individual scents interact, mix and become stronger.

The sample product was then placed in a bottle with a funnel, covered and placed in a cool dark place then left to age for three weeks for future use. Under the ranges of the quality and strength as provided by www.sensoriam.com, the product obtained falls in the range of Eau de Parfum which has a fragrance concentration between 15% and 20% which can lasts for about four to five hours on an average, though below Parfum known as extrait de parfum or pure perfume having the highest fragrance concentration between 15% to 40% fragrance that last up to six to eight hours. However, it has higher lasting concentration fragrance above Eau de Toilette (EDT) which has a fragrance concentration of between 5% and 15% which can only last between two to three hours. It was also higher in fragrance concentration above Eau de cologne (EAU) which serves between 2% and 4% of fragrance and contains a very high concentration of alcohol

V. CONCLUSION

An essential oil was produced from lemongrass (Cymbopogon citratus) using solvent extraction (soxhlet extraction method which is one of the best techniques that increases oil output, separating the solvent from the oil at 60°C and regulate the oil's composition which enable fragile plants in achieving better yield of essential oil with a smaller amount of harvesting. The extract was further employed for the production of perfume which result falls under the range of Eau de Parfum having a fragrance concentration between 15% and 20% that can lasts for about four to five hours on an average. The extraction method is one specialized separation processes used for heating sensitive materials such as essential oils, resins, hydrocarbons that are insoluble in water and may decompose at their boiling point. The temperature of the steam was high enough to vaporize the essential oils present while not destroying or burning them. Furthermore, in varying temperature and time, yield increases with both time and temperature respectively. And to be precise every necessary application and methods were used of chemical engineering unit operations such as leaching, liquid-liquid extraction, and evaporation.

REFERENCES

Oloyede, O. I. (2009). Chemical profile and antimicrobial activity of Cymbopogon Citrus leaves. *Journal of Natural Medicine, 2*, 98-103.

Ugbogu, A. E., Akubugwo, E. I.,Uhegbu, F. O., Chinyere, C. G., Ugbogu, O. C., Oduse, K. A. (2014). Quality assessment profile of Jatropha curcas (L) seed from Nigeria. *International Food Research Journal 21*(2), 735-741.

www.worldhistory.org/article/1777/thespice-trade--the-age-of-exploration World History Encyclopedia. 2021. (Accessed 16th November, 2022)

www.nhb.gov.in, National Horticulture Board. 2014. (Accessed 16th November, 2022)

Suryawanshi, M. A., Mane, V. B., and Kumbhar, G. B. (2016). Methodology to extract Oils from Lemongrass Leaves: Solvent Extraction Approach. *International Research Journal of Engineering and Technology, 8*, 1775-1780.

Haldar S.K, B.B Ghosh, A. Nag 2009. Utilization of Unattended *Putranjiva roxburgurghii* Non-edible Oil as Fuel in Diesel Engine. Renewable Energy, Volume 34, January 2009,pagea 343-347

Atitegeb Abera 2022. Extraction and Physicochemical Analysis of Essential Oils in Lemongrass leaves grown in Arbaminch, Ethiopia. International Journal of Engineering Research & Technology (IJERT) ISSN: 2278-0181

Alhassan, M., Lawal, A., Nasiru, Y., Suleiman, M., Safiya, A.M. and Bello, N. Extraction and Formulation of Perfume from Locally Available Lemon Grass Leaves Department of Chemistry, Sokoto State University, P.M.B. 2134-Birnin Kebbi Road, Sokoto-Nigeria

Agbafor, K. N. and Akubugwo, E. (2007). Hypocholesterolaemic effect of ehanolic extract of fresh leaves of Cybogon Citratus (Lemongrass). *Afr .J. Biotechnol, 6*, 596-598.

Kotzekidou, P., Giannakidis, P. and Boulamatsis, A. (2008). Antimicrobial activity of some plant extracts and essential oils against foodborne pathogens in *vitro* and on the fate of inoculated pathogens in chocolate. *LWT-Food Sci. Technol, 41*, 119-127.

Mahanta, J.J., Chutia, M., Bordoloi, M., Pathak, M.G., Adhikary, R.K., and Sarma, T.C. (2007), *Cymbopogon Citratus* L. essential Oil as a potential antifungal agent against key weed moulds of *Pleurotus spp.* Spawns. *Flavour Fragr, 22*, 525 - 530.

Ekpenyong, C. E., and Akpan, E. E. (2017). Use of Cymbopogon citratus essential oil in food preservation: Recent advances and future perspectives. *Critical reviews in food science and nutrition*, 57(12), 2541-2559.

Hesham H. A., Abdurahman H. N., and Rousli M. Y., (2016). Techniques For Extraction of Essential Oils From Plants: A Review, Australian Journal of Basic And Applied Science, 10(16): 117- 127.

Chrissie, W., (1996). *The Encyclopedia of Aromatherapy. Vermont*: Healing Arts Press, pp: 16- 21.

Akowuah, G.A., Zhari, I., (2010). Effect of Extraction Temperature on Stability of Major Polyphenols and Antioxidant Activity of Orthosiphon stamineus Leaf, *Journal of Herbs, Spices and Medicinal Plants* 16(3-4):160-166.

Hanaa, A.M., Sallam, Y.I., El-Leithy, A.S. and Aly, S.E., (2012). Lemongrass (Cymbopogon citratus) essential

oil as affected by drying methods. *Annals of Agricultural Sciences*, 57(2): 113-116.

Samson O.O. and Ifeanyichukwu E. (2022) Parametric Study on the Extraction of Essential Oil from Lemongrass (Cymbopogon Citratus). *International Journal of Food Science and Agriculture*, 2022, 6(3), 282-286

Jigisha, K.P., Meghal A.D., (2011), Hydrodistillation of Eseential Oil from Cymbopogon flexuosus. *International Journal of Food Engineering*, 7: 1-11.

Tajidin, N.E., Ahmad, S.H., Rosenani, A.B., Azimad, H., and Munirah, M. (2012). "Chemical Composition and Citral Content in Lemongrass (Cymbopogon Citratus) Essential Oil at Three Maturity Stages", *African Journal of Biotechnology*, 11, (11) 2685-26

www.sensorian.com/blogs/blog/how-to-distinguish-between-different-perfume-types. (Accessed 16th November, 2022

Journal of Engineering, Emerging Technologies and Applied Sciences -– Volume 1 Issue 1, April 2023

Available at ***www.ndu.edu.ng/ journalofengineering***

RESEARCH ARTICLE OPEN ACCESS

Effects of Non-Standard Refined Diesel Fuel Oil on the Combustion Characteristics of a Diesel Engine and on the Environment

Oyinkepreye Lucky Bebeteidoh[1,2], Kayvan Pazouki[1], Rose Norman[1],
[1]School of Engineering, Newcastle University, Newcastle upon Tyne, United Kingdom
[2]Department of Marine Engineering, Faculty of Engineering, Niger Delta University, Bayelsa State, Nigeria
Email: engrpreye@ndu.edu.ng

----------**********----------

Abstract:

The Niger Delta Region of Nigeria is presently inundated with non-standard refined diesel fuel oils, available in major towns and communities. To investigate the impact of burning these fuels, where no scientific evidence of their impacts is available, an experimental study was conducted to examine the effects of the non-standard refined diesel on engine performance and emission characteristics in comparison with standard refined diesel. The experiments were performed in a naturally aspirated, air-cooled, single-cylinder Cussons Engine Testbed, P8252, with a 3.5kW Lombardini engine. In this study, the engine was run at a constant speed of 2500 rpm with varying loads to replicate the typical usage of non-standard refined diesel fuels in generator engines in the Niger Delta Region of Nigeria. The exhaust emissions were analysed using a Testo 350 exhaust gas analyzer, and cylinder pressure was determined using a piezoelectric transducer. An Agilent Cary 630 FTIR spectrometer with an absorbance range of 4000 cm^{-1} to 650 cm^{-1} was used to identify functional groups within the fuel samples and the band equivalent to various radiations. Three non-standard refined diesel fuel oil samples obtained from the creeks of the Niger Delta Region of Nigeria, were tested along with a fourth sample of standard diesel obtained from a government retail outlet in Nigeria which was designated as the control sample. Results from the FTIR analysis indicated the presence of aromatic stretch around 1600 cm^{-1} for the non-standard refined fuel samples and the performance and emission analysis revealed low levels of brake thermal efficiency (BTE) with high levels of NO_x, CO, and CO_2 emissions for some of the locally refined samples.

Keywords — Compression ignition engine, Non-standard diesel, NO_x emissions, Carbon monoxide, Environment, Niger Delta Region

----------**********----------

I. INTRODUCTION

Diesel engines offer efficient combustion technology [EL-Seesy et al. 2019] and therefore, they are the main source of power in industries, ships, and small power generation plants [Sen, 2019], [Emiroğlu, 2019], [Tadros et al. 2019]. The diesel engine is also known for its high output torque and low consumption of fuel compared to the gasoline engine [Yu et al. 2020]. However, the emissions from the diesel engine have a harmful effect on the environment and humans [Santhosh et al. 2020], [Raman et al. 2019], [Mejia et al. 2020]. Based on a review from the World Health Organization (WHO), diesel engine exhaust emissions are classified as a carcinogenic substance [IARC, 2012].

Exhaust emissions from diesel engines have become a source of worry for many countries [Sadeq et al. 2019]. High levels of tailpipe emissions have led to stringent emission regulations especially for conventional diesel combustion engines [Lujan et al. 2019], [Elwardany et al. 2020]. Diesel engines are responsible for high particulate matter (PM) and nitrogen oxide (NO_x) levels in the environment [Benajes et al. 2020], [Sundaram et al. 2020]. The formation of NO_X in diesel engines is a function of the residence time, oxygen concentration, and combustion temperatures [Patil and Thipse, 2015].

Engines are designed and manufactured to operate on specified fuel [Ale, 2003], and the life of an engine is largely dependent on the quality of the fuel being used [Verma et al. 2018]. Refined diesel fuel oils, before being supplied to the market, are required to meet a set of regulatory requirements [Vempatapu and Kanaujia, 2017]. Sub-standard diesel fuel oil will not only affect engine performance, but it also increases the noxious emissions as well as greenhouse gases [Wang et al. 2020], and causes drops in engine pressure, difficulties in starting, and irreparable damage to engines [Cunha et al. 2016]. Also, [Bhowmik et al. 2019] reported that low quality diesel fuel oil reduces brake thermal efficiency (BTE) while it increases brake specific energy consumption (BSEC), carbon monoxide, and unburned hydrocarbon (UHC). The constituents in diesel exhaust emissions vary considerably depending on the fuel, lubricating oil, engine type, and operating conditions [Zielinska et al. 2004], [Nelson et al. 2008]. However, [Senthikumar et al. 2012] reported that emission reduction and performance enhancement in diesel engines could be achieved by the addition of fuel additives, engine modification, and exhaust gas post-treatment. Fuel modification could be achieved by increasing the percentage of oxygen in the fuel by the use of additives that are cost-effective, eco-friendly, and readily available [Kumar et al. 2020]. Several studies have been carried out on exhaust emission analysis of diesel engines using diesel fuel oil refined to meet standards and then blended with other fuels like kerosene, white spirit, tyre oil, nanoparticles, waste paint, and ethanol as presented in Table 1.

The quality assessment of diesel fuel oil is very important but comes at a very high cost while using standard methods [Nespeca et al. 2018]. Studies have shown that no technically straightforward solution has been developed in the petroleum industry to detect and identify compounds in substandard fuels [Adesina et al. 2020]. Fourier Transform Infrared Spectroscopy Infrared (FTIR) is a reliable and non-destructive method that provides a quick and straightforward analysis of a sample [Barra et al. 2019]. It determines fuel adulteration by measuring the absorbance bands of certain components in the fuel [Gong et al. 2016]. Spectra obtained from FTIR allow for functional group identification [Edney et al. 2020]. FTIR was used for the determination of biodiesel adulteration with raw vegetable oil [Soares et al. 2011], whilst [Barra et al. 2019] highlighted the dissimilarities between two diesel classes. The rapid and simultaneous prediction of eight quality parameters through FTIR analysis was highlighted by [Nespeca et al. 2018].

Nonstandard refining of crude oil is described as the method of refining petroleum products like gasoline, diesel, and kerosene without expertise or technology [Bebeteidoh et al. 2020]. These products are very common in the Niger Delta Region of Nigeria [Bebeteidoh et al. 2020]. In [Attah, 2012] the author described non-standard refineries as very inefficient, they produce low-grade diesel fuel oil and as much as 80% of the heavy end of the crude oil cannot be refined and is dumped into the environment. In [Nrior et al. 2018] it was reported that the non-standard refined products contain a lot of impurities and unsaturated hydrocarbons, which cause knocking in vehicles and generator engines, and have caused fires in residential houses. In [Patil and Thipse, 2015] the authors reported that non-standard refined diesel fuel contained adulterants, a higher than standard concentration of volatile organic compounds, and also had very low flashpoints.

TABLE 1: Literature review on diesel fuel blended with other fuels

Reference	**Fuel Blends**	**Findings**
[Kalligeros et al. 2005]	Diesel / Domestic heating oil/white spirit	Increased nitrogen oxide (NO_x), unburned hydrocarbon (HC), particulate matter (PM), a slight decrease in volumetric fuel consumption
[Czechlowski, 2020]	Diesel Fuel Oil	Increase in engine load results in a significant reduction in a significant reduction in specific NO_x emissions
[Yang et al. 2017]	Diesel /kerosene blend	Fuel with a higher percentage of kerosene gives maximum power output and lower carbon monoxide emission
[Patil and Thipse, 2015]	Diethyl ether/kerosene/diesel blend	Low brake thermal efficiency, high brake specific fuel consumption, high smoke at full load, low smoke at part load, low NO, almost similar CO, high HC, and low HC at part load
[Bodisco et al. 2019]	Diesel/tyre oil	No significant difference in NO_x emission. On-road NO_x emission significantly exceeded set regulations and significant variability in on-road emission.
[Bhowmik et al. 2017]	Diesel/kerosene/ethanol	The addition of ethanol to the diesel/kerosene blend substantially improved the brake thermal efficiency (BTE), brake specific energy consumption (BSEC), oxides of nitrogen (NO_x), total hydrocarbon (THC), carbon monoxide (CO) emissions of the engine
[Wani and Charoo, 2013]	Diesel/kerosene	Reduction in the brake specific fuel consumption and opacity with increased kerosene substitution in diesel
[Lee et al. 2013]	Diesel/waste engine oil/waste paint	Substantial increase in THC, NO_x, CO, PM, and CO_2. Also, high levels of VOCs (volatile organic compounds), benzene, toluene, ethylbenzene, and xylenes were recorded.
[Kadhim, 2011]	Diesel/kerosene	Reduced brake specific fuel consumption (BSFC). Increase in exhaust gas temperature, brake thermal efficiency (BTE), carbon dioxide (CO_2), NO_X
[Kumar et al. 2020]	Diesel/TiO_2 nanoparticles	By adding 50 and 100 ppm of TiO2 nanoparticles to diesel there was a significant reduction in CO, HC, NO_x, and smoke emissions
[Ithnin et al. 2018]	Water-in-Diesel emulsion	The result showed that emulsion fuel without surfactant does give significant improvement to the engine. There was also an increase in the BSFC compared to diesel fuel. Reduction in particulate matter (PM) and nitrogen oxide (NO_x)

Non-standard refined diesel fuel oil was used in this study. The diesel fuels were locally refined in the creeks of the Niger Delta Region of Nigeria using crude techniques [Bebeteidoh et al. 2020]. To produce non-standard refined diesel fuel oil, the crude oil was heated in 220 litre metal drums welded together to serve as pots [Umukoro, 2018]. The heated crude oil evaporates and goes through two pipes attached to the drums and placed inside a wooden water bath with the refined product emerging at the end of the pipe [Evbuomwan and Alete, 2020]. These refined products are classed as diesel fuel oil. A huge volume of these products has found its way into the Nigerian market, where unsuspecting customers buy them for their daily use in diesel-run small craft, generators, and vehicles.

The purpose of this study was to investigate the impact of the usage of non-standard refined diesel fuel oil on engines and the environment. Though cheap and readily available in the region, there is no scientific evidence of their impact available. The emission characteristics in terms of NO_x, CO, and CO_2, of the non-standard refined diesel fuel oil from three different camps in the creeks of the Niger Delta Region of Nigeria, and the brake specific fuel consumption (BSFC) and brake thermal efficiency (BTE) were determined. FTIR technique was used to determine the chemical bonds present in the test fuels.

The rest of the paper is outlined as follows. Section II introduces the materials used and methodology. In Section III, the results and discussions are presented, while the effect of non-standard refined diesel fuel on the environment is presented in Section IV. Finally, the concluding remarks are given in Section V.

II. MATERIALS AND METHODS

A. Experimental Fuels and their Properties

The locally refined samples designated as A, B, and C were obtained from three different local refineries in the Niger Delta region of Nigeria. For comparison, a fourth sample, designated as D, is the control sample obtained from a government retail outlet in Port Harcourt, Rivers State, Nigeria. The physicochemical properties of the test diesel fuel oils are presented in Table 2 as adapted from [Bebeteidoh et al. 2020].

TABLE 2: Physicochemical properties of test fuels [Bebeteidoh et al. 2020]

Property	Units	A	B	C	D
Density	kgm^{-3}	850.7	854.5	854.4	862.8
Kinematic viscosity	mm^2s^{-1}	2.946	3.587	3.689	3.20
Water Content	mg/kg	77	87	214	78
Cetane Index		46.6	45.8	45.7	45.9

Samples A, B, and C are locally refined diesel fuel samples
D fuel obtained from a government retail outlet in Nigeria

B. Fourier Transform Infrared Analysis

The FTIR analysis was carried out to analyse the chemical bonds present in the test fuels. An Agilent Cary 630 FTIR spectrometer with an absorbance range of 4000 cm^{-1} to 650 cm^{-1} was used for the analysis to identify functional groups and the bands equivalent to various vibrations. Before measuring the spectral intensity, the sample holder was cleaned with acetone, and the CARY 630 FTIR instrument was connected to a computer with the software installed for data processing. Using a pipette, a sample was added to the sample holder and the spectra were captured. The infrared vibrational groups of the diesel fuel samples are shown in Table 3.

TABLE 3: Infrared Vibrational Groups of Diesel Samples [Nespeca et al. 2018].

Attribution	**Wavenumber (cm^{-1})**
CH_3 asymmetrical stretch	2953
CH_3 symmetric stretch	2870
CH_3 angular deformation	1379
CH_2 asymmetrical stretch	2922
CH_2 symmetrical stretch	2853
CH_2 angular deformation	1464
C=O carbonyl stretch	1750-1735
C-O stretch (aliphatic ester)	1300-1000
C=O stretch (aromatics)	1600 and 1475
=C-H stretch (aromatic)	900-690

C. Experimental Setup and Procedure

The experiment was conducted with a single-cylinder Cussons Engine Testbed P8252 with a 3.5 kW (4.8 Hp) Lombardini engine as illustrated in Fig. 1. The engine is a naturally aspirated fuel injected four-stroke compression ignition engine (CIE). The engine drives a 3-phase alternator via a toothed pulley and a toothed belt, has a 69mm bore cylinder, a 60mm stroke, and a maximum output of 3.5 kW

(4.8hp) at 3500 rpm. Specifications of the engine are listed in Table 4. This type of engine is most widely used for fishing boats and in the processing of farm produce around the coastal region of Nigeria.

To ensure that the engine was running in a steady-state condition during the tests, it was started and allowed to run under a no-load condition for 5-10 minutes. Tests were conducted at four different engine loads (0.12kW, 0.43kW, 0.95kW, and 1.71kW) and the rated speed of 2500rpm. The speed was held constant to mimic the operational profile of a constant speed standby generator and thereby determine the performance of the fuel in these generators. To ensure that the fuel system of the test engine was not contaminated by other fuels, a different external fuel tank, and fuel filter were used for each test case. At the end of each experiment, the fuel line was purged with clean diesel fuel, and the engine allowed to run for an ample time to consume any residual fuel from the previous experiment. This was to ensure that there was no contamination in the process of fuel replacement. The tests were conducted three times for each fuel sample. The repeatability analysis was based on the technical standard ISO/IEC 17025:2017 [Trishch et al. 2019], [LAI, 2019].

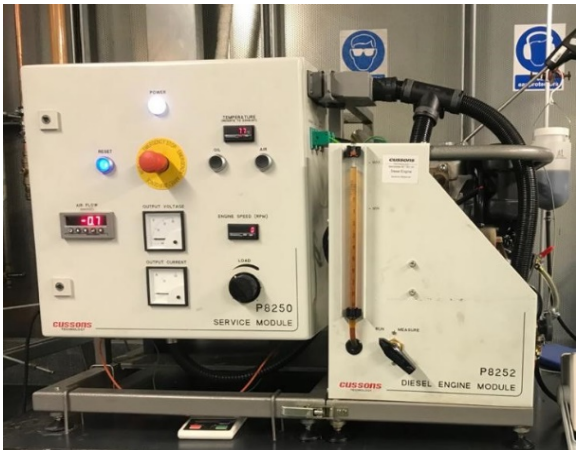

Fig. 1: Cussons Engine Test Bed P8252 with a 3.5 kW (4.8 Hp) Lombardini Engine.

TABLE 4: Specification of the Test Engine

Manufacturer Model	**P8252**
Engine type	4-stroke
Number of cylinders (N)	1
Bore (mm)	69
Stroke (mm)	60
Swept volume (cm^3)	224
Compression ratio	21.1
RPM	3600
Power (kW)	3.5
Fuel consumption (g/kW.hr)	267

A Testo 350 exhaust gas analyzer as illustrated in

Fig. 2: Testo 350 exhaust Gas Analyzer and Printer

Fig. 2, was utilised to determine the concentrations of NO_x, CO, and CO_2 in the exhaust emissions. The Testo 350 analyzer is comprised of the sensor system and the electronics that are required for emission measurement. The specification of the Testo 350 gas analyzer is presented in Table 5.

A piezoelectric transducer (6052 Kistler high-temperature pressure sensor) was installed in the engine cylinder head to measure the in-cylinder pressure, and its output signal fed to a Type 5018A Kistler single channel charge amplifier. The signal from the single-channel charge amplifier was fed to a 100MHz GW INSTEK GDS-1102A-U Digital Storage Oscilloscope.

TABLE 5: Specification of the Testo 350 emission gas analyzer

Measurement Parameter	Range (ppm)	Accuracy	Resolution (ppm)
CO, H_2- Compensated	0-10000	±10ppm (0-199ppm) ±5% of mv (200-2000ppm) ±10% of mv (rest of range)	1
CO_{low}, H_2-Compensated	0-500	±2ppm (0-39.9ppm CO) ±5% of mv	0.1
NO	0-4000	±5ppm (0-99) ±5% of mv (100-1999.9ppm) ±10% of mv (2000-4000ppm)	1
NO_{low}	0-300	±2ppm (0-39.9ppm) ±5% of mv (40-300ppm)	0.1
NO_2	0-500	±5ppm (0-99.9ppm) ±5% of mv (100-500ppm)	0.1ppm

***mv stands for measured value

III. RESULTS AND DISCUSSIONS

Results from the FTIR are discussed in this section along with engine performance parameters including brake thermal efficiency and brake specific fuel consumption and the emission analysis.

1. FTIR Analysis

Fig. 3 illustrates the FTIR spectrum images for the four samples. The spectral peak around 2952 cm^{-1} appears in all samples and indicates the presence of asymmetric stretch CH_3 of a methyl group which can be found in diesel. A similar peak was reported by [Nespeca et al. 2018], [Barra et al. 2019], [Barra et al. 2020], [Li et al. 2020]. CH_2 is the most available functional group in standard diesel fuel, hence the most pronounced in the FTIR. The spectral peaks around wave numbers 2920 cm^{-1} and 2850 cm^{-1} are the asymmetric and symmetric stretch for CH_2 with a strong peak of its angular deformation appearing around 1457 cm^{-1}. All the samples analysed to show the presence of these spectral peaks which are all found in standard diesel fuel oil. This agrees with the work of [Nespeca et al. 2018], [LAI, 2019]. A trace of the spectral peak was identified around 1600 cm^{-1} which indicates aromatic stretch. All samples except D (standard diesel fuel oil) show the presence of this peak. This means that samples A, B, and C (non-standard refined diesel fuel oil) have a traceable amount of aromatic compounds such as benzene, toluene, and xylene (BTEX) [Barra et al. 2020]. This was also reported in [Ale, 2003] where there were high concentrations of toluene, and m-, p-, and o-xylenes, which was attributed to inadequate fractionation in the refining process. Various studies have reported the problems associated with the contamination of soil and water by BTEX [Ahmed et al. 2019], [Sun et al. 2021], [Kim et al. 2021], [Ashok et al. 2020]. BTEX contamination is serious because of its volatility, toxicity, solubility in water, and the ability to migrate [Ahmed et al. 2019]. BTEX contamination in soil has caused alarming issues in human health and ecosystems [Li et al. 2020].

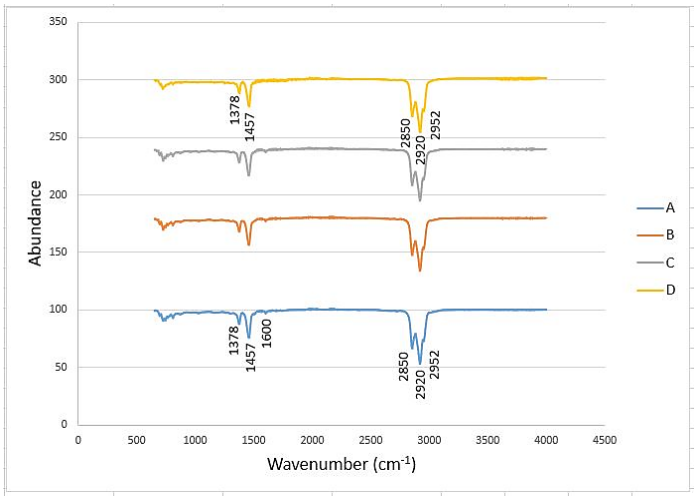

Fig. 3: Infrared spectra of all diesel samples

2. Brake Thermal Efficiency (BTE)

The correlation between the output power derived to the heat imparted in the engine is called brake thermal efficiency [Ashok et al. 2020]. It is used to evaluate how well an engine converts the heat from fuel to mechanical energy [Rahman et al. 2013]. The effect of the test samples A, B, C, and

the control sample D on the brake thermal efficiency (BTE) at different load conditions is illustrated in Fig. 4. The brake thermal efficiency increased with the increase in load for all test samples. The BTE is superior at all loads for samples A and D. With increasing load there is a noticeable increase in the difference in the BTE between samples A, D, and B, C which could be attributed to higher fuel viscosity for samples B and C [Venu et al. 2020].

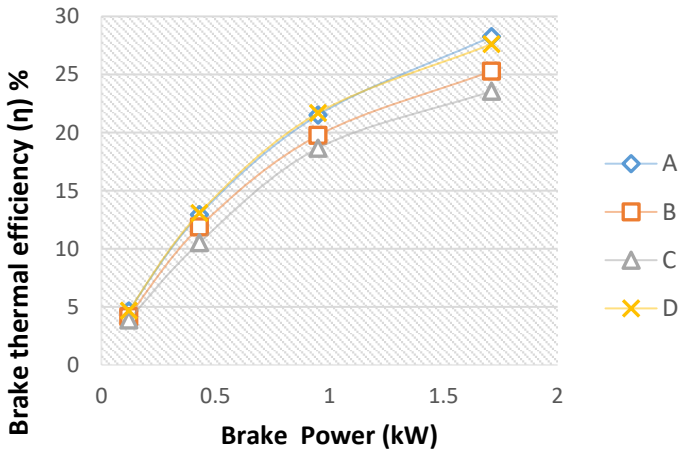

Fig. 4: Brake Thermal Efficiency (BTE)

3. *Brake specific fuel consumption (BSFC)*

The brake specific fuel consumption is defined as the quantity of fuel consumed for a unit power output [Hariram et al. 2020]. It is an important parameter to analyse the performance of the diesel engine [Shrivastava and Verma, 2020]. Change of BSFC at different loads for the test fuels A, B, C, and D is illustrated in Fig. 5. For all test cases, the BSFC increased with increasing load [Shrivastava et al. 2020], [Almohammadi et al. 2020]. The brake specific fuel consumption values for all test fuel samples is presented in Table 6. A slight difference could be observed between sample D and samples A, B, and C.

TABLE 6: Brake specific fuel consumption for test fuels

Engine Load (kW)	Samples (kg/kW.hr)			
	A	B	C	D
0.12	1.705	1.776	1.779	1.790
0.43	0.613	0.619	0.653	0.640
0.95	0.369	0.373	0.369	0.385
1.71	0.281	0.291	0.292	0.303

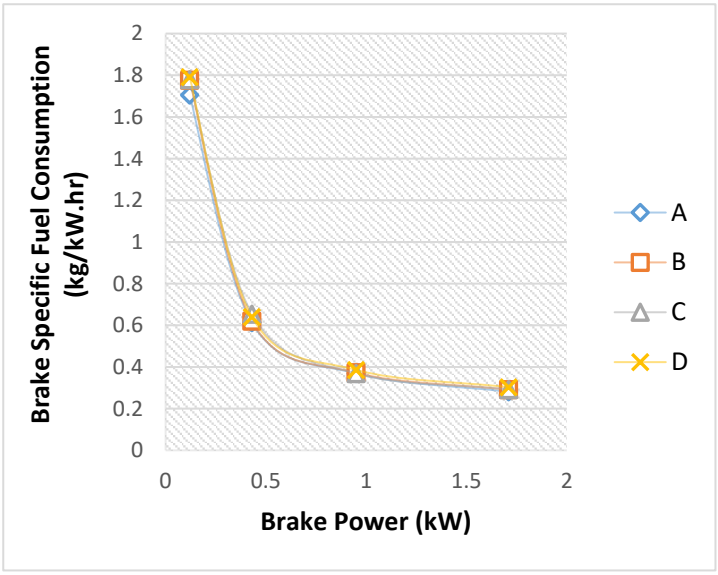

Fig. 5: Brake specific fuel consumption (BSFC)

4. *Oxides of Nitrogen (NOx) Emission*

Fig. 6 shows the variation in NOx emissions under different load conditions. As can be seen, the NOx emission increased with an increase in engine load for all the tested fuel samples. The non-standard refined diesel sample C had higher NOx compared to samples A, B, and the control sample D. Sample B had the lowest NOx value. The lower NOx formation indicated in sample B could be due to the lower temperature formed in the combustion chamber [Shrivastava et al. 2019]. Also, increased NOx in the test fuel samples could be attributed to aromatic content in the locally refined diesel fuel samples A, and C [Ale, 2003], [Sharma et al. 2020]. The NOx value for the test samples is presented in Table 7. Comparing the results of sample B to C,

there was a 34.26%, 53.21%, 68.29%, and 33.79% increase in NOx emissions at the different load conditions. Also comparing the non-standard refined diesel fuel sample C to the control sample D, results showed an increase of 10.96%, 26.27%, 29.93%, and 27.64% in NOx emissions. The usage of non-standard refined fuel could lead to an increase in oxides of nitrogen which poses a great danger to humans and the environment [Lopatin, 2020]. NOx emission from diesel engines causes harm to human health, pulmonary problems, chest tightness, and chronic cough [Lopatin, 2020]. The effect of NOx emissions on the environment also includes ozone depletion, haze, acid rain, and the production of greenhouse emissions [Mohammadi et al. 2020].

TABLE 7: Oxides of nitrogen results for test fuels at varying loads

Engine Load (kW)	Samples (ppm)			
	A	B	C	D
0.12	264.73	226.93	304.67	274.57
0.43	352.37	286.87	439.50	348.07
0.95	552.87	402.30	677.03	521.07
1.71	791.53	696.80	932.27	730.37

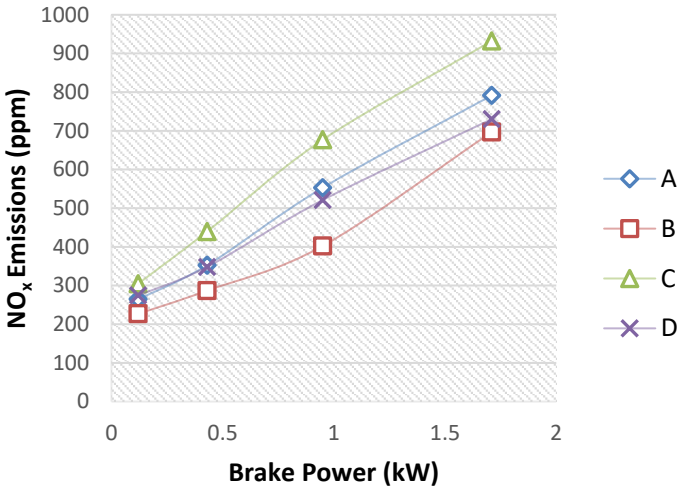

Fig. 6: Oxides of nitrogen (NOx)

5. Carbon Monoxide Emission

Fig. 7 shows the variation in carbon monoxide emission of the test fuels. A lack of oxygen during combustion could result in the formation of CO [Pan et al. 2019]. Samples A, C, and D had higher levels of CO emissions. Sample B on the other hand produced the highest CO emission at the highest load condition. The combustion temperature of an internal combustion engine could also affect the CO emission [Hazar et al. 2019]. In ICE, carbon monoxide emissions occur due to incomplete combustion [Yusri et al. 2019]. CO is a major environmental pollutant [Kalaimurugan et al. 2020]. It is one of the most significant pollutants and also the most harmful pollutant to human health [Liu et al. 2020]. It can be observed that carbon monoxide emissions decreased as the engine load increased in all the test samples. The CO emission value for test samples is presented in Table 8. There was an increase of 60.99%, 45.92%, 38.47%, and 41.59% between non-standard refined diesel fuel sample B and sample C. Also, comparing the control sample D with the non-standard refined diesel sample C, there was a percentage increase in carbon monoxide (CO) emission of 44.91%, 23.22%, 25.29%, and 29.08% at the four load conditions.

TABLE 8: Carbon monoxide results for test fuels at varying loads

Engine Load (kW)	Samples (ppm)			
	A	B	C	D
0.12	368.67	303.33	488.33	337.00
0.43	305.00	249.67	364.33	295.67
0.95	210.67	183.67	254.33	259.67
1.71	267.33	329.67	294.00	306.00

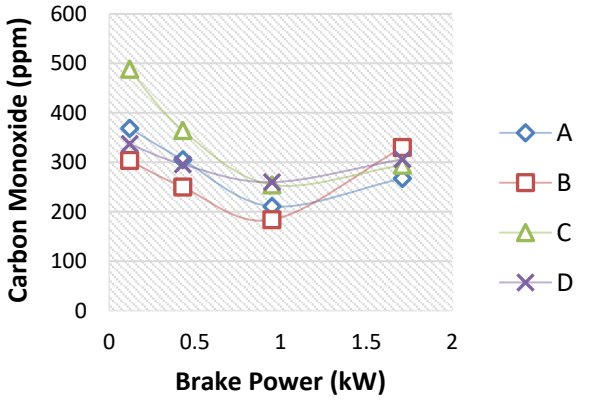

Fig. 7: Carbon monoxide (CO)

6. Carbon Dioxide Emission

Fig. 8 shows the variation in carbon dioxide emissions for the test fuel samples. This variation could be attributed to inconsistency in the refining process from the non-standard refineries A, B, & C. It can be seen from the figure that CO2 emission was highest for test sample C and lowest for sample B. With an increase in load, CO2 emission increased for all samples. The CO2 emission value for test samples is presented in Table 9. Increased CO2 emission aggravates the greenhouse effect, leading to global warming and human health risk [Harris et al. 2020].

TABLE 9: Carbon dioxide results for test fuels at varying loads

Engine Load (kW)	Samples (%)			
	A	B	C	D
0.12	2.07	1.77	2.46	2.02
0.43	2.52	2.12	3.25	2.46
0.95	3.49	2.79	4.23	3.46
1.71	4.77	4.61	5.74	4.64

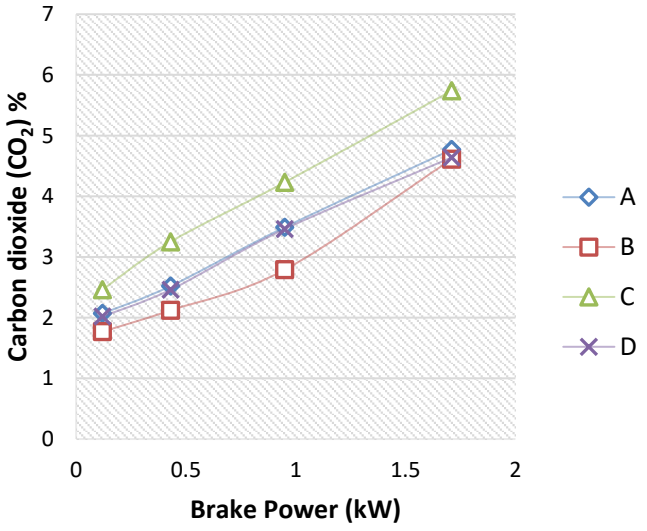

Fig. 8: Carbon dioxide emission (CO_2)

7. Exhaust Gas Temperature

The variations in the exhaust gas temperature (EGT) at different loads are illustrated in Fig. 9. Generally, there was an increase in the exhaust gas temperature with load for all the tested fuels. This could be attributed to an increased supply of fuel into the combustion chamber as a result of the higher load [Shrivastava et al. 2019]. The exhaust gas temperature also indicates the quality of combustion in the combustion chamber [Kalaimurugan et al. 2020]. The EGT for the test samples is presented in Table 10. It is dependent on the quantity of oxygen, the fuel-burning time, and pre-mixed fuel combustion time [Sharma et al. 2020].

TABLE 10: Exhaust gas temperature results for test fuels at varying loads

Engine Load (kW)	Samples (°C)			
	A	B	C	D
0.12	139.67	130.33	143.33	146.00
0.43	171.67	160.67	179.33	175.00
0.95	223.67	209.67	229.67	225.67
1.71	299.33	311.30	309.33	307.00

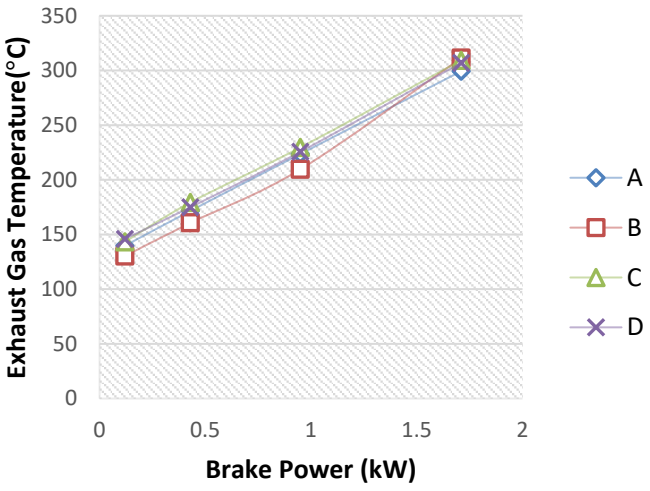

Fig. 9: Exhaust Gas Temperature

8. Cylinder Pressure

The difference in cylinder pressure under different loading conditions for all test fuels is presented in Fig. 10. There is a noticeable increase in cylinder

pressure as the engine load in increased for all test fuels. At 0.12kW and 0.43kW brake power, the cylinder pressure of the non-standard refined diesel fuel oils was slightly higher than that of the control sample D. At 0.95kW brake power, sample C was slightly higher than the control sample D. At 1.71kW brake power, sample C was 3.35% higher than the control sample D. Comparing the cylinder pressure from the three different camps to that of the control sample as shown in Fig. 10 and Table 11, it was observed that at all load conditions the non-standard refined diesel fuel oil from camp C was higher than the control sample D. The higher pressure when using the non-standard refined diesel fuel oil may reflect shortened ignition delay time. According to [Ozer, 2020] the addition of solvents like toluene to diesel fuel oil results in shortened ignition delay; toluene reduces the flash, and ignition point of fuel. The addition of toluene is believed to start the burning in the first phase of the spray before the target point, possibly reducing the duration of the combustion [Simsek and Colak, 2019]. Due to its very low boiling point, toluene is easily gasified, and mixed with the charged air at the end of compression, could lead to a higher rate of combustion and higher cylinder pressure. The higher cylinder pressure could be damaging to internal engine parts like piston, piston rings and valves.

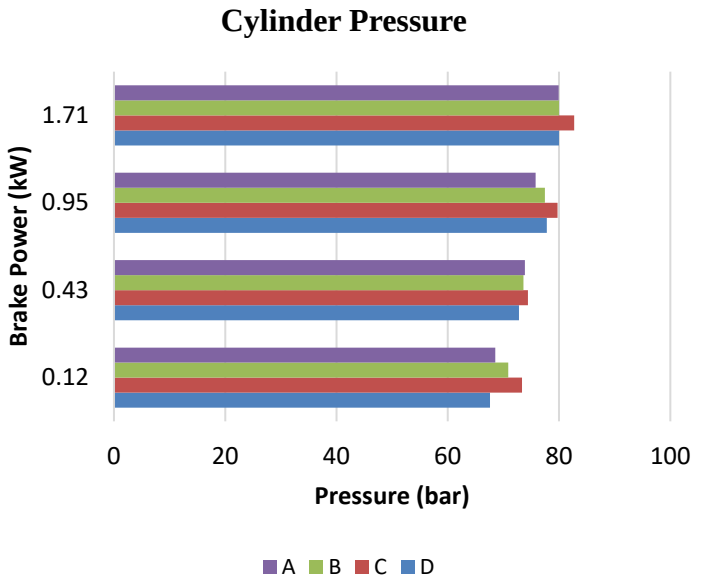

Fig. 10: Cylinder Pressure

TABLE 11: The percentage difference between the non-standard refined diesel fuel oils and the control sample at 1.71kW

Sample	Sample	% Difference Between
A	NGR	0.087
B	NGR	0
C	NGR	3.35%

IV. THE EFFECT OF NON-STANDARD REFINED DIESEL FUEL ON THE ENVIRONMENT

FTIR analysis of the tested fuel samples revealed the presence of aromatics in the non-standard refined diesel fuel oils compared to the control sample. VOCs which are characterized as unregulated emissions are much more dangerous to the environment and human health [Tian et al. 2018]. While VOCs can be from natural and anthropogenic origins, with natural sources mainly from vegetation emissions, volcanic eruptions, and forest fires the major anthropogenic sources comprise combustion and volatile emission [Niu et al. 2021].

In the controlled environment under which the experiment was conducted, there was a noticeable increase in harmful environmental pollutants from the usage of the non-standard refined diesel fuel oil. Results from the experimental analysis of the test fuels showed an increase in nitrogen oxide (NO_x), carbon monoxide (CO), and carbon dioxide emissions for samples A and C compared to sample B and the control sample. The increase in the level of these gases released into the environment could affect inhabitants and the environment of the Niger Delta Region where these fuels are refined and sold to the public at cheap rates. Nitrogen oxide emission is a source of acid rain, photochemical smog, stratospheric ozone depletion, tropospheric ozone formation, and even climate change [Tian et al. 2018], [Niu et al. 2021]. Also, an increase in carbon monoxide emission was observed from the results. CO is a component of motor vehicle exhaust and is

found to be a small contributor in photochemical reactions leading to ozone formation and could cause pathological and physiological changes and untimely death in humans [Amid et al. 2020]. Results also revealed an increased level of CO_2 emission while using the non-standard refined diesel fuel oil with notable increases in samples A and C as compared to sample B and the control samples. With the world moving in the direction of reducing GHG emissions, to protect the environment, the continuous use of non-standard refined diesel fuel oil might lead to increased GHG emissions [Amid et al. 2020]. Finally, results also showed inconsistency in the non-standard refined products, which creates uncertainty when attempting to do corrective engine adjustments to burn these fuels. With this, the end-users of the products may not be getting value for monies spent.

V. CONCLUSION

The present study experimentally investigated the effect of non-standard refined diesel fuel oil on the environment and combustion characteristics of the diesel engine. The BTE, BSFC, cylinder pressure, and emission characteristics were obtained from the engine performance analysis while the chemical bonds present in the test fuels were determined using the FTIR. The conclusions can be summarized as follows:

1. The FTIR analysis indicated the presence of asymmetric stretch CH_3 of the methyl group which can be found in diesel. The most pronounced functional group was the asymmetric stretch of CH_2 with wavenumber 2920 cm^{-1} and 2850 cm^{-1}.
2. The FTIR analysis indicated the presence of a spectral peak of aromatic stretch around 1600 cm^{-1} for the nonstandard refined diesel fuel samples. Trace number of aromatic compounds such as benzene, toluene, and xylenes.
3. Decreases were found in the BTE for samples with higher fuel viscosity. There was no major difference in the BSFC for the samples at all test loads
4. NO_x emissions increased as the load increased for all the samples. The usage of non-standard refined fuel could lead to an increase in oxides of nitrogen which causes grave danger to the environment and humans.
5. CO_2 emissions increased as the engine load increased. Despite the engine's constant speed at 2500 rpm, the CO_2 emission for sample C was higher and sample B lower compared to samples A and D. The variability in the CO_2 emissions could be attributed to the inconsistency in the refining process. Increased CO_2 emissions aggravate the greenhouse effect.
6. The high cylinder pressure from sample C could be damaging to piston rings, pistons, and valves.

REFERENCES

Adesina, F., Ekoh-Chukwukalu, Adeyemi, G., Abolarin, O., Mkpaoro, I., 2020. A Fast and Cost-Efficient Method to Detect Ethanol as Adulterant in Gasoline. MethodsX 100974. https://doi.org/10.1016/j.mex.2020.100974

Ahmed, N., Ok, Y.S., Jeon, B.-H., Kim, J.R., Chae, K.-J., Oh, S.-E., 2019. Assessment of benzene, toluene, ethyl-benzene, and xylene (BTEX) toxicity in soil using sulfur-oxidizing bacterial (SOB) bioassay. Chemosphere 220, 651–657. https://doi.org/10.1016/j.chemosphere.2018.12.102

Ale, B. B. (2003). Fuel adulteration and tailpipe emissions. *Journal of the Institute of Engineering*, *3*(1), 12-16.

Almohammadi, B.A., Singh, P., Sharma, S., Kumar, S., Khandelwal, B., 2020. Impact of alkylbenzenes in formulated surrogate fuel on characteristics of compression ignition engine. Fuel 266, 116981. https://doi.org/10.1016/j.fuel.2019.116981

Amid, S., Aghbashlo, M., Tabatabaei, M., Hajiahmad, A., Najafi, B., Ghaziaskar, H.S., Rastegari, H., Hosseinzadeh-Bandbafha, H., Mohammadi, P., 2020. Effects of waste-derived ethylene glycol diacetate as a novel oxygenated additive on performance and emission characteristics of a diesel engine fueled with diesel/biodiesel blends. Energy Conversion and Management 203, 112245. https://doi.org/10.1016/j.enconman.2019.112245

Ashok, B., Nanthagopal, K., Chyuan, O.H., Le, P.T.K., khanolkar, K., Raje, N., Raj, A., Karthickeyan, V.,

Tamilvanan, A., 2020. Multi-functional fuel additive as a combustion catalyst for diesel and biodiesel in CI engine characteristics. Fuel 278, 118250. https://doi.org/10.1016/j.fuel.2020.118250

Attah, T. (2012, December). Oil Theft and Artisanal (illegal) Refining in Nigeria–Scale, Impacts and the need for a multi-dimensional response. In *Chatham House–Gulf of Guinea Security Conference, London Vice President HSE & Corporate Affairs, Shell Sub-Saharan Africa December* (Vol. 6).

Barra, I., Kharbach, M., Bousrabat, M., Cherrah, Y., Hanafi, M., Qannari, E.M., Bouklouze, A., 2020. Discrimination of diesel fuels marketed in Morocco using FTIR, GC-MS analysis and chemometrics methods. Talanta 209, 120543. https://doi.org/10.1016/j.talanta.2019.120543

Barra, I., Mansouri, M.A., Cherrah, Y., Kharbach, M., Bouklouze, A., 2019. FTIR fingerprints associated to a PLS-DA model for rapid detection of smuggled non-compliant diesel marketed in Morocco. Vibrational Spectroscopy 101, 40–45. https://doi.org/10.1016/j.vibspec.2019.02.001

Bebeteidoh, O.L., Kometa, S., Pazouki, K., Norman, R., 2020. Sustained impact of the activities of local crude oil refiners on their host communities in Nigeria. Heliyon 6, e04000. https://doi.org/10.1016/j.heliyon.2020.e04000

Bebeteidoh, O.L., Pazouki, K., Norman, R., 2020. An experimental investigation of the physio-chemical properties of locally refined diesel oil. Sustainable Chemistry and Pharmacy 15, 100200. https://doi.org/10.1016/j.scp.2019.100200

Benajes, J., García, A., Monsalve-Serrano, J., and Martínez-Boggio, S., (2020). Potential of using OMEx as substitute of diesel in the dual-fuel combustion mode to reduce the global CO2 emissions. Transportation Engineering 1, 100001. https://doi.org/10.1016/j.treng.2020.01.001

Bhowmik, S., Panua, R., Debroy, D., Paul, A., (2017). Artificial Neural Network Prediction of Diesel Engine Performance and Emission Fueled With Diesel–Kerosene–Ethanol Blends: A Fuzzy-Based Optimization. Journal of Energy Resources Technology 139, 042201. https://doi.org/10.1115/1.4035886

Bhowmik, S., Paul, A., Panua, R., Ghosh, S.K., Debroy, D., 2019. Artificial intelligence-based gene expression programming (GEP) model prediction of Diesel engine performances and exhaust emissions under Diesosenol fuel strategies. Fuel 235, 317–325. https://doi.org/10.1016/j.fuel.2018.07.116

Bodisco, T.A., Rahman, S.M.A., Hossain, F.M., Brown, R.J., (2019). On-road NOx emissions of a modern commercial light-duty diesel vehicle using a blend of tyre oil and diesel. Energy Reports 5, 349–356. https://doi.org/10.1016/j.egyr.2019.03.002

Cunha, D.A., Montes, L.F., Castro, E.V.R., Barbosa, L.L., 2016. NMR in the time domain: A new methodology to detect adulteration of diesel oil with kerosene. Fuel 166, 79–85. https://doi.org/10.1016/j.fuel.2015.10.078

Czechlowski, M., (2020). Effect of Diesel Fuel Temperature on the Nitrogen Oxides Emission from a Compression-Ignition Engine. J. Ecol. Eng. 21, 164–170. https://doi.org/10.12911/22998993/118283

Edney, M.K., Barker, J., Reid, J., Scurr, D.J., Snape, C.E., 2020. Recent Advances in the Analysis of GDI and Diesel Fuel Injector Deposits. Fuel 272, 117682. https://doi.org/10.1016/j.fuel.2020.117682

EL-Seesy, A.I., Kosaka, H., Hassan, H., and Sato, S., (2019). Combustion and emission characteristics of a common rail diesel engine and RCEM fueled by n-heptanol-diesel blends and carbon nanomaterial additives. Energy Conversion and Management 196, 370–394. https://doi.org/10.1016/j.enconman.2019.05.049

Elwardany, A.E., Marei, M.N., Eldrainy, Y., Ali, R.M., Ismail, M., El-kassaby, M.M., (2020). Improving performance and emissions characteristics of compression ignition engine: Effect of ferrocene nanoparticles to diesel-biodiesel blend. Fuel 270, 117574. https://doi.org/10.1016/j.fuel.2020.117574

Emiroğlu, A.O., (2019). Effect of fuel injection pressure on the characteristics of single cylinder diesel engine powered by butanol-diesel blend. Fuel 256, 115928. https://doi.org/10.1016/j.fuel.2019.115928

Evbuomwan B.0 and Alete O.G (2020) Comparative Analysis of Locally Refined Petroleum Product (Diesel) In Niger Delta Region, Nigeria. *American Journal of Engineering Research (AJER)*, Vol., 9, Issue 2, pp 25-32, ISSN: 2320-0936

Gong, X., Tian, H., Sun, Y., Li, J., 2016. Research on Fuel-Dilution Monitoring of Engine Lubricant by FT-IR Spectroscopy, in: Proceedings of the 2016 5th International Conference on Energy and Environmental Protection (ICEEP 2016). Presented at the 2016 5th International Conference on Energy and Environmental Protection (ICEEP 2016), Atlantis Press, Shenzhen, China. https://doi.org/10.2991/iceep-16.2016.81

Hariram, V., Solomon, G.R., Raj, D.S., Dev, M.J., Kumar, U.N., Gokulakesavan, M., Premkumar, T.M., Seralathan, S., 2020. Impact of compression ratio in the emission and performance phenomenon of a CI engine fuelled with jojoba biodiesel blends. Materials Today: Proceedings S2214785320340190. https://doi.org/10.1016/j.matpr.2020.05.439

Harris, A., Soban, D., Smyth, B.M., Best, R., 2020. A probabilistic fleet analysis for energy consumption, life cycle cost and greenhouse gas emissions modelling of bus technologies. Applied Energy 261, 114422. https://doi.org/10.1016/j.apenergy.2019.114422

Hazar, H., Sevinc, H., Sap, S., 2019. Performance and emission properties of preheated and blended fennel vegetable oil in

a coated diesel engine. Fuel 254, 115677. https://doi.org/10.1016/j.fuel.2019.115677

IARC. (2012) Diesel Engine Exhaust Carcinogenic; [Online] Available from <https://www.iarc.fr/en/media-centre/pr/2012/pdfs/pr213_E.pdf>.

Ithnin, A.M., Yahya, W.J., Ahmad, M.A., Ramlan, N.A., Abdul Kadir, H., Sidik, N.A.C., Koga, T., (2018). Emulsifier-free Water-in-Diesel emulsion fuel: Its stability behaviour, engine performance and exhaust emission. Fuel 215, 454–462. https://doi.org/10.1016/j.fuel.2017.11.061

Kadhim, N. S (2011) Study the Effect of Blending Kerosene with Diesel fuel on the Performance and Emissions of diesel engine. *IJESRT*, 4(8), 772-776

Kalaimurugan, K., Karthikeyan, S., Periyasamy, M., Mahendran, G., 2020. Experimental investigations on the performance characteristics of CI engine fuelled with cerium oxide nanoparticle added biodiesel-diesel blends. Materials Today: Proceedings S2214785320315625. https://doi.org/10.1016/j.matpr.2020.02.778

Kalligeros, S., Zannikos, F., Stournas, S., Lois, E., Anastopoulos, G., (2005). Impact of using automotive Diesel fuel adulterated with heating Diesel on the performance of a stationary Diesel engine. Energy Conversion and Management 46, 677–686. https://doi.org/10.1016/j.enconman.2004.05.003

Kim, J., Kwon, E.E., Lee, J.E., Jang, S.-H., Jeon, J.-K., Song, J., Park, Y.-K., 2021. Effect of zeolite acidity and structure on ozone oxidation of toluene using Ru-Mn loaded zeolites at ambient temperature. Journal of Hazardous Materials 403, 123934. https://doi.org/10.1016/j.jhazmat.2020.123934

Laboratory accreditation in India including latest ISO/IEC 17025:2017: An overview, 2019. . IJPO 6, 1–8. https://doi.org/10.18231/2394-6792.2019.0001

Lee, Jong-Tae, Moon, Sunhee, Kim, Jeong-Soo, Kim, Sun Moon, Park, Gyutae, Lim, Yunsung, (2013). Atomization characteristics of similar diesel and normal diesel and environmental evaluation of exhaust gas. Journal of The Korean Liquid Particulate Chemistry 18, 106–111. https://doi.org/10.15435/JILASSKR.2013.18.2.106

Li, Y., Wei, M., Liu, L., Xue, Q., Yu, B., 2020. Adsorption of toluene on various natural soils: Influences of soil properties, mechanisms, and model. Science of The Total Environment 740, 140104. https://doi.org/10.1016/j.scitotenv.2020.140104

Liu, W., Chen, J., Luo, Y., Shi, Z., Ji, X., Zhu, H., 2020. Study on the Annual Reduction Rate of Vehicle Emission Factors for Carbon Monoxide: A Case Study of Urban Road Tunnels in Shenzhen, China. Advances in Civil Engineering 2020, 1–17. https://doi.org/10.1155/2020/1686753

Lopatin, O.P., 2020. The effect of operational modes of diesel engines to emissions of nitrogen oxides. IOP Conf. Ser.: Mater. Sci. Eng. 862, 062087. https://doi.org/10.1088/1757-899X/862/6/062087

Luján, J.M., García, A., Monsalve-Serrano, J., and Martínez-Boggio, S., (2019). Effectiveness of hybrid powertrains to reduce the fuel consumption and NOx emissions of a Euro 6d-temp diesel engine under real-life driving conditions. Energy Conversion and Management 199, 111987. https://doi.org/10.1016/j.enconman.2019.111987

Mejía, A., Leiva, M., Rincón-Montenegro, A., Gonzalez-Quiroga, A., and Duarte-Forero, J., (2020). Experimental assessment of emissions maps of a single-cylinder compression ignition engine powered by diesel and palm oil biodiesel-diesel fuel blends. Case Studies in Thermal Engineering 19, 100613. https://doi.org/10.1016/j.csite.2020.100613

Mohammadi, M., Neshat, E., 2020. Accurate prediction of NOx emissions from diesel engines considering in-cylinder ion current. Environmental Pollution 266, 115347. https://doi.org/10.1016/j.envpol.2020.115347

Nelson, P.F., Tibbett, A.R., Day, S.J., (2008). Effects of vehicle type and fuel quality on real world toxic emissions from diesel vehicles. Atmospheric Environment 42, 5291–5303. https://doi.org/10.1016/j.atmosenv.2008.02.049

Nespeca, M.G., Hatanaka, R.R., Flumignan, D.L., Oliveira, J.E. de, 2018. Rapid and Simultaneous Prediction of Eight Diesel Quality Parameters through ATR-FTIR Analysis. Journal of Analytical Methods in Chemistry 2018, 1–10. https://doi.org/10.1155/2018/1795624

Niu, Z., Kong, S., Zheng, H., Yan, Q., Liu, J., Feng, Y., Wu, J., Zheng, S., Zeng, X., Yao, L., Zhang, Y., Fan, Z., Cheng, Y., Liu, X., Wu, F., Qin, S., Yan, Y., Ding, F., Liu, W., Zhu, K., Liu, D., Qi, S., 2021. Temperature dependence of source profiles for volatile organic compounds from typical volatile emission sources. Science of The Total Environment 751, 141741. https://doi.org/10.1016/j.scitotenv.2020.141741

Nrior, R.R., Akani, N.P., Wilcox, A., (2018). Ecotoxicological Assessment of Nigeria Locally Refined Diesel and Kerosene on Aspergillus niger a Key Fungal Pollution Biomarker. AJOB 6, 1–8. https://doi.org/10.9734/AJOB/2018/43896

Pan, M., Huang, R., Liao, J., Jia, C., Zhou, X., Huang, H., Huang, X., 2019. Experimental study of the spray, combustion, and emission performance of a diesel engine with high n-pentanol blending ratios. Energy Conversion and Management 194, 1–10. https://doi.org/10.1016/j.enconman.2019.04.054

Patil, K.R., Thipse, S.S., (2015). Experimental investigation of CI engine combustion, performance and emissions in DEE–kerosene–diesel blends of high DEE concentration. Energy Conversion and Management 89, 396–408. https://doi.org/10.1016/j.enconman.2014.10.022

R. Senthilkumar, K. Ramadoss, R. Manimaran and M. Prabu, "Emission, combustion, performance and characteristics of a CI engine using MTBE blended diesel fuel," IEEE-International Conference On Advances In Engineering,

Science And Management (ICAESM -2012), Nagapattinam, Tamil Nadu, 2012, pp. 360-364.

Rahman, S.M.A., Masjuki, H.H., Kalam, M.A., Abedin, M.J., Sanjid, A., Sajjad, H., 2013. Production of palm and Calophyllum inophyllum based biodiesel and investigation of blend performance and exhaust emission in an unmodified diesel engine at high idling conditions. Energy Conversion and Management 76, 362–367. https://doi.org/10.1016/j.enconman.2013.07.061

Raman, L.A., Deepanraj, B., Rajakumar, S., and Sivasubramanian, V., (2019). Experimental investigation on performance, combustion and emission analysis of a direct injection diesel engine fuelled with rapeseed oil biodiesel. Fuel 246, 69–74. https://doi.org/10.1016/j.fuel.2019.02.106

Sadeq, A.M., Bassiony, M.A., Elbashir, A.M., Ahmed, S.F., and Khraisheh, M., (2019). Combustion and emissions of a diesel engine utilizing novel intake manifold designs and running on alternative fuels. Fuel 255, 115769. https://doi.org/10.1016/j.fuel.2019.115769

Santhosh, K., Kumar, G.N., Radheshyam, and Sanjay, P.V., (2020). Experimental analysis of performance and emission characteristics of CRDI diesel engine fueled with 1-pentanol/diesel blends with EGR technique. Fuel 267, 117187. https://doi.org/10.1016/j.fuel.2020.117187

Şen, M., (2019). The effect of the injection pressure on single cylinder diesel engine fueled with propanol–diesel blend. Fuel 254, 115617. https://doi.org/10.1016/j.fuel.2019.115617

Senthil kumar, J., Ramesh Bapu, B.R., Gugan, R., (2020). Emission examination on nanoparticle blended diesel in constant speed diesel engine. Petroleum Science and Technology 38, 98–105. https://doi.org/10.1080/10916466.2019.1683579

Sharma, A., Singh, Y., Ahmad Ansari, N., Pal, A., Lalhriatpuia, S., 2020. Experimental investigation of the behaviour of a DI diesel engine fuelled with biodiesel/diesel blends having effect of raw biogas at different operating responses. Fuel 279, 118460. https://doi.org/10.1016/j.fuel.2020.118460

Shrivastava, P., Verma, T.N., 2020. Effect of fuel injection pressure on the characteristics of CI engine fuelled with biodiesel from Roselle oil. Fuel 265, 117005. https://doi.org/10.1016/j.fuel.2019.117005

Shrivastava, P., Verma, T.N., David Samuel, O., Pugazhendhi, A., 2020. An experimental investigation on engine characteristics, cost and energy analysis of CI engine fuelled with Roselle, Karanja biodiesel and its blends. Fuel 275, 117891. https://doi.org/10.1016/j.fuel.2020.117891

Shrivastava, P., Verma, T.N., Pugazhendhi, A., 2019. An experimental evaluation of engine performance and emisssion characteristics of CI engine operated with Roselle and Karanja biodiesel. Fuel 254, 115652. https://doi.org/10.1016/j.fuel.2019.115652

Simsek, D., & Colak, N.Y. (2019). Investigation of the effects of biodiesel/propanol fuel mixtures on diesel engine emissions. Al-Cezeri Journal of Science and Engineering, 6, 166-174

Soares, I.P., Rezende, T.F., Pereira, R. de Cássia.C., Santos, C.G. dos, Fortes, I.C.P., 2011. Determination of biodiesel adulteration with raw vegetable oil from ATR-FTIR data using chemometric tools. J. Braz. Chem. Soc. https://doi.org/10.1590/S0103-50532011000700005

Sun, P., Shen, G., Tan, Q., Chen, Q., Song, R., Hu, J., 2021. Degradation of BTEXS with stable and pH-insensitive iron-manganese modified biochar from post pyrolysis. Chemosphere 263, 128092. https://doi.org/10.1016/j.chemosphere.2020.128092

Sundaram, S., Ramasamy, V., Natarajan, N., and Sivakumar, J., (2020). Investigation on performance and emission characteristics of cardanol–diesel blends in a single cylinder DI diesel engine. Energy Sources, Part A: Recovery, Utilization, and Environmental Effects 42, 486–496. https://doi.org/10.1080/15567036.2019.1587093

Tadros, M., Ventura, M., and Guedes Soares, C., (2019). Optimization procedure to minimize fuel consumption of a four-stroke marine turbocharged diesel engine. Energy 168, 897–908. https://doi.org/10.1016/j.energy.2018.11.146

Tian, J., Tan, J., Hu, N., Liu, T., Wang, Y., Zhong, H., Cheng, J., Zhang, X., 2018. Characteristics analysis for total volatile organic compounds emissions of methanol-diesel fuel. Journal of the Energy Institute 91, 527–533. https://doi.org/10.1016/j.joei.2017.04.004

Trishch, R., Maletska, O., Hrinchenko, H., Artiukh, S., Burdeina, V., Antonenko, N., 2019. Development and validation of measurement techniques according to ISO/IEC 17025:2017, in: 2019 IEEE 8th International Conference on Advanced Optoelectronics and Lasers (CAOL). Presented at the 2019 IEEE 8th International Conference on Advanced Optoelectronics and Lasers (CAOL), IEEE,

Umukoro, N., 2018. Home-grown Solution to African Problem: Harnessing Innovation for Petroleum Refining in Nigeria. Strategic Planning for Energy and the Environment 37, 58–73. https://doi.org/10.1080/10485236.2018.12002426

Vempatapu, B.P., Kanaujia, P.K., 2017. Monitoring petroleum fuel adulteration: A review of analytical methods. TrAC Trends in Analytical Chemistry 92, 1–11. https://doi.org/10.1016/j.trac.2017.04.011

Venu, H., Raju, V.D., Subramani, L., Appavu, P., 2020. Experimental assessment on the regulated and unregulated emissions of DI diesel engine fuelled with Chlorella emersonii methyl ester (CEME). Renewable Energy 151, 88–102. https://doi.org/10.1016/j.renene.2019.11.010

Verma, R.K., Suwalka, P., Yadav, J., (2018). Detection of adulteration in diesel and petrol by kerosene using SPR based fiber optic technique. Optical Fiber Technology 43, 95–100. https://doi.org/10.1016/j.yofte.2018.04.011

Wang, S., Liu, S., Yuan, Y., Zhang, J., Wang, Z., and Che, X., (2020). A novel CC-tSNE-SVR model for rapid determination of diesel fuel quality by near infrared spectroscopy. Infrared Physics & Technology 106, 103276. https://doi.org/10.1016/j.infrared.2020.103276

Wani, M. M., & Charoo, M. S. (2013). Performance and emission characteristics with kerosene blending with diesel on a single cylinder four stroke cycle direct injection diesel engine. *International Journal of Managment, IT and Engineering*, *3*(2), 274-282.

Yang, W., Tay, K.L., Kong, K.W., (2017). Impact of Various Factors on the Performance and Emissions of Diesel Engine Fueled by Kerosene and Its Blend with Diesel. Energy Procedia 142, 1564–1569. https://doi.org/10.1016/j.egypro.2017.12.609

Yu, W., Zhao, F., and Yang, W., (2020). Qualitative analysis of particulate matter emission from diesel engine fueled with Jet A-1 under multivariate combustion boundaries by principal component analysis. Applied Energy 269, 115068. https://doi.org/10.1016/j.apenergy.2020.115068

Yusri, I.M., Mamat, R., Akasyah, M.K., Jamlos, M.F., Yusop, A.F., 2019. Evaluation of engine combustion and exhaust emissions characteristics using diesel/butanol blended fuel. Applied Thermal Engineering 156, 209–219. https://doi.org/10.1016/j.applthermaleng.2019.02.028

Zielinska, B., Sagebiel, J., McDonald, J.D., Whitney, K., Lawson, D.R., (2004). Emission Rates and Comparative Chemical Composition from Selected In-Use Diesel and Gasoline-Fueled Vehicles. Journal of the Air & Waste Management Association 54, 1138–1150. https://doi.org/10.1080/10473289.2004.10470973

Journal of Engineering, Emerging Technologies and Applied Sciences -– Volume 1 Issue 1, April 2023

Available at ***www.ndu.edu.ng/ journalofengineering***

RESEARCH ARTICLE OPEN ACCESS

An Improved Wearable Medication Reminder System Using Peripheral Interface Controller for Persons with Arrhythmia

Samuel Adeniyi*, Kufre Esenowo Jack*, Abdullah Oreoluwa Bankole*,
Abiodun Ayodele Oguntuyi*, Adamu Abdullahi Ginyan*, Olamilekan Muftaudeen Yusuf**

*Department of Mechatronics Engineering, School of Electrical Engineering and Technology,
Federal University of Technology Minna, Niger State, Nigeria
kufre@futminna.edu.ng

**Department of Electrical & Electronics Engineering, School of Electrical Engineering and Technology,
Federal University of Technology Minna, Niger State, Nigeria

----------**********----------

Abstract:

Arrhythmia condition affects millions of people worldwide, and the management of the disease requires adherence to strict medication schedules. Wearable medication reminding systems have shown a great deal of benefits in improving medication adherence rates among patients with various chronic diseases such as coronary artery disease. In this study, an improved wearable medication reminding system for persons with arrhythmia was proposed and utilizes Peripheral Interface Controller (PIC) for the designed model. The system as designed functions to remind patients to take their medication at the appropriate times while monitoring the patient's heart rate. Hence, reporting the patient's adherence to the doctor's prescription. The wearable device was connected via the global system for mobile communication (GSM) to the patient's and medical advisor's smartphone for notification purposes, and the device was equipped with a heart rate sensor to detect any abnormality occurring in the patient's heartbeat. A simulation was carried out to test the system's effectiveness in promoting medication adherence and the results indicates the system significantly improved medication adherence rates among patients. Haven tested for performance validation, it is recommended that this system be adopted as a tool for managing arrhythmia and improving medication adherence rates. Long-term medication adherence and arrhythmia management are key areas that need more study to establish the system's potential.

Keywords*:* Heart, Arrhythmia, Medication Adherence, Wearable Technology

----------**********----------

I. INTRODUCTION

Arrhythmia of the heart is a heart disease characterized by an abnormal heartbeat pattern that results in severe health complications, including stroke, heart failure, and even sudden death (Biniyam, et al., 2017). According to (Abdi, *et al*., 2015; Babu, 2021), Patients with cardiac arrhythmia need to have their heart rates closely monitored else this could result in severe complications caused by the inability to properly manage the disease. Managing this disease requires the patients to take their medications as prescribed by their medical advisors. Due to the lack of consistent adherence to

medication, non-adherence to medication has become a prevalent issue among patients with chronic conditions.

Due to the innovation introduced by technological advancement, a device is tasked with the responsibility of reminding patients with arrhythmia to consistently adhere to medications has been designed and it is known as Wearable Medication Reminding System (WMRS). Wearable medication reminding systems (WMRS) are designed and properly equipped with features that notify the patients to adhere to medication at the right time thereby resulting in consistent adherence to medication by the patient (Verma & Gupta, 2012). A WMRS typically consists of a wearable device, a microcontroller, and a smartphone connectivity feature, which work together to provide personalized medication reminders.

In recent years, there has been a growing interest in developing WMRS specifically for individuals with arrhythmia (AmolGosavi, *et al*., 2017).

These systems are designed to provide patients with reminders to take their anti-arrhythmic medication at the right time, and to help monitor their heart rhythm to detect any abnormalities (Parihar, *et al*., 2017; Balakumar, *et al*., 2016; Shabaan¸ *et al*., 2020).

In the context of WMRS for individuals with heart arrhythmia, a PIC microcontroller was used to collect and process data from wearable sensors and provide patients with reminders to take their medication at the right time (Satpathy, *et al*., 2020; Tan, *et al.*, 2021).

The WMRS for persons with arrhythmia disease using PIC microcontroller consists of a wearable device that includes a heart rate sensor and an accelerometer, which are used to monitor the patient's heart rhythm and detect any abnormalities (Trivedi & Cheeran, 2017).

There have been several studies conducted on the use of WMRS for promoting medication adherence among individuals with arrhythmia. In one of the studies (Kumar, *et al.*, 2016) found that the use of a wearable medication reminding system resulted in a significant improvement in medication adherence rates among patients with atrial fibrillation, a type of arrhythmia (Lin, *et al*., 2016). Also, (Palanivel, *et al*., 2013) found that a WMRS that included personalized reminders and feedback helped to improve medication adherence among patients with chronic conditions.

Hence, WMRS using PIC microcontroller are a promising tool for promoting medication adherence among individuals with heart arrhythmia. These systems are designed for abnormalities.

As technology continues to advance, it is likely that wearable medication reminding systems could become increasingly sophisticated and effective in promoting medication adherence among individuals with arrhythmia and other chronic conditions, lack of social support was a barrier to adherence, as patients did not have access to adequate support from family, friends, or healthcare providers and may as well claim to have forgotten when to take the medication and which of the medication was to be taken. Thus necessitates the need for the development of this model.

Therefore, the aim of this research is to develop an enhanced wearable medication reminder system for persons with arrhythmia disease using a PIC16F877 microcontroller. The following objectives were used to achieve this aim: to design an improved wearable system for medication reminders with a patient-medical advisor intra-communication channel; to develop the medication reminder model with a notification scheme.

REVIEWED LITERATURE

Medication adherence is a critical aspect of disease management among patients with heart arrhythmia. Poor adherence to medication regimens can lead to suboptimal health outcomes and increased healthcare costs. Wearable medication reminding systems have emerged as a promising tool for managing medication schedules and improving adherence rates among patients with chronic diseases, including Arrhythmia disease. In this section, several kinds of literature on heart rate and visual representation of Electrocardiogram (ECG) Signal, heart rate measurement, medication

adherence among patients with Arrhythmia disease, the use of wearable technology in promoting medication adherence, and the development of wearable medication reminder systems were reviewed.

A. Heart Rate and Visual Representation of Electrocardiogram (ECG) Signal

The heart circulates blood throughout the body. The human heart has four chambers—two atria and two ventricles—and may be found in the center of the thorax, somewhat off to the left, and surrounded by the lungs. Blood from the entire body is pumped back into the heart and enters through the right atrium. After being pumped by the right ventricle, blood travels to the lungs to be oxygenated before returning to the heart via the left atrium. From there, it is pumped once again by the left ventricle and distributed to the body via the arteries (Casillas & Americas, 2010). Between different parts of the body, a voltage potential of about 1 mV occurs (Sundararaj, 2016). The number of times the heart beats in a minute is the heart rate (bpm). Several devices, such as pulse oximeters, heart rate monitors, electrocardiographs, and even an ECG strap, are used to take readings of the heart's electrical activity as shown in Fig. 1. The average heart rate varies widely from person to person based on a number of factors including age, health, and environment. The rate at which the heart beats is controlled by a central organ in the brain (Acharya, *et al.*, 2017). This control hub adjusts the heart rate based on input from various muscles and sensors.

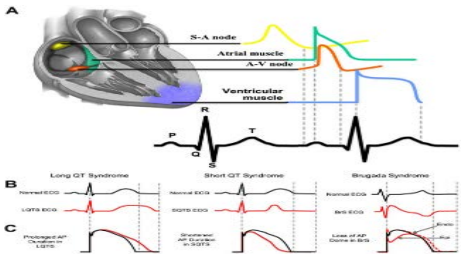

Fig. 1: Electrical Activity of the Heart in Health and Disease *(*Murat, *et al.*, 2020*)*

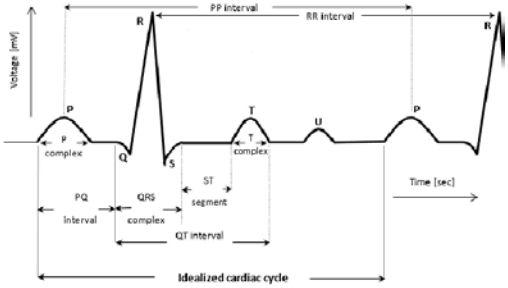

Fig. 2: The ECG Signal Waveform *(Tutuko, et al., 2022)*

B. Heart Rate Measurement

Fig. 2 shows how the heart rate is determined by analyzing an electrocardiogram (ECG) and looking for the peaks. The best indicator of a person's fitness is their resting heart rate before, during, and after exercise. If done manually, counting heartbeats over time requires the subject to pause their current activity. Electric circuits allow for more rapid and precise measurement of the heart rate. Checking a person's heart rate is a crucial diagnostic tool because of how vital it is to the functioning of the cardiovascular system. A normal resting adult heart rate is somewhere about 72 beats per minute (bpm). As a general rule, athletes have healthier heart rates than the general population. Young infants' heart rates average 120 beats per minute (bpm), whereas those of school-aged children average 90 bpm. The increase in heart rate during exercise is moderate, as is the subsequent decrease to resting levels. The fitness of a person is gauged by how quickly their pulse returns to normal after being disturbed. An abnormally slow heart rate, or bradycardia, and a rapid heart rate, or tachycardia, are two extremes of the same disorder (Kranjec, *et al.*, 2014). The average resting heart rate of an endurance athlete is quite low. One's pulse is a reliable indicator of heart rate. Pressing one's fingertips against an artery is just as accurate as using medical equipment for measuring the pulse (typically on the wrist or the neck). It is generally agreed that auscultation, or listening to the heart with a stethoscope, is the most accurate way to determine a person's heart rate. Phonocardiograms (PCG), electrocardiograms (ECG), blood pressure waveforms and pulse meters are only a few of the many alternative ways, but they

are all clinical and expensive (Fernandes, *et al.*, 2020).

C. Medication Adherence Among Patients with Arrhythmia

Medication adherence among patients with arrhythmia is often poor, which lead to adverse health outcomes (Elhag, *et al.*, 2022). Several studies have evaluated medication adherence rates among patients with arrhythmia.

Jackevicius, *et al.*, (2017) conducted a study involving patients with atrial fibrillation and found that only 36% of patients were adherent to their medication regimen. Non-adherent patients had a significantly higher risk of stroke, bleeding, and hospitalization as compared to adherent patients. Similarly, Salmasi, *et al.*, (2020) found that only 35 percent of patients with arrhythmia were adherent to their medication regimen, and non-adherent patients had a significantly higher risk of mortality compared to adherent patients.

Several factors contribute to poor medication adherence among patients with arrhythmia. Forgetfulness is a common reason for non-adherence, as patients may forget to take their medication at the appropriate times (Reading *et al.*, 2019). Complex medication regimens can also be a barrier to adherence, as patients may find it difficult to manage multiple medications with different dosing schedules. Medication side effects also contribute to non-adherence, as patients may discontinue their medication due to unpleasant side effects (Chang *et al.*, 2018).

D. Wearable Technology in Promoting Medication Adherence

Wearable technology has shown promise in promoting medication adherence among patients with various chronic diseases, including arrhythmia (Hsieh **et al.**, 2021). Wearable devices, such as smartwatches and fitness trackers provide patients with real-time reminders to take their medication, monitor their medication adherence, and provide feedback on their adherence behavior.

Several studies have evaluated the effectiveness of wearable technology in promoting medication adherence among patients with arrhythmia. Ahmed *et al.* (2018) conducted a study involving patients with atrial fibrillation and found that a smartwatch-based medication reminder system significantly improved medication adherence rates compared to standard care. Patients in the intervention group received real-time reminders to take their medication, and the system also provided feedback on their medication adherence behavior.

Similarly, a study conducted by Aldeer *et al.* (2018) evaluated the effectiveness of a wearable medication reminder system among patients with arrhythmia. The system consisted of a wearable device that provided real-time reminders to take medication, as well as a smartphone application that allowed patients to track their medication adherence. Results indicated that the system significantly improved medication adherence rates among patients, and they also reported an improvement in their overall quality of life.

E. Wearable Medication Reminding Systems

Wearable medication reminding systems have emerged as a promising tool for managing medication schedules and improving adherence rates among patients with chronic diseases, including arrhythmia (Greiwe and Nyenhuis, 2020). These systems provide patients with real-time reminders to take their medication, monitor their medication adherence, and provide feedback on their adherence behavior.

Several studies have evaluated the effectiveness of wearable medication reminding systems among patients with arrhythmia. A study conducted by the following researchers Rosner *et al.* (2015) and Kalantarian *et al.* (2016) evaluated the effectiveness of a wearable medication reminder system among patients with Atrial fibrillation. The system consisted of a smartwatch that provided real-time reminders to take medication, as well as a smartphone application that allowed patients to track their medication adherence. Results indicated that the system significantly improved medication adherence rates

among patients, and they also reported a higher level of satisfaction with the system compared to standard care.

The use of microcontrollers, such as PIC microcontrollers, has become increasingly popular in the development of wearable medication reminding systems. PIC microcontrollers are low-cost and low-power devices and are programmed to perform specific tasks, such as providing real-time reminders to take medication. Several studies have used PIC microcontrollers in the development of wearable medication reminding systems.

Furthermore, a study conducted by Jayanth *et al*. (2017) developed a wearable medication reminding system using a PIC microcontroller. The system consisted of a wearable device that provided real-time reminders to take medication, as well as a smartphone application that allowed patients to track their medication adherence. Results indicated that the system significantly improved medication adherence rates among patients, and a higher level of satisfaction with the system compared to standard care was reported.

Another study conducted by Mondol, *et al*., (2016); Choi, *et al.*, (2013) developed a wearable medication reminding system using a PIC microcontroller. The system consisted of a smartwatch that provided real-time reminders to take medication, as well as a smartphone application that allowed patients to track their medication adherence. Results indicated that the system significantly improved medication adherence rates among patients, and they also reported an improvement in their quality of life.

Lin, *et al.*, (2016) developed a device which was connected to PIC microcontroller, and responsible for processing the data and providing the patient with medication reminders. The reminders are personalized based on the patient's medication schedule and a short message service (SMS) was sent to the patient's smartphone via a GSM module (Chuquimarca, *et al*., 2020). The SMS also provides report of the patient's heart rhythm, which helps patients to better understand their condition and the importance of adherence to their medication regimen.

The literature reviewed so far suggests that wearable medication reminding systems are effective in improving medication adherence rates among patients with arrhythmia. But further enhancement is required in terms of creating a documentary platform for the medical advisors to evaluate the arrhythmia patient's rate of adherence to prescribed medication. Among other enhancements in this research work, the system seeks to develop a viable means of communication between the patient and the medical advisors in case of failure to adhere to the medication regimen by the patient. In this case, the proposed model has the capability of allowing the medical advisor alert the patients whenever the patient fails to adhere to the regimen.

II. METHODOLOGY

This section highlights the various materials and methods that were utilized in the development of this system model for patients suffering from arrhythmia conditions. Several different pieces of hardware and software were utilized in this study for the development of an enhanced microcontroller-based heart rate monitor.

A. Materials

The software materials used for the development of this system model were Proteus Design Suite (PDS) and mikroC PRO for PIC. The heart rate sensor, temperature sensor, global system for mobile communication (GSM) module, LCD display, and buzzer were the hardware components utilized for the construction of this system.

B. Method

The comprehensive embedded system results to the detailed system model in Fig. 3.

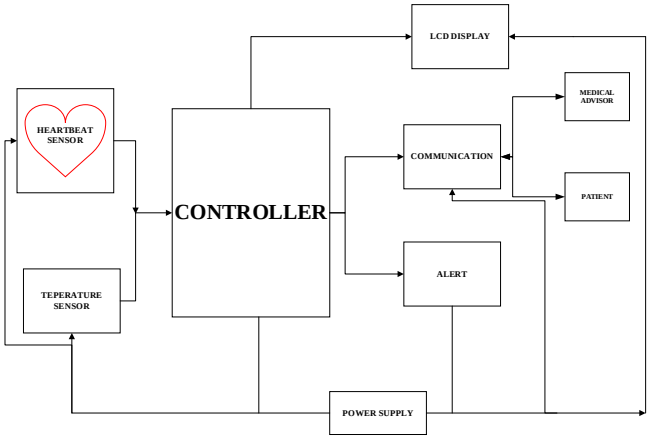

Fig. 3: Block Diagram of the System

1) Heart Rate Sensor

When a finger is placed on the pulse detector, it produces a more precise reading. The sensor's thump Light Emitting Diode (LED) flashes in a zigzag pattern with each heartbeat while the heartbeat indication is active. The PIC regulator is then linked to the sensor's output to approximate the BPM rate. It uses the thumb rule of light law to detect changes in blood flow in the finger in time with each heartbeat. LEDs are used to monitor heartbeats and generate high-pulse output, and in the specifications, the operational voltage was capped at +5V DC, the operating current was 100mA, the output data levels are Transistor-Transistor Logic (TTL) was 5V, and the light source is 660nm super red LEDs.

2) Temperature Sensor

The LM35 provides an instantaneous voltage output proportional to the temperature in Celsius. The outer adjustment was unnecessary for the LM35 to operate because of its low impedance output and operates between 4 and 30 volts with 0.5^{o}C accuracy guaranteed at +25^{o}C, a temperature range from 55^{o}C to 150^{o}C, and a linear scale factor of +10mV/^{o}C were specified.

3) Peripheral Interface Controller (PIC)

PIC regulators were used to improve sensor circuit outputs. The small, adaptable size are easily revised and updated without a hitch in the assembly. The PIC16F877A microcontroller has the following features, making it suitable for use in various types of apparatus and control systems: a DC-20MHz clock input, the PIC controller processes up to 8 channels from the ADC's 10-bit resolution. Data memory in EEPROM hold up to bytes, whereas flash memory can hold up to words.

4) LCD Display

To show data, liquid crystal displays (LCDs) was used. LCD screens come in both 14-pin and 16-pin varieties. In this experiment, a 16-pin, 16 x 2 LCD screen was used. The LCD displays data in a two-line, sixteen-character-by-two-character format.

5) Communication System

The communication system provides a medium for interaction between the controller, medical advisor and the patient. GSM modem uses a 12V power supply, a communication interface RS232, and a Subscriber Identity Module (SIM) card establishes connectivity for the wearable device. When communicating with a GSM modem, the accompanying AT-Commands are used.

TABLE I
AT-Command for GSM

AT-Command	Description
AT	Enter
AT+CMGF	Select SMS Message Format
AT+CMGS	Send SMS Message

6) *Alert System*

A beeping device was wired to the microcontroller output to serve as the alert mechanism. The microcontroller's signal was amplified by a transistor amplifier before it reaches the beeping device. To bias the transistor's base, a 4.7K and 2.2k resistor are needed. Once the sensor detects an irregular heartbeat, it produces a beep sound to alert and signal the need for immediate medical attention.

C. Discrete Fourier Transform

Computing the Fourier Transform of the heartbeat data was necessary for determining blood pressures (bps), and the mathematical model represented thus. The minimum sampling rate were calculated using the Nyquist-Shannon sampling theorem in the following way, considering a comparatively high heart rate of 120 beats per minute.

The heartbeats per second = $\frac{120}{60}$ = 2bps

The minimum sampling frequency = $2 \times 2 = 4$ samples per second.

The system controller reads the input signal at 20 samples per second, which was significantly higher than the aforementioned bare minimum. This ensures that Fourier Transforms are highly accurate and that the calculated pulse rate was accurate. 100 samples are taken over the course of 5 seconds to ensure that the gadget was as precise as possible.

Let's suppose that the function g represents the continuously occurring analogue signal g(t). The signal's Fourier Transform (G(f)) is then specified as something like 0:

$$G(f) = \int g(t)e^{-j2\pi ft}dt \quad (1)$$

where information about the signal and the length of time an observation was made defined the bounds within which an integration was performed. Let's say that over the course of time T, a total of N samples were taken. The signal could possibly be expressed as a sequentially step level, sample and hold, if the duration between samples is t:

$$G(t) = g(t_i)\ where\ i\Delta t \leq t < (i+1)\Delta t \quad (2)$$

From the ADC's discrete input, the Fourier Transform was calculated as follows:

$$G(f) = \sum_{i=1}^{N} g(t_i)\, e^{-j2\pi f t_i} \quad (3)$$

Thus, the actual and imaginary parts as is expressed as:

$$Re(G(f)) = \sum_{i=1}^{N} g(t_i)\cos(2\pi f t_i) \quad (4)$$

$$Im(G(f)) = -\sum_{i=1}^{N} g(t_i)\sin(2\pi f t_i) \quad (5)$$

D. Wearable System Model for Medication Reminder

The PIC microcontroller-based wearable system model for the medication reminder system was developed in this sub-section. Fig. 4 depicts the circuit, together with the block diagram which reveals the system's functionality.

MAXHR - Maximum Heart Rate and HR – Heart Rate

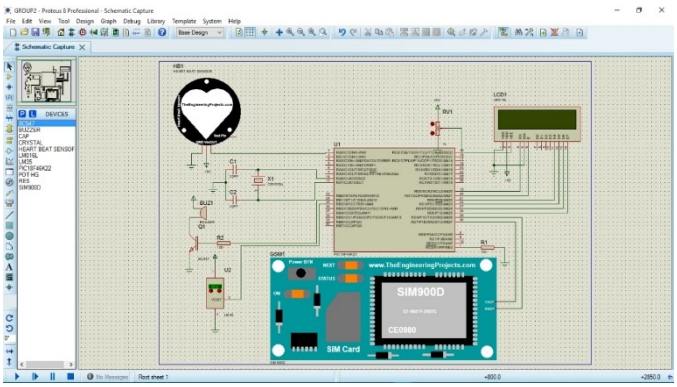

Fig. 4: Circuit design for improved wearable medication system model

Heartbeat PIC Algorithm: Pseudo Code:

Initialize the microcontroller:
Clock frequency
ADC configuration:
Initialize I/O Ports
Initialize LCD
Serial communication settings
Insert the user's information (i.e name, age, gender, and, phone number)
Calculate the maximum HR
Start measuring the HR
Display the HR
If
Then, display HR into LCD
Send text message to use's specified phone

number
Set counter = 0
Turn on the buzzer and LED
Delay for 1s
Turn off the buzzer and LED
If counter is less than 5
Then, urn on the buzzer and LED
If HR < MAXHR, display HR into LCD
Start measuring the HR

Body Temperature PIC Algorithm: Pseudo Code:

Start system
Initialize all Ports
Turn off Alert
Let system count the Heart beat for 1 minute
Read Body Temperature
If Body Temperature and Heart Beat Exceeded
Then turn on alert
Send heart beat and body temperature via SMS
Else
Read Body Temperature
Stop system

III. RESULT AND DISCUSSION

The system model was actualized, findings were analysed and, the implications discussed. The research aim and objectives were achieved as the improved wearable medication reminder system for patients with arrhythmia was developed. This section presents the system performance analysis and evaluation metrics of the developed model.

A. System Performance

The performance of the wearable medication reminding system for persons with arrhythmia using PIC microcontroller was evaluated through a series of experiments. The system was tested in terms of its accuracy, reliability, security, and compatibility, and effectiveness in reminding patients to take their medications. The following are the results of the system performance: The system was found to be highly accurate in reminding patients to take their medications. The reminders were delivered at the right time, and the system was able to detect if the patient had taken their medication or not; the system was found to be highly reliable in terms of delivering reminders consistently. The system was able to operate continuously for several weeks without any downtime or failure; the system was secure, with measures in place to protect patient data and prevent unauthorized access; the system was compatible with a range of devices and operating systems, such as smartphones and computers, to allow for easy data access and sharing with healthcare professionals.

The results of the experiments demonstrate that the wearable medication reminding system for persons with arrhythmia using PIC microcontroller was highly accurate, reliable, and effective. The system has the potential to improve patient adherence to medication regimens and ultimately lead to better health outcomes for patients with arrhythmia

B. Wearable System Model for Medication Reminder

i. HEART SENSOR

Since the correctness of the signal at the output was crucial to the testing process, this means that the testing could proceed to the next phase. So, the first step was to make sure the signal was strong before actually testing it. The power for the circuit comes from a 5V source. Taking the reliability of the infrared sensor into account, the finger was placed very close to the sensor.

Connecting the oscilloscope connector helps to verify the output signal after the amplifier and filter were tested.

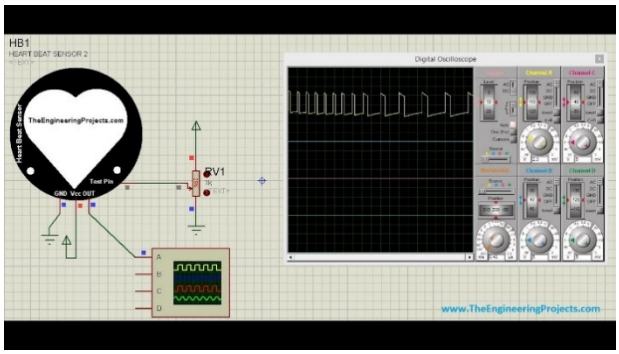

Fig. 5: The output signal by Oscilloscope on Proteus for heart sensor

Comparing the ECG waveform in Fig. 2 with the one in Fig. 5, it was observed that the output signal

was well-suited for transmission to the microcontroller.

The ADC channel of the microcontroller was subjected to sinusoidal waveforms with frequencies ranging from 1 HZ to 3 HZ, and the corresponding beats per minutes were recorded. These tests were carried out in both a simulated environment (using Proteus) and the actual world. Table 2 displays the identical results observed in both settings. The negligible disparity between the two documentaries could be attributed to design error.

TABLE 2: MEASURING FREQUENCY OF SINUSOIDAL SIGNALS

Frequency (Hz)	Result on Proteus (bpm)	Result on real world (bpm)
1	55	59.52
2	105	120.15
2.7	142	163.33
3	160	179.52

ii. USER HEART BEAT PULSE TESTING

After the device's circuitry and display were validated, the user's heart beat pulse was used to ensure the device was functioning properly. A total of five human subjects, male and female, were employed to test this model. The user paused for one minute, then places the finger on the center of the infrared sensor, and the software began to execute based on the programmed algorithm. The infrared sensor picked up the pulse of the heart, the circuit amplified and filtered it, and the microcontroller converts it to a digital signal within 5 seconds, and the controller then spends another 9 seconds performing the Fourier transform on the signal. When successful, the controller needs about 4 seconds to locate the frequency, this includes the time needed to setup the system and collect user information, the entire procedure took less than a minute.

The Electrocardiogram (ECG) data from the patient's fingertip sensor is used to evaluate the Heart Rate Monitor (HRM) device's functionality on an oscilloscope. The percentage error was determined by:

$$E = \frac{(A - M)}{A} \times 100 \qquad (6)$$

Here, A = Actual heart rate

M = Measured heart rate

E = Error rate

TABLE 3: HEART RATE AND TEMPERATURE RESULT

Activity	Patient A		Patient B		Patient C	
	Heart (bpm)	Temp (^{0}F)	Heart (bpm)	Temp (^{0}F)	Heart (bpm)	Temp (^{0}F)
Resting	80	98	75	98.2	70	98.4
Running	130	99.2	170	99.4	135	99.3
Walking	90	98.5	95	98.6	100	98.8

The result of the testing process is represented in Table 3 as three patients' (Patient A, Patient B, and Patient C) resting, running, and walking heart rates and temperatures are displayed. This information was presented in the context of an enhanced wearable medication reminder system for people with arrhythmia. This system employs a Peripheral Interface Controller (PIC) to provide medication reminders and heart rate monitoring. The findings show that heart rate and temperature fluctuate considerably across a wide range of demographics, including age, gender, health, and physical activity. However, the given heart rate data demonstrates that the wearable medication reminder device was successful in keeping tabs on the patients' heart rates throughout the day for three respective patients.

All three patients' resting heart rates were within a healthy range, with Patient (A) having the slowest heart rate and Patient (C) having the fastest, both when the patients were sitting still and while they were walking. There was no abnormality in any of the three patients' temperatures, keeping a steady heart rate during less strenuous activities may have been made easier thanks to the medication reminder system. However, Patient (B's) heart rate reached 170 bpm while running, which was much greater than that of the other patients. It's also possible that the runner's elevated heart rate had nothing to do with the wearable reminder system. Patient (B) may have been too preoccupied during the runs for the medication reminder system to be as efficient as it was during the walks and rests scenario, this emphasizes the significance of taking into account

the influence of physical exercise on heart rate and the efficacy of the medication reminder system when engaging in a variety of activities.

Furthermore, the data in Table 3 suggests that the enhanced wearable medication reminder system with a Peripheral Interface Controller was useful for monitoring heart rate during less strenuous activities like sleeping and walking. The system's efficacy may be diminished, however, during more strenuous sports like jogging due to factors including physical exertion and the patient's compliance with the system developed.

TABLE 4: MEDICATION ACTIVITY STATUS

Activity/Feedback	**Patient**	
	Yes	**No**
Medication Taken	Alert: Okay	Alert: Please Take your Medication
Medication Not Taken	Alert: Please Take your Medication	Alert: Okay

Patient reactions to an enhanced wearable medication reminder systems are shown in table 4. In order to ensure that patients with arrhythmia take their medication at the right times, the system makes use of a Peripheral Interface Controller (PIC) and GSM module to communicate the patient's activities from cloud. There were two types of patient feedback recorded: "Medication Taken" and "Medication Not Taken."

There were two possible outcomes in the "Medication Taken" section: either the patient took the medication after being reminded ("Alert: Okay") or the patient did not need to be reminded ("Alert: Please Take your Medication"). Both "Alert: Please Take your Medication" and "Alert: Okay" fall under the "Medication Not Taken" heading, indicating that the patient has either ignored the reminder and hence not taken the prescription, or has taken the medication but was just not responding to the reminder.

Based on the data in the Table 4, it appears that the upgraded wearable medication reminder system was successful in getting the patient to take the medication when it is due. The "Alert: Please Take your Medication" response indicates that the system was successful in reminding the patient to take their prescription. Patients with arrhythmia may have a better chance of taking their medications as prescribed with this system implementation.

TABLE 5: MEDICATION ACTIVITY COMPARISON RESULT

Gender	**Age**	**HR on Display Device**	**HR on Oscilloscope**	**Error rate (%)**
Male	22	97	96	1.03
Male	22	83	81	2.41
Male	20	78	78	0
Male	22	90	87	3.33
Male	20	80	79	1.25
Female	22	77	77	0
Female	22	104	103	0.96
Female	19	75	75	0
Female	20	69	71	2.081
Female	22	83	85	2.35

In Table 5, the device precision was approximately 1.414 but changes depending on the results of the tests. Women typically have a greater HR than men, where there was a significant weight or lifestyle difference such as kind of work, health, inheritance of heart disease, and doing exercises.

In another test, two male heart rates were measured before and after a five minutes run. The resting heart rates were taken after the volunteers had rested for about two minutes. Comparing the device measurement to human measurement, which is done by counting pulses at the wrist as in Table 6.

TABLE 6: MANUAL AND WEARABLE SYSTEM MODEL COMPARISON TEST

Age	**Case**	**HR on Display Device**	**HR by Manual Measurement**
24	Before Exercise	65	64
	After Exercise	90	88
15	Before Exercise	91	88
	After Exercise	110	100

The test results indicate that different types of people have varying resting heart rates; the first test subject was a young man who regularly engages in physical activity, and the recorded resting heart rate

was the lowest of all the test subjects. The other young man whose resting HR was recorded to be the highest of the two. Being aware that the healthy heart rate is between 60 and 100 beats per minute, it was assumed that anything above or below this indicates a health problem prior to testing. The research revealed a more accurate range of 60 to 120 bpm as the healthy range for heart rate. Therefore, it is very necessary to provide users with more response information of body condition, such as heart rate, to help know the healthy condition and prevent risk of disease.

iii. NOTIFICATION

There were also other tests done to guarantee that the alert mechanisms are activated if the HR was found to be too high. By providing false information about the user's age and gender, the MAXHR was reduced so that it was easily exceeded.

The result obtained was an efficient and reliable wearable medication reminding system that helps persons with arrhythmia to remember to take their medication at the right time. By using the Discrete Fourier Transform (DFT) algorithm on the PIC microcontroller, the system performed real-time signal processing and provided accurate heart rate measurements for medication reminders.

IV. CONCLUSION

The primary goal of the system model was to alert the patient's medical advisors via short message service on the case of arrhythmia on a monitored patient with wearable device and also notifies the medical advisor on the patient's adherence to medical prescription from the medical advisor using a two-way communication channel enabled by the GSM modem. The system was tested with its performance evaluated to ensure optimum results. This device is deployable in hospitals, private homes, and emergency vehicles. The data presented in the research work indicates that the upgraded wearable medication reminder system was helpful in increasing medication adherence among patients with arrhythmia, but that further work could be needed to identify when medication has been given to prevent needless reminders.

ACKNOWLEDGMENT

Sincere gratitude to everyone who contributed to the development of the wearable medication reminding system for persons with arrhythmia using PIC microcontroller. Thank you all for your contributions to this research work, which has the potential to improve the lives of those with arrhythmia through the use of technology.

REFERENCES

Abdi, M., Karimi, A., Navidbakhsh, M., Pirzad Jahromi, G., & Hassani, K. (2015). A lumped parameter mathematical model to analyze the effects of tachycardia and bradycardia on the cardiovascular system. *International Journal of Numerical Modelling: Electronic Networks, Devices and Fields*, *28*(3), 346-357.

Acharya, U. R., Fujita, H., Oh, S. L., Hagiwara, Y., Tan, J. H., & Adam, M. (2017). Application of deep convolutional neural network for automated detection of myocardial infarction using ECG signals. *Information Sciences*, *415*, 190-198.

Ahmed, I., Ahmad, N. S., Ali, S., Ali, S., George, A., Danish, H. S., ... & Darzi, A. (2018). Medication adherence apps: review and content analysis. *JMIR mHealth and uHealth*, *6*(3), e6432.

Aldeer, M., Javanmard, M., & Martin, R. P. (2018). A review of medication adherence monitoring technologies. *Applied System Innovation*, *1*(2), 14.

AmolGosavi, M., DnyaneshwarKandekar, M., Ghadge, M. N., Behere, M. A., & Patil, D. R. (2017). Pulse Rate Monitoring Alert via SMS-Conclusion. *International Journal of Engineering Research and Management (IJERM), 3(6),* 1-4.

Babu, S. I. (2021). A PIC controlled based heart rate miniaturization using GSM. *Turkish Journal of Computer and Mathematics Education (TURCOMAT)*, *12*(10), 4765-4771.

Balakumar, P., Maung-U, K., & Jagadeesh, G. (2016). Prevalence and prevention of cardiovascular disease and diabetes mellitus. *Pharmacological research*, *113*, 600-609.

Biniyam, A., Tesema, A. G., Mohammed, A. A., Ramaiah, N. S., & Dilla, A. E. (2017). Design and implementation of heart beat monitoring using PIC microcontroller. In *2017 IEEE International Conference On Smart Technologies For Smart Nation (SmartTechCon)* pp. 784-787.

Casillas, C., & Americas, R. T. A. C. (2010). Heart rate monitor and electrocardiograph fundamentals. *Freescale Semiconductor*, 1-21.

Chang, L. L., Xu, H., DeVore, A. D., Matsouaka, R. A., Yancy, C. W., Fonarow, G. C., ... & Hernandez, A. F. (2018). Timing of postdischarge follow-up and medication adherence among patients with heart failure. *Journal of the American Heart Association*, *7*(7), e007998.

Choi, Y. M., Olubanjo, T., Farajidavar, A., & Ghovanloo, M. (2013). Potential barriers in adoption of a medication compliance neckwear by elderly population. In *2013 35th Annual International Conference of the IEEE Engineering in Medicine and Biology Society (EMBC)* (pp. 4678-4681). IEEE.

Chuquimarca, L., Roca, D., Torres, W., Amaya, L., Orozco, J., & Sánchez, D. (2020). Mobile IoT device for BPM monitoring people with heart problems. In *2020 International Conference on Electrical, Communication, and Computer Engineering (ICECCE)* (pp. 1-5). IEEE.

Elhag, M., Awaisu, A., Koenig, H. G., & Mohamed Ibrahim, M. I. (2022). The Association Between Religiosity, Spirituality, and Medication Adherence Among Patients with Cardiovascular Diseases: A Systematic Review of the Literature. *Journal of Religion and Health*, *61*(5), 3988-4027.

Fernandes, S. L., Gurupur, V. P., Sunder, N. R., Arunkumar, N., & Kadry, S. (2020). A novel nonintrusive decision support approach for heart rate measurement. *Pattern Recognition Letters*, *139*, 148-156.

Greiwe, J., & Nyenhuis, S. M. (2020). Wearable technology and how this can be implemented into clinical practice. *Current allergy and asthma reports*, *20*, 1-10.

Hsieh, H. L., Kao, C. W., Cheng, S. M., & Chang, Y. C. (2021). A Web-Based Integrated Management Program for Improving Medication Adherence and Quality of Life, and Reducing Readmission in Patients With Atrial Fibrillation: Randomized Controlled Trial. *Journal of Medical Internet Research*, *23*(9), e30107.

Jackevicius, C. A., Tsadok, M. A., Essebag, V., Atzema, C., Eisenberg, M. J., Tu, J. V., & Pilote, L. (2017). Early non-persistence with dabigatran and rivaroxaban in patients with atrial fibrillation. *Heart*, *103*(17), 1331-1338.

Jayanth, S., Poorvi, M. B., Shreyas, R., Padmaja, B., & Sunil, M. P. (2017). Wearable device to measure heart beat using IoT. In *2017 International Conference on Inventive Systems and Control (ICISC)* (pp. 1-5). IEEE.

Kalantarian, H., Motamed, B., Alshurafa, N., & Sarrafzadeh, M. (2016). A wearable sensor system for medication adherence prediction. *Artificial intelligence in medicine*, *69*, 43-52.

Kranjec, J., Beguš, S., Geršak, G., & Drnovšek, J. (2014). Non-contact heart rate and heart rate variability measurements: A review. *Biomedical signal processing and control*, *13*, 102-112.

Lin, B. S., Wong, A. M., & Tseng, K. C. (2016). Community-based ECG monitoring system for patients with cardiovascular diseases. *Journal of medical systems*, *40*, 1-12.

Mondol, A. S., Emi, I. A., & Stankovic, J. A. (2016). MedRem: An interactive medication reminder and tracking system on wrist devices. In *2016 IEEE Wireless Health (WH)* (pp. 1-8). IEEE.

Mondol, A. S., Emi, I. A., & Stankovic, J. A. (2016,). MedRem: An interactive medication reminder and tracking system on wrist devices. In *2016 IEEE Wireless Health (WH)* (pp. 1-8). IEEE.

Murat, F., Yildirim, O., Talo, M., Baloglu, U. B., Demir, Y., & Acharya, U. R. (2020). Application of deep learning techniques for heartbeats detection using ECG signals-analysis and review. *Computers in biology and medicine*, *120*, 103726.

Palanivel Rajan, S., & Sukanesh, R. (2013). Experimental studies on intelligent, wearable and automated wireless mobile tele-alert system for continuous cardiac surveillance. *Journal of applied research and technology*, *11*(1), 133-143.

Parihar, V. R., Tonge, A. Y., & Ganorkar, P. D. (2017). Heartbeat and temperature monitoring system for remote patients using Arduino. *International Journal of Advanced Engineering Research and Science*, *4*(5), 237161.

Reading, S. R., Black, M. H., Singer, D. E., Go, A. S., Fang, M. C., Udaltsova, N., ... & Reynolds, K. (2019). Risk factors for medication non-adherence among atrial fibrillation patients. *BMC cardiovascular disorders*, *19*(1), 1-12.

Rosner, D., Jurba, A. T., Tataroiu, R., Ilas, C., Vasile, S., & Matei, S. (2015). Wearable medication reminder architecture enhancement: Focus group based assessment and scenario based testing. In *2015 20th International Conference on Control Systems and Computer Science* (pp. 279-284). IEEE.

Salmasi, S., Loewen, P. S., Tandun, R., Andrade, J. G., & De Vera, M. A. (2020). Adherence to oral anticoagulants among patients with atrial fibrillation: a systematic review and meta-analysis of observational studies. *BMJ open*, *10*(4), e034778.

Satpathy, S., Mohan, P., Das, S., & Debbarma, S. (2020). A new healthcare diagnosis system using an IoT-based fuzzy classifier with FPGA. *The Journal of Supercomputing*, *76*, 5849-5861.

Shabaan, M., Arshid, K., Yaqub, M., Jinchao, F., Zia, M. S., Bojja, G. R., & Munir, R. 2020).

Survey: smartphone-based assessment of cardiovascular diseases using ECG and PPG analysis. *BMC medical informatics and decision making*, *20*, 1-16.

Sundararaj, V. (2016). An efficient threshold prediction scheme for wavelet based ECG signal noise reduction using variable step size firefly algorithm. *Int J Intell Eng Syst*, *9*(3), 117-126.

Tan, L., Yu, K., Bashir, A. K., Cheng, X., Ming, F., Zhao, L., & Zhou, X. (2021). Toward real-time and efficient cardiovascular monitoring for COVID-19 patients by 5G-enabled wearable medical devices: A deep learning approach. *Neural Computing and Applications*, 1-14.

Tutuko, B., Rachmatullah, M. N., Darmawahyuni, A., Nurmaini, S., Tondas, A. E., Passarella, R., ... & Firdaus, F. (2022). Short single-lead ECG signal delineation-based deep learning: implementation in automatic atrial fibrillation identification. *Sensors*, *22*(6), 2329.

Verma, S., & Gupta, N. (2012). Microcontroller-based Wireless Heart Rate Telemonitor for Home Care. *IOSR J Eng (IOSRJEN)*, *2*(7), 25-31

.

Journal of Engineering, Emerging Technologies and Applied Sciences – Volume 1 Issue 1, April 2023

Available at ***www.ndu.edu.ng/journalof engineering***

RESEARCH ARTICLE OPEN ACCESS

Development of a Robot Arm Using Electromagnet as End Effector To Carry Out Pick and Drop Operation

Fred Oyinbonogha Agonga *, Justice Chikezie Anunuso**, Ayuba Elkanah Jatau***

*(Department of Mechanical Engineering, Niger Delta university, Amassoma
Email: agongofred@ndu.edu.ng)

** (Department of Mechatronics Engineering, Federal University of Technology Minna, Niger State
Email : j.aunuso@futminna.edu.ng)

***(Department of Mechanical Engineering Technology, Niger State Polytechnic Zungeru
Email : elkanahayubaj@gmail.com)

----------**********----------

Abstract:

Owing to labour issues in industry, such as pick and drop operation of hazardous and heavy materials, there is a need to procure an autonomous solution. This article shows the creation and use of a model robotic arm that uses a magnetic gripper to load and unload light metal sheets. Two servo motors operate as actuators to control the arm's movement and the wrist's alignment. An Arduino microprocessor controls the arm, while a DC power source powers the electromagnet. To depict how the actual system will seem, the design was created using CAD software. This was subsequently physically applied to a functional system. The physical system is created through the combination of several components, and the electrical control system utilized an Arduino Uno microcontroller, for which a program was generated using the Arduino IDE to direct the movement of the servo motors and regulate the electromagnet. According to the results of the experiments, the robotic arm equipped with a magnetic end effector is capable of picking and dropping objects with a high degree of accuracy and effectiveness. The creation of a robot manipulator using an electromagnet as the end effector for pick and drop operations is discussed in this study, offering a practical solution for sectors that need to do repetitive tasks.

Keywords — **Actuators, Electromagnet end effector , Industrial Automation, Microcontrolle , Magnetic Gripper, Robotic Arm, Simulation.**

----------**********

I. INTRODUCTION

A robot is an electromechanical device connected with joints and links, driven by motors or actuators guided by sensors and controlled through a software program to perform many different kinds of work (Moe Myint et al., 2016). The term ‘robotics’ was coined by a well-known Russian Science fiction writer Isaac Asimov sequel to this period, Karl Capek had written a play titled Rossum’s Universal Robots which gave popularity to the term robotics in the 1920s (Ropo et al., 2018).

A robotic arm with an electromagnet as its end effector is a machine designed to pick up and drop objects using an electromagnet. This type of arm is commonly used in manufacturing and industrial settings where objects need to be moved and manipulated with precision and efficiency.

The electromagnet at the end of the arm can be turned on and off using an electric current, allowing it to attract and hold onto objects made of magnetic materials. The arm itself is typically made up of several joints that can be moved and rotated to position the end effector in the desired location (Islam & Islam, 2014)

settings where objects need to be moved and manipulated with precision and efficiency.

The electromagnet at the end of the arm can be turned on and off using an electric current, allowing it to attract and hold onto objects made of magnetic materials. The arm itself is typically made up of several joints that can be moved and rotated to position the end effector in the desired location.(Islam & Islam, 2014).

The design of a robotic arm with an electromagnet as its end effector requires careful consideration of factors such as the weight of the objects to be moved, the precision required for positioning, and the range of motion needed for the arm. Additionally, the power source for the electromagnet and the control systems for the arm must also be carefully designed and integrated (Islam & Islam, 2014).

Over the years, robotics has found applications in several fields ranging from space exploration to medical fields, homes applications, laboratory research, manufacturing, and industries. Robots are generally used to perform highly repetitive and unpleasant tasks that seem strenuous and hazardous to human agents. The more the number of industries increases in developing countries and even developed countries, the higher the demands for laborers in carrying out several operations in these industries (Harish et al., 2019) Time and adequate manpower are major constraints in carrying out large-scale tasks in industries hence the need for machines or systems to save human efforts in the industries. The costs of maintaining human labour in the industries keep rising, the price of buying and maintaining robots is reducing (Ropo et al., 2018). While robots become more cost-effective at their jobs, human labour continues to be expensive and less productive, hence more industrial jobs are being taken over by robots.

An industrial robot is a re-programmable multifunctional manipulator designed to move material, parts, tools, or specialized devices through variable programmed motion for the performance of a variety of tasks - the definition from the Robot Institute of America to reflect main features of modern robot systems. An industrial robot system can include any devices or sensors together with the industrial robots to perform its tasks as well as sequencing or monitoring communication interfaces. (Elfasakhany et al., 2011)

One of the vital functions of an industrial robot is the pick and place function. This operation includes lifting a payload from within its workspace, or carrying it to a predetermined location where the load is released. The picking and dropping of loads in industries seem to be one of the most highly repetitive processes with a high call for timeliness and accuracy. Human's efforts most times fall short of these demands hence the need for a smarter and more efficient system in handling this process.By simply introducing the autonomous robotics applications, simple repetitive tasks can be accomplished by keeping demands of accuracy and speed in mind which will result in optimal utilization of the machine and manpower. An essential goal in the development of robots is to have them interact with their surroundings. Typically, an arm and a grasping tool or end effectors are used to execute this interaction. A robot manipulator is programmed to perform similar functions to that of a human arm; the arm may be part of a more complex robot. The links of such a manipulator are connected by joints allowing either rotational motion or translational (linear) displacement and can be considered to form a kinematic chain, the terminus of which is called the end effector and it is analogous to the human hand (Kruthika et al., 2017).

II. MAIN COMPONENTS

To make the robotic arm the following parts/components are required (as shown in Table 1).

TABLE I
PARTS/COMPONENTS OF THE ROBOTIC ARM

Servo motor	Voltage regulator (7806)
Electro magnet	Transistor BC555
Wooden and metal links	Regulator: constant 5V
Pattress box	Bero-board
Relay (6V)	Switch
Arduino Uno	Pattress box
19v power supply	

Servo motor: Servo motors as seen in Figure 1 are electronic actuators devices that rotate pushing parts of a machine with precision. A servomotor is a motor, which forms part of a servomechanism often paired with some type of encoder to provide position/speed feedback.

Fig. 1 Servo motor

Electromagnet: Electromagnets as seen in figure 2 are made of **coils** of wire with electricity passing through them. Moving charges create magnetic fields, so when the coils of wire in an electromagnet have an electric current passing through them, the coils behave like a magnet. Electromagnets are used in a lot of electronic devices when magnetic forces are only needed for short periods of time. Electromagnetic gripper is a type of end effector mounted at the end of the robotic arm, that can catch and transfer steel parts or ferrous materials in automated assembly operations (Islam & Islam, 2014). Magnetic end effector, also known as magnetic grippers or robot magnetic end-of-arm tool, is a must-have for robotic pick and place of steel parts, especially in intelligent manufacturing

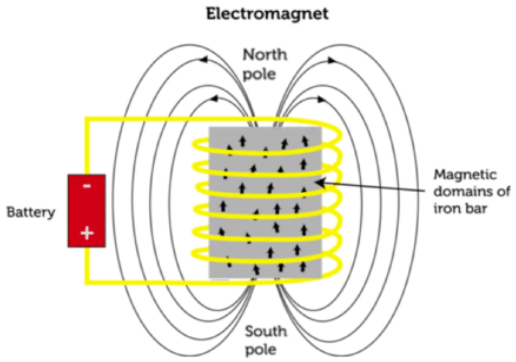

Fig. 2 Electromagnets (Islam & Islam, 2014)

Arduino Uno: Arduino Uno as seen in Figure 3 is a microcontroller board based on the ATmega328P (datasheet) having 14 digital input/output pins, 6 analogue inputs, a 16 MHz ceramic resonator (CSTCE16M0V53-R0), a USB connection, a power jack, an ICSP header and a reset button. It can simply be connected to a computer using a USB cable or powered with an AC-to-DC adapter or battery. Arduino uno is a low-cost, flexible, and easy-to-use programmable open-source microcontroller board that can be integrated into a variety of electronic projects (Jambotkar, 2017) which can also be interfaced with other Arduino boards, Arduino shields, Raspberry Pi boards and can control relays, LEDs, servos, and motors as an output.

Fig. 3 Arduino uno ATmega328P (Jambotkar, 2017)

III. METHODOLOGY

This research work follows three stage which solves its objectives. This can be seen from the design block in Figure 4.

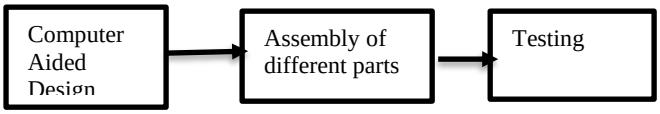

Fig. 4 Design block diagram

A. Computer Aided Design (CAD)

The first stage is the Computer Aided Design (CAD) design stage. In this stage, solid works 2018 software was used to design a 3D model of the system. The software was used to design the individual component that makes up the robotic arm as seen in figure 5 then assembly drawing was then used to bring together these parts. Figure 6 shows the 3D model of the whole system.

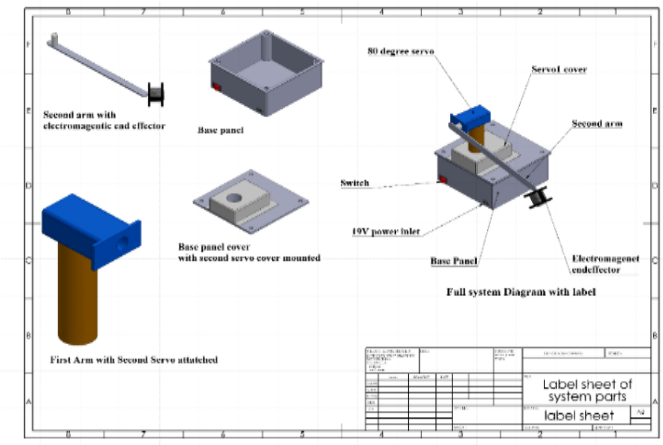

Fig. 5 System parts label

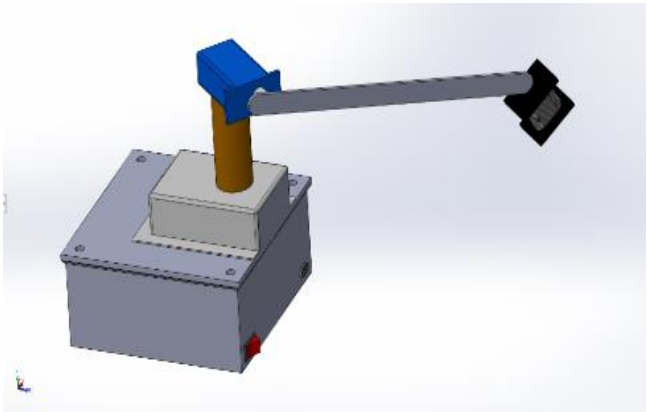

Fig. 6 System 3D model

B. Fabrication And Assembly

The robot arm was designed using a top-down technique; however, it was constructed piece by piece and then its individual components were assembled to form the entire arm.

For equilibrium, the actuators (two servo motors) are positioned in the centre of the upper base. The motors are controlled by a 5-volt power supply. By programming the microcontroller, the servo motor that is attached to the upper base is rotated 180 degrees. The second servo motor is also angled between 180 and 270 degrees. Three relays that operate on 5 volts are utilized to magnetize the gripper. The relays are magnetized and connected to one another so that they may grasp any metallic object. The model is powered by a battery that has a 5 volt and 1 ampere capacity as depicted in Figure 7.

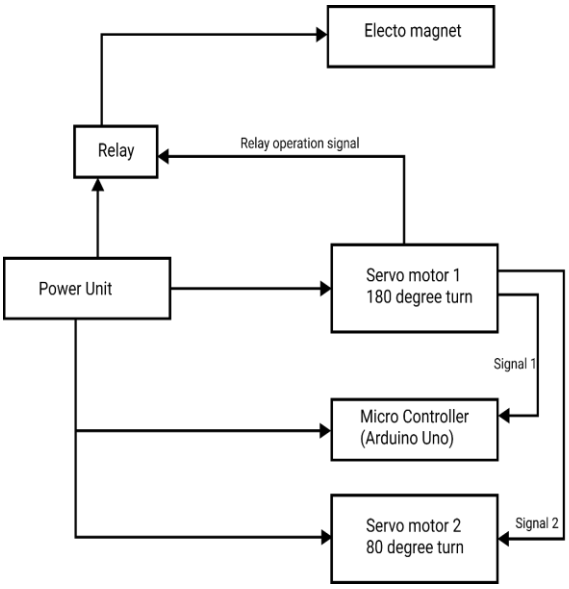

Fig. 7 System operation block diagram

The robotic arm functions just like a human hand. Because of the magnet, it has a strong grip. It can retain a light metal sheet in a moving position using the grasping. After some time, the magnet's power turns on, holding the sheet metal as it is moved from one location to another.

Two servo motors are employed in this situation to carry the sheet metal. One servo motor rotates horizontally, moving hand to the horizontal position, while another rotates vertically, moving the hand to the vertical position. Microcontrollers control the entire system. The microcontroller is pre-programmed to make a decision for any input and transmit that decision to the motors and magnetic grip as shown in Figure 8. The microcontroller generates the output for the magnetic grip when the hand is in the correct alignment. The motor in this case is swung by the BD555 Transistor. An LM7805 acts as a consistent power source in the circuit.

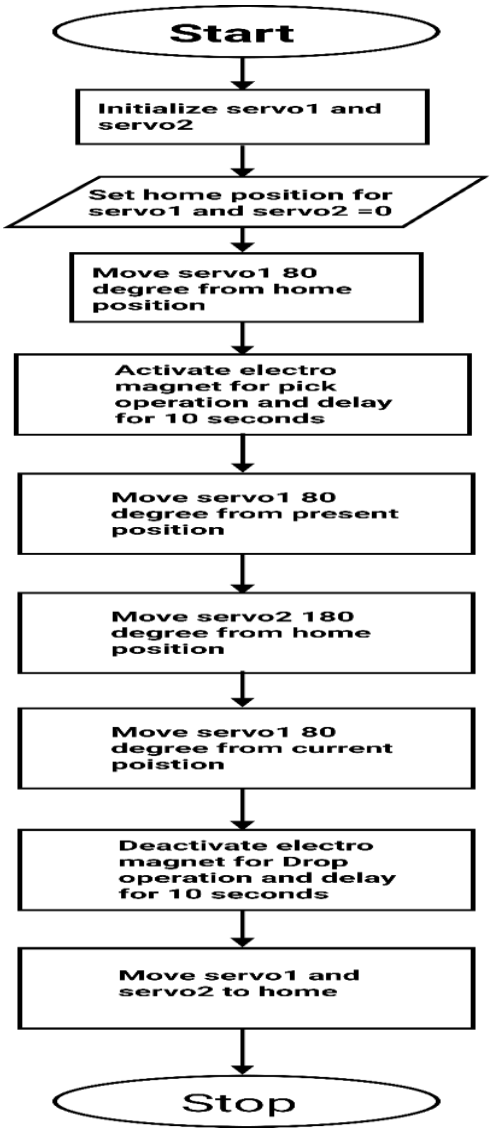

Fig. 8 Flow chat of the operation of the robotic arm

C. Testing

The testing phase, the solid works was used to obtain the graph for the angular displacement, velocity and acceleration via motion study feature. And the proteus was used to simulate the electrical circuit to see how it works. Figure 9 shows the proteus schematic circuit diagram.

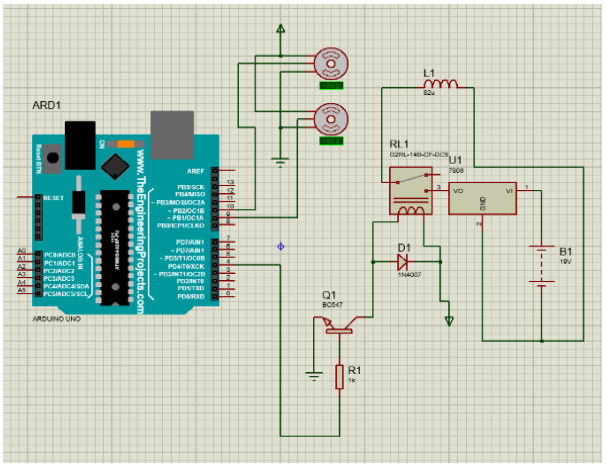

Fig. 9 Circuit diagram

Figures 10 and 11 shows the graph of the angular displacement of the system for link 1 and link 2 respectively. The angular displacement is plotted against the time it takes from the link to move from home position to the final position. The graph presented from Figure 12 and Figure 13 describes the angular velocity of the links 1 and 2 respectively as they transform from one position to the other with respect to time. The graph presented from Figure 14 and Figure 15 describes the angular acceleration of the links 1 and 2 respectively as they transform from one position to the other with respect to time.

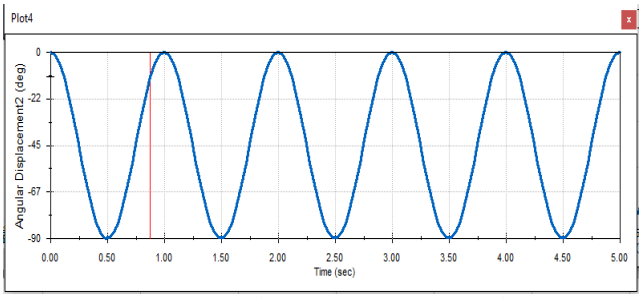

Fig. 10 The graph of the angular displacement of link 1

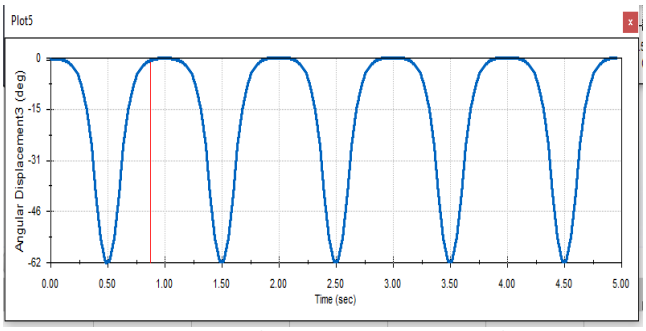

Fig. 11 The graph of the angular displacement of link 2

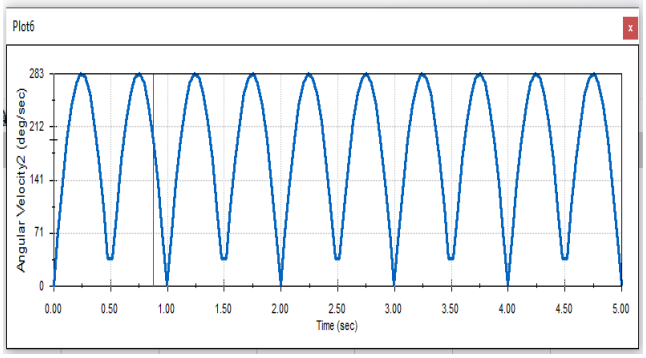

Fig. 12 The graph of the angular velocity of link 1

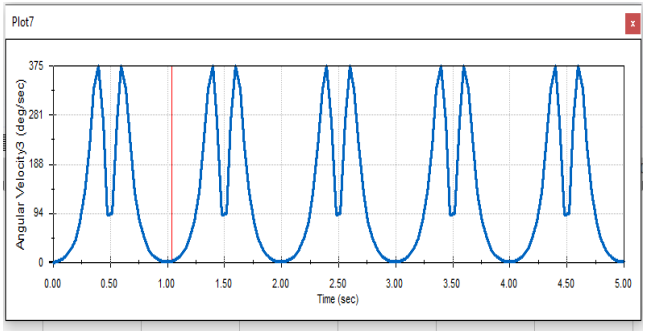

Fig. 13 The graph of the angular velocity of link 2

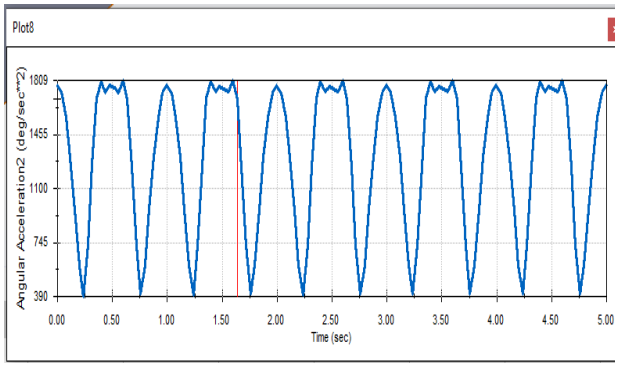

Fig. 14 The graph of the angular acceleration of link 1

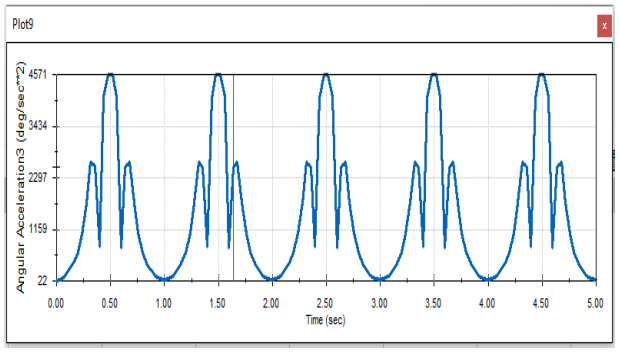

Fig. 15 The graph of the angular acceleration of link 2

IV. DISCUSSION OF RESULT

The goal of this research work was to develop, and control a prototype robotic arm that loads and unloads light metal sheets using electromagnetic grippers.

The outcome demonstrates that servo motors 1 and 2 are at a 0-degree angle, which is the home position for the robotic arm. This is to ensure that the picking link is at a convenient workspace for it to pick the sheet metal. Then the electro magnet is then actuated by the relay connected to pin 4 of the Arduino. This allows 19 volts to flow to the electromagnet to pick the sheet metal. After this is completed by delaying the system for 10 seconds, then the servo 1 is then set to 0 degree again in other to put the arm in a safe workspace for the second servo to move to the drop position. Then the second servo is then move to 180 degrees (the drop position). The servo 1 is then moved again to 80 degree and the electromagnet is deactivated.

V. CONCLUSION

Robotic arms are perfect for tasks that need to be repeated, reliable, and of a very high calibre. The pick-and-drop process can be made more accurate, economical, and predictable by automating it. Using a robotic arm offers various benefits, including increased production capacity and manufacturing process precision. Assembling, packaging, bin selecting, and other tasks are some of the uses for pick and drop robots.

The goals are established based on these requirements, and the research activities (design, fabrication, installation, and controlling the robotic arm) have been successfully completed.

The robotic arm's mechanical and electrical architecture is fairly straightforward. By using a magnetic gripper, the robotic arm is capable of loading and unloading steel metal objects. The arm has a 180-degree vertical range of motion. The program of the microcontroller makes it simple to regulate the arm's speed and direction.

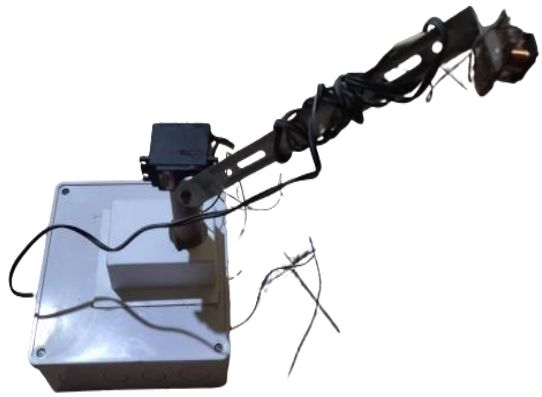

Fig. 16 Image of the final design.

ACKNOWLEDGMENT

We want to express our sincere thanks to the Almighty God. We also value the kind assistance and collaboration friends and colleagues for their inputs for the successful completion of this project. We also like to thank the workshop staff and students for their kind support in making this project a success and producing the required results.

REFERENCES

Harish, K., Megha, D., Shuklambari, M., Amit, K., & Jambotkar, C. K. (2019). *Pick and Place Robotic Arm Using Arduino*. *April*.

Islam, T., & Islam, M. R. (2014). *05-P-15:* DESIGN & FABRICATION OF A ROBOTIC ARM MODEL WITH MAGNETIC GRIPPER ABIOTIC PHYSIOLOGY VIEW PROJECT INVESTIGATION AND PERFORMANCE ANALYSIS OF A SMALL SCALE SAVONIUS WATER CURRENT TURBINE IN PERSPECTIVE OF BANGLADESH View project. https://www.researchgate.net/publication/344844111

Jambotkar, C. K. (2017). Pick and Place Robotic Arm Using Arduino. International Journal of Science, Engineering and Tech. *Research (IJSETR)* (Vol. 6). https://www.researchgate.net/publication/332565132.

Kruthika, K., Kiran Kumar, B. M., & Lakshminarayanan, S. (2017, September 27). Design and development of a robotic arm. *2016 International Conference on Circuits, Controls Communications and Computing, I4C 2016*. https://doi.org/10.1109/CIMCA.2016.8053274.

Moe Myint, K., Min Min Htun, Z., & Myo Tun, H. (2016). Position Control Method For Pick And Place Robot Arm For obj. Sorting System. INTERNATIONAL JOURNAL OF SCIENTIFIC & TECHNOLOGY RESEARCH, 5(06). www.ijstr.org

Ropo, O. O., Adekunle, O. F., Oluwaseun, O. A., & Babatope O. P. (2018). Design of a Pick and Place Serial Manipulator. IOP Conference Series: Materials Science and Eng. *413*(1). https://doi.org/10.1088/1757-899X/413/1/012056

Elfasakhany, A., Yanez, E., Baylon, K., & Salgado, R. (2011).Design and Development of a Competitive Low-Cost Robot Arm with Four Degrees of Freedom. Modern Mechanical Eng. *01*(02), 47–55. https://doi.org/10.4236/mme.2011.12007

Journal of Engineering, Emerging Technologies and Applied Sciences -– Volume 1 Issue 1, April 2023

Available at ***www.ndu.edu.ng/ journalofengineering***

RESEARCH ARTICLE OPEN ACCESS

A Review on the Effect of Reaction Parameters on Biodiesel Production

Biebelemo Jethrow Jonathan and Branly Eric Yabefa

Department of Agricultural & Environmental Engineering, Niger Delta University, Amassoma, Bayelsa State, Nigeria

Corresponding Author: jonathanbiebelemo@ndu.edu.ng

----------**********----------

Abstract

Biodiesel is an environment friendly fuel that comes with less pollution compared to the fossil fuel, which diesel engines can use fully or as partial replacement, to the petroleum based conventional diesel. It is normally produced from locally available materials such as plants, waste cooking oil, animal fats etc. The production of biodiesel can be done through a transesterification reaction which is affected by some reaction parameters including; reaction time, reaction temperature, catalyst concentration, content of free fatty acid etc. however, literature is scarce on the review of factors affecting the transesterification reaction. Hence, this study intends to discuss the factors that influence biodiesel production.

Keywords: Biodiesel, reaction-time, reaction-temperature, catalyst-concentration, FFA

----------**********----------

I. INTRODUCTION

The increasing demand for a less expensive and environment friendly alternative source of energy has attracted researchers' attention to the biodiesel production which can be easily processed from locally available wastes materials as feedstock, and it comes with less emissions to pollute the environment compared to the petroleum based fuel and it is a renewable source of energy (Mathiyazhagan et al., 2011). Feedstock for biodiesel production can be vegetable oil from plants, animal fats, waste cook oils etc. the biodiesel can be produced in a transesterification reaction. This process involves the reaction of triglycerides with methanol or ethanol (i.e. alcohol) in a given temperature, time mixing rate, produce fatty acids alkyl esters called the biodiesel glycerol with the aid of a catalyst (Lalita et al., 2004). Transesterification reaction can be of the following types; acid catalyzed, alkaline, enzyme catalyzed and the supercritical methanol transesterification (i.e. non catalyzed). However, the alkaline catalyzed transesterification is the most conventionally used method because it is fast and easy. Examples of raw materials such as, soybean oil, jastropa oil, coconut oil, rapseed oil etc are used for producing biodiesel (Lalita et al., 2004)

The transesterification reaction is affected by different factors such as; reaction time (RT), reaction temperature (RTM), methanol to oil ratio (MOR), catalyst concentration (CC) etc. (Mathiyazhagan et al., 2011; Lalita et al., 2004). However, literature is scarce on the review of biodiesel yield based on the reaction parameters influence. Hence, this study intends to extensively report the influence of the reaction parameters to biodiesel production.

II. LITERATURE REVIEW

A. Reaction Temperature (RTM)

The RTM in a transesterification reaction is a significant factor that determines the yield of biodiesel. The variation in the reaction temperature can give a duration under which a better yield can be obtained. In most cases, when the RTM is increased, it lowers the viscosity of the bio-oil thereby reducing the reaction time (Mathiyazhagan et al., 2011). However, the biodiesel yield can reduce drastically

when the temperature goes beyond the maximum level, (Eevera et al 2009). Leung et al., (2006) presented that, the maximum reaction temperature for a transesterification reaction is dependent on the alcohol and the bio-oil to be used. However, the range of 50oC to 60oC was recommended to be the best in their study. Encinar et al., (2001) presented a report on the production of biodiesel from *Cynara cardunculus* oil and obtained almost 92% yield at ambient temperature. Lalita et al., (2004) reported the production of biodiesel from crude palm oil using a range of temperature from 30oC to 60oC, and revealed that, the yield reduced as the reaction temperature increased, because the separation between the biodiesel and glycerol was reduced by the higher solubility based on the increased temperature. Hence room temperature was recommended by them in their study.

B. Reaction Time

This is another important reaction parameter for consideration in biodiesel production i.e. the best duration under which the maximum yield can be produced. Lalita et al., (2004) presented a report on the production of biodiesel from crude palm oil using different reaction times. Lalita et al, (2004) revealed that, there was a gradual increase but biodiesel yield was not significantly affected, but the biodiesel concentration increased with the increase in reaction time. The reversible reaction of transesterification leads to the reduction on biodiesel production in a prolong reaction period, resulting in formation of soap and loss of ester. Hence lesser reaction time is recommended in transesterification, because, further increase in reaction time does not increase the biodiesel yield. (Ma et al., 1998).

C. Oil to Methanol ratio

The mix ratio of methanol to the vegetable oil for the transesterification is another major reaction parameter that affects yield of biodiesel (Leung et al., 2006). Too much of alcohol in the mixture drastically accelerates the rate of fats conversion to sugar very quckly. Hence, biodiesel production increases, as the alcohol concentration increases to a certain level and at the same time, the cost of alcohol recovery becomes more expensive (Leung and Guo., 2006). The type of catalyst used may also determine the ratio of alcohol content required in the mixture. For instance, a ratio of 6:1 for alcohol to catalyst is required when using alkali catalyst in the transesterification reaction for biodiesel production (Lalita et al., 2004). However, an acid catalyst will be needed, if there is much free fatty acid (FFA) in the oil because, alkali catalyst will not give a good result in such condition. Hence, using the acid catalyst will require more volume of alcohol in the reaction than the former. The simple reason is because, the acid catalyst can withstand the water and FFA presence in the samples of oil. Lalita et al., (2004) reported that, raising the reactants mass ratio enhances the interaction of the oil and methanol to produce a higher concentration of methyl ester. But as the mass ratio of reactant increases, the production yield drops.

D. Catalyst Concentration (CC)

The yield of biodiesel in the transesterification reaction can also be influenced by the conc. of the catalyst used in the reaction. The most commonly used catalysts in transesterification reaction for biodiesel production are sodium hydroxide and potassium hydroxide. However, in a study by Freeman et al., (1984) stated that, the use of sodium hydroxide as a catalyst in biodiesel production results in a little quantity of water, which in turn inhibits a good yield of the biodiesel due to the hydrolysis reaction. Therefore, it is always advisable to mix the catalyst with the methanol before adding to the oil.

Again, when the concentration of the catalyst in the oil is increased, it will significantly increase the yield of the production of biodiesel from the triglycerides. Also, insufficient catalyst causes partial conversion of triglycerides to fatty acid esters (Leung et al., 2006). The best yield of the catalyst approached 1.5wt%, but increasing the concentration of the catalyst also had some negative impacts on the yield of biodiesel because, formation of more soap will result when an excess of alkali

catalyst reacts with the triglycerides (Leung and Guo 2006).

E. Content of Water and Free Fatty Acid (FFA)

In a transesterification reaction, the availability of water and FFA are significant factor that enhance the rate of biodiesel production. The raw materials normally used for biodiesel production must be water free and low acid value of less than one (Demirbas, 2009). However, when there is too much FFA contained in the oil for the biodiesel production, then such reaction will need much catalyst to certainly neutralize the FFA to obtain a better yield of the biodiesel. The presence of water in the oil can enhance the production of soap and foaming which is not a good requirement in biodiesel production, because, it increases the viscosity of the oil there by making it more difficult to be converted to biodiesel. Also, the development of gels and foams makes it difficult for glyceryl separation from the biodiesel (Demirbas 2009). The presence of water and FFA in the oil is always known for negative effects in the transesterification reaction that leads to the formation of soap which consumes much of catalyst. Again, the presence of water and FFA in the oil for transesterification can as well reduce the methyl ester. Hence, Kusdiana and Saka (2001) suggested supercritical methanol approach, when they used a temperature of 623K and a pressure of 43MPa for 4 minutes of treatment for an oil to methanol ratio of 1:42. The result obtained in their study was compared with the alkaline and acid catalyzed methods. It was revealed that, water has less effect on the supercritical methanol approach.

III. CONCLUSION

Biodiesel production and usage had been widely encouraged around the globe due to its renewability and low cost of production. Biodiesel which is normally produced from vegetable oils, animal fats etc. by a transesterification reaction which reduces the viscosity of the oils in the presence of a catalyst. This process is normally affected by some reaction parameters including reaction time, reaction temperature, oil to methanol ratio, catalyst concentration and FFAs.

ACKNOWLEDGMENT

Sincere appreciation goes to everyone who contributed to this review of reaction parameters affecting production of biodiesel. Thank you all for your contributions to this study which can be a useful reference material for further studies in biodiesel production in the area of renewable energy.

REFERENCES

Demirbas A. (2009) Progress and recent trends in biodiesel fuels. *Energy Convers Manage*; 50:14–34.

Eevera T, Rajendran K, Saradha S (2009): Biodiesel production process optimization and characterization to assess the suitability of the product for varied environmental conditions. *Renew Energy*; 34:762– 5

Encinar. J.M., Gonzalez, J.F., Rodriguez, J.J., and Tejedor, A., (2001): Biodiesel fuels from Vegetable oil; Transesterification of Cynara cardunculus L. Oils with Ethanol, Energy & Fuels.

Freeman., B., Pryde, E.M and Mounts, T.L. (1984): Variables Affecting the yield of Fatty Esters from Transesteried Vegetables Oils. J.Am. Oil Chem. Soc. 61. Pp. 1638-1643.

Kusdiana, D.; Saka, S (2001): Kinetics of transesterification in rapeseed oil to biodiesel fuel as treated in supercritical methanol. *Fuel*, 80, 693–698.

Lalita , A, Sukunya M., Peesamai J., (2004): Factors affecting Biodiesel from Crude Palm Kernel Oil. The Joint International Conference on Sustainable Energy and Environment (SEE) Hua Hin, Thailand. 3-045

Leung DYC, Guo Y. (2006): Transesterification of neat and used frying oil: optimization for biodiesel production. *Fuel Process Technol*; 87:883–90

Ma F, Clement L.D, Hana M. A, (1998): the effects of catalyst free fatty acids, and water on trans esterification of beef tallow. Trans Am Soc Eng; 41:1261-5

Mathiyazhagan, M., Ganapathi, A., (2011): Factors affecting Biodiesel Production. A review article. Research in Plant Biology 1(2): 01 – 05. ISSN: 2231 -5101

